On wave-wind interactions and implications for offshore wind turbines

by

Siri M. Kalvig

Thesis submitted in partial fulfillment of
the requirements for the degree of
PHILOSOPHIAE DOCTOR
(PhD)

Faculty of Science and Technology
Department of Mechanical and Structural
Engineering and Materials Science
2014

University of Stavanger
N-4036 Stavanger
NORWAY
www.uis.no

ISBN 978-82-7644-581-7
ISSN 1890-1387
PhD Thesis UiS, 235

Abstract

Offshore wind technology has many similarities with wind energy on land, but it is still recognized as an immature industry. Also, there are special challenges associated with the offshore environment. As a part of this thesis, it has been documented that there is a gap between 'best knowledge' and 'best practice' in boundary layer meteorology in the field of offshore wind energy. One part of this gap is to consider the sea surface as level and smooth. In reality, the sea surface is constantly changing and this results in a dynamical roughness of the sea surface. The wind whips up the ocean surface and creates waves, and the waves themselves influence the wind. However, the latter effect is usually ignored in the contexts of offshore wind energy.

The shape of the wind profile is very important for wind turbine performance. For an offshore wind turbine, operating over the ever-changing sea surface, it is therefore crucial to investigate how waves will affect the wind profile and the wind shear in the swept area of the wind turbine rotor. Consequently, the main topic of investigations for this thesis has been wave-wind interaction and the implications for offshore wind turbines.

Computational fluid dynamics (CFD) has been used for both wave influenced wind modelling, and for wind turbine performance and wake predictions. These two areas were first investigated separately, and different turbulence calculation techniques were tested. Thereafter, a coupled CFD setup was developed that allows a direct modelling of the effects of wave influenced wind on wind turbine performance.

The model experiments show that waves influence the wind field above them. The effect is notable far up into the marine atmospheric boundary layer and depends on the wave state and the direction of the waves and the wind. As a result, the wind turbine rotor will be exposed to wind profiles and turbulent levels other than what is predicted with the usual assumption of a logarithmic wind profile and low turbulence levels over a flat surface. Model simulations with the coupled setup further show that wave influenced wind will affect the turbine performance, as well as the loads and fatigue. The wave influenced wind induces oscillations in the power output with the same frequency as the waves. Wave influenced wind turbine simulations, linked to the structural response tool FAST, demonstrated that swell will increases the fatigue damage compared to a situation with no waves, especially for the cases where the wave field opposes the wind field.

Key words: Offshore wind turbine, marine atmospheric boundary layer, actuator line, wind wave interaction, k-ε turbulence model, CFD, OpenFOAM

Preface and acknowledgements

This thesis is submitted in partial fulfillment of the requirements for the degree of Doctor of Philosophy (PhD) at the University of Stavanger (UiS), Norway. The research work was carried out at the UiS and StormGeo in the period from September 2009 to June 2014 (paused by a period of maternity leave). The project was funded by the Norwegian Research Council and StormGeo. The compulsory PhD courses followed have been offered at the UiS and at Aalborg University in Denmark.

My four supervisors have been very supportive. I would especially like to acknowledge Eirik Manger, at Acona Flow Technology, for all his invaluable help regarding the development of the new wave influenced wind turbine solver. Without his programming expertise and supreme CFD knowledge, this PhD would have taken a different and undesirable course. Nina Winther in StormGeo motivated me in the first place and I have learned a lot from her clear and wise thoughts. Jasna B Jakobsen and Bjørn Hjertager, at the University of Stavanger, have also given valuable support and guidance, and I have benefited from their long experience in relevant research fields. A great thanks to my main surpervisor, Bjørn Hjertager, for allowing me to be his PhD student. It has been hard work, enlightening and fun!

The computations carried out have been quite computationally demanding and I would like to acknowledge Theodor Ivesdal at University of Stavanger for his excellent technical support regarding the Linux cluster.

I would also like to thank Matthew Churchfield at NREL for his hospitality and assistance regarding my visit to the research center in Boulder last year. Although I could not stay for many weeks, it was a very educational visit to one of the world's most recognized renewable energy laboratories. Churchfield and NREL have done impressive work with the open source CFD tool SOWFA, which I have used for this thesis. My PhD project has been a part of the Norwegian Centre for Offshore Wind Energy (NORCOWE). The participation in this research consortium have given me valuable insight into the field of offshore wind energy research. I have appreciated all the good workshops and discussions NORCOWE have facilitated.

Undertaking a PhD has been a fantastic opportunity for me, and has been realized with the support from StormGeo. I am very grateful for this opportunity from my employer.

In order to finalize this PhD project, support was of course also needed from my family. I am really looking forward to spending more time with Kjell-Erik, Sara, Silje and Lilly again without thinking about wave influenced wind!

Siri M. Kalvig

Artistic representation of an offshore wind turbine.
Silje Kalvig Østdahl (aged 10)

Contents

Nomenclature

Abbreviations

BEM	Blade element momentum
CFD	Computational Fluid Dynamics
ECMWF	The European Centre for Medium Range Forecast
FAST	Aero elastic code that can model the dynamic response of horizontal-axis wind turbines
Hindcast	Numerical we models in a historical mode. Often used as a substitute to observations in order to give a representation of the wave climate or weather in a period.
LES	Large Eddy Simulations
MABL	Marine Atmospheric Boundary Layer
MetOcean	Abbreviation for 'meteorological and oceanographic'
MO	Monin-Obukhov similarity theory
NORCOWE	Norwegian Centre for Offshore Wind Energy
NOWITECH	Norwegian Research Center for Offshore Wind Technology
NREL 5 MW	National Renewable Energy Laboratory's reference turbine of 5 Mega Watt
NREL	National Renewable Energy Laboratory
PIMPLE	Numerical algorithm for solving the time-dependent fluid flow equations
PISO	Numerical algorithm for solving the time-dependent fluid flow equations
QUICK	Numerical discretization scheme, Quadratic upwind interpolation for convective kinematics
RANS	Reynolds Averaged Navier-Stokes
SGS	Subgrid-scale model
SOWFA	Simulator fOr Wind Farm Applications
SWAN	Simulating Waves Nearshore, wave model
URANS	Unsteady Reynolds Averaged Navier-Stokes
WBL	Wave boundary layer
WIWiTS	Wave Influenced Wind Turbine Simulations
WRF	The Weather Research and Forecasting model
XFOIL	Airfoil development system, name of software

Symbols

c_p	Phase speed of the peak of the wave spectrum
U_{10}	Wind speed at 10 m height
z_0	Roughness length
u_*	Friction velocity
g	Acceleration due to gravity
ρ	Density of the air
C_D	Surface drag coefficient
z	The height
L	Obukhov length
a	Wave amplitude
T	Wave period
c	Wave speed
U	Velocity vector
f_{ϵ_G}	Body force
F_L	Lift force
F_D	Drag force
e_L	Unit vectors in the direction of the lift
e_D	Unit vectors in the direction of the drag
Re	Reynolds number
r	Distance between the CFD cell center and the actuator section point
c_{chord}	Turbine rotor blade chord length (in the papers c is used)
k	Turbulent kinetic energy
u_i'	Fluctuating part of the velocity vector U
$C_{\varepsilon 1}$	Model constant in the k-ε model
$C_{\varepsilon 2}$	Model constant in the k-ε model
C_μ	Model constant in the k-ε model
Cs	Model constant in the Smagorinsky subgrid-scale turbulence model
S_{ij}	Filtered deformation rate
S'_{ij}	Fluctuating deformation rate

Greek symbols

δ_{ij}	Kronecker delta, if i≠j δ=0, if i=j δ=1
θ_v	Mean virtual potential temperature
μ_t	Turbulent eddy viscosity
σ_k	Model constant in the k-ε model
σ_ε	Model constant in the k-ε model
Φ_m	Non-dimensional function
ψ_m	Non dimensional function, an empirical relation
A	Charnock parameter (in the Papers α is used)
α	Angle of attack
Δ	Filter width related to the grid cell size
ε_G	Gaussian width element (in the papers ε is used)
ε	Turbulent dissipation of kinetic energy
ξ	Sea surface elevation (in the papers η is used)
η_{ϵ_G}	Regulation kernel
κ	von Kármán's constant (in the papers k is used)
λ	Wave length (in the papers L is used)
μ	Dynamic viscosity of the air
ν	Viscosity of the air
τ	Surface stress, force per unit area exerted by the ground surface
χ_{10}	Wave age parameter

List of appended papers

Paper 1 Kalvig, S., Gudmestad, O.T. and Winther, N. (2013) 'Exploring the gap between 'best knowledge' and 'best practice' in boundary layer meteorology for offshore wind energy'. *Wind Energy*, 17: 161–171. doi: 10.1002/we.1572

Paper 2 Kalvig. S., Manger, E. and Kverneland, R. (2013) 'A method for wave driven wind simulations with CFD', *Energy Procedia*, vol. 35, pages 148-156, ISSN 1876-6102, http://dx.doi.org/10.1016/j.egypro.2013.07.168.

Paper 3 Kalvig, S., Manger, E. and Hjertager, B. (2014) 'Comparing different CFD wind turbine modelling approaches with wind tunnel measurements', *Journal of Physics, Conference series.* 555.

Paper 4 Kalvig, S., Churchfield, M., Manger, E. and Hjertager, B. (In review), 'URANS versus LES based simulations of wind turbine performance and wakes - comparison with wind tunnel measurements', *Journal of Renewable and Sustainable Energy (JRSE), AIP.*

Paper 5 Kalvig, S., Manger, E., Hjertager, B. and Jakobsen, J.B. (2014) 'Wave influenced wind and the effect on offshore wind turbine performance', *Energy Procedia,* Volume 53, 2014, Pages 202-213, ISSN 1876-6102, http://dx.doi.org/10.1016/j.egypro.2014.07.229.

Paper 6 Kalvig, S., Eliassen, L. and Manger, E. (In review), 'On offshore wind turbine fatigue caused by wave influenced wind', 2nd Symposium on OpenFOAM in Wind Energy, May 2014, Boulder, Colorado, USA. *E3S Web of Conferences*

Part I – Thesis summary

1 Introduction

Imagine thousands of meters of swirling air masses above your head. Hot and cold air mixes, rises and falls. The air masses move quickly, sometimes at over 100 km per hour. They are never steady, but always gusty and turbulent. Below, you have the dense, slower moving water. The ocean surface is seldom calm and level, but constantly oscillating, sometimes with waves over twenty meters high. In this restless zone, where the air stirs up the ocean surface and where the ocean alters the air above, we are building thousands of wind turbines. In the transition between these two fluids, the ever-changing sea and the fast blowing air, there is a tremendous energy potential that can solve large parts of the world's energy demand in a clean and affordable way.

The boundary layer between these two fluids - water and air - is quite challenging to understand, describe and not least, to model. The Marine Atmospheric Boundary Layer (MABL) is the part of the troposphere that directly 'feels' the ocean surface. Offshore wind parks operate in the MABL and the dynamics in this layer impose constraints, as well as possibilities, for offshore wind energy.

Over 2000 European wind turbines (EWEA[a], 2014) are now transferring the wind energy over the ocean into electric power. The installation of wind turbines in the ocean has just begun. The first semi offshore wind park started up off the coast of Denmark at a pier near Ebeltoft. This was in 1985 and the park consisted of 16 units of 55 kW. In 1991, Vindeby wind park was erected and with that the first real offshore wind park in the world. In 2009, Horns Rev 2 was officially declared the largest offshore wind park with its 91 units of 2 MW turbines. In 2013, London Array in the UK became operational. This wind park has in total 175 wind turbines and can produce 630 MW. This is now the world's largest wind park (London Array, 2014). While Denmark, the UK and Germany are leading players for bottom fixed offshore wind turbines, Norway can be proud of housing the world's first full-scale floating offshore wind turbine. Statoil's Hywind is located 10 km west of Karmøy. The test turbine has generated 32.5 GWh since it became operational in 2010. The next step for Statoil is to develop pilot parks based on the floating Hywind concept (Statoil, 2012).

From the start in Vindeby in 1991, to London Arrey in 2014 – a lot of technological development has been undertaking. Nevertheless, compared with

the land based wind energy industry, the offshore wind industry is a new field with new technological barriers.

Moving wind energy from onshore to offshore and to deeper waters with increasing turbine sizes, introduces new challenges. The harsh climate represents several technological barriers and the construction, installation and maintenance part is significantly more expensive offshore than onshore. On the other hand, the wind resources are better, and offshore wind parks have much smaller negative impacts on aesthetics of the landscape compared to onshore wind parks. There will be vast investments in offshore wind technology in the near future, and the industry is now the fastest growing power sector in Europe. It is estimated to increase to 64% by 2020 compared to 2013 figures (EWEA[b], 2014).

Accurate knowledge and modelling of the MABL are essential during the whole life cycle of an offshore wind park; from the earliest project plans on the drawing table, to the point where all the turbines are erected and in operation. The different stages during the life cycle require different information about the MABL: not only meteorological information, but also oceanographic information. In the first phase – the financial decision and site selection – the wind resource potential will be estimated based on either observational records, or by running meteorological and oceanographic models (MetOcean models) in a historical mode, hindcasts. In this initial phase, the applied technology will be chosen. Again, this is based on anticipation of representative and extreme MetOcean conditions. Representative wind profiles for the current site, and extreme turbulence levels as well as wave heights are important inputs for the design choices. The operation and maintenance stages require operational, high quality day to day (or hour by hour) MetOcean forecasts. The Offshore wind energy is hence a large ‘consumer’ of high quality MetOcean information and with the growing offshore wind energy new focus and resources have been put into MABL research. This will not only benefit the offshore wind industry but all industries operating offshore.

This PhD work contributes to understanding the processes in the MABL. More specifically, it will examine how the waves influence the wind and thereby affect offshore wind turbines. The direct effect of the waves on the offshore wind turbine structures has been ignored. The focus has rather been on the indirect effect of waves on the wind profile and turbulent intensity in the rotor swept area. Up until now, this is an effect few have studied.

1.2 Motivation and research question

When starting on this PhD in 2009 a ‘saying’ in the industry was; “the offshore wind industry takes ‘old’ technology over land, and expect it to work over sea”. This oral assertion is perhaps hard to validate, but it motivated the starting point of this work. If one could find out whether or not the differences between boundary layer meteorology over land versus that over sea were taken into account in the governing standards, it could perhaps shed light on the oral statement regarding onshore technology being used offshore. Therefore, a parallel investigation on the governing offshore wind energy standards, combined with a literature study of boundary layer meteorology related issues, was conducted. The governing standards should represent the best practice for an industry, whereas the research literature should represent the best knowledge. If a clear gap was found between best practice and best knowledge, this could then indicate that there was some accuracy in the above statement. The first task in this PhD work (the literature review) resulted in the formulation of the research question as well as the appended Paper 1.

Will wave influenced wind at an offshore wind site result in different wind shear and more turbulence than expected? And if so, how will this affect the turbines?

While working with the literature review and Paper 1, it became clear that this PhD work would span over two large scientific disciplines: wind turbine engineering and boundary layer meteorology. In order to seek an answer to the research question, it became necessary to look into both disciplines. Thus, this thesis can be seen as quite cross-disciplinary.

Wave measurements, wind and turbulence profiles, and turbine wake and performance measurements from an operating offshore wind park, all recorded simultaneously, would be the ideal data set to study in order to answer the research question. Unfortunately, offshore field measurements are very sparse and to my knowledge data sets such as these do not exist in an openly available way. Instead, this PhD work relies heavily on computational fluid dynamics (CFD) modelling. The research question calls for understanding and modelling of both the MABL and wind turbines.

1.3 Thesis structure

The structural outline of this PhD work is visualized in Figure 1. The outline can be seen as a road towards an answer to the research question. The starting point leads into two paths that will later be combined. The appended papers represent milestones along this road and are indicated with numbers in Figure 1.

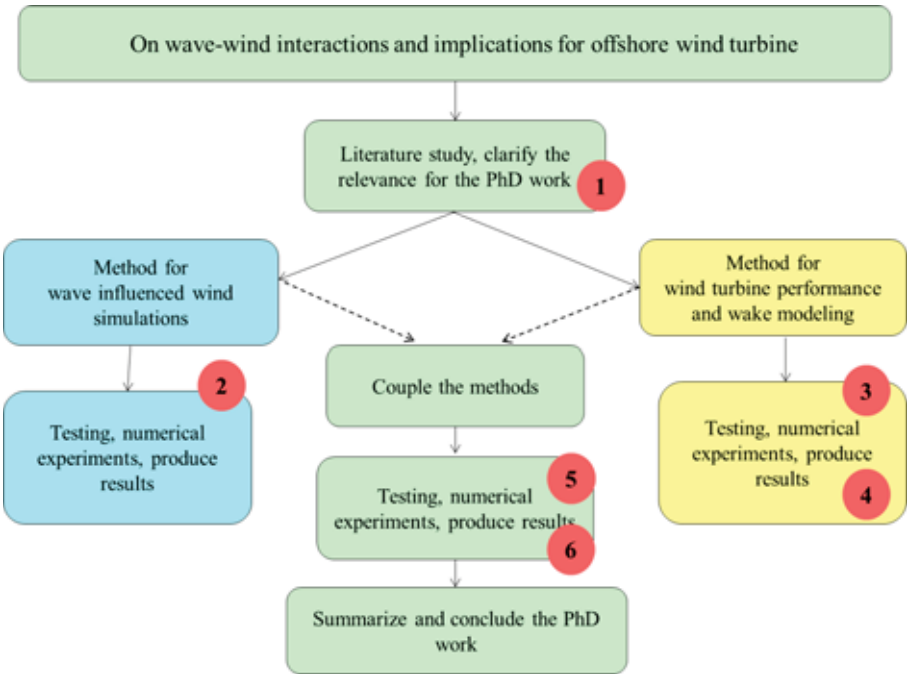

Figure 1: Structure of the PhD work. Red dots, with numbers, refers to paper numbering. Placement of dots indicates area of research.

One path targets wave influenced wind modelling, whilst the other targets wind turbine performance and wake modelling. The wave influenced wind modelling part represented new development, and model testing was challenging. The results have not been directly compared with measurements. Instead, testing of different inflow conditions and wave states was conducted and to some extent compared with the literature, even though it was difficult to find comparable results that were based on the same modelling approaches. The wind turbine modelling path was based on pre-existing methods for wind turbine modelling. Here, testing was more feasible because wind tunnel data was available.

The method chosen for the wave influenced wind simulations (Paper 2) defined some restrictions for the wind turbine modelling, since the work was aimed at directly coupling wave simulations with wind turbine modelling. One restriction was that the method should be based on the Reynolds Averaged Navier-Stokes (RANS) approach. In addition, it should be able to handle a moving computational mesh as well as be executed in transient mode. The wind tunnel blind test project, undertaken by the Norwegian Centre for Offshore Wind Energy (NORCOWE) and the Norwegian Research Center for Offshore Wind Technology (NOWITECH), was started in 2011 at the Norwegian University of Science and Technology (NTNU). StormGeo/University of Stavanger participated with a simplified wind turbine wake model, the actuator disk model. Acona Flow Technology participated with a fully resolved method (Krogstad & Eriksen, 2013). Just after participation in the first blind test experiment, it was discovered that National Renewable Energy Laboratory (NREL) in the United States was working with actuator line for their open source Simulator fOr Wind Farm Applications (SOWFA). This included an actuator line model set up. Based on the work done for the blind test and new work performed with the actuator line method, Paper 3 was published. This paper contains a comparison of the three very distinct methods – all based on RANS compared with the measurements from the blind test wind tunnel experiment.

SOWFA was at this point only used in combination with Large Eddy Simulations (LES), and it was appealing to investigate if unsteady RANS could serve as a substitute to LES. Since it was necessary to resolve the waves in the coming combined modelling approach of wave influenced wind with a full-scale wind turbine representation, it would not have been computationally feasible to use LES. This work resulted in Paper 4.

After a separate investigation of wave influenced wind modelling and wind turbine modelling, the work combining these two modelling methods started. This work was challenging because there was a need for simulation on realistic scales. When including a full-scale wind turbine in the wave simulation domain, two-dimensional calculations were not possible. Even if the computations were parallelized, every scenario took several days to calculate and post processing quickly filled up the available disk space. Paper 5 and 6 are based on the coupled set up.

In the next chapters, theoretical background and numerical methods for the problem studied are presented in a very compact form. Note that in the title of

Paper 2 the words ‘wave driven’ were used. Later I became aware that ‘wave influenced’ is probably a better term, since the wave only influences the wind; it is not the main driver of the wind. Hence, the term ‘wave influenced’ is, except in Papers 1 and 2, used throughout this PhD. The first paper was published in Wiley Wind Energy under Broader Perspectives. This paper represents much of the background and state of the art, and I would recommend reading this as part of the introduction.

2 Wave wind interactions

The wind whips up the ocean surface and creates waves. This is the most visual form of energy transfer, but the atmosphere and the ocean interplay with each other in various ways. Air and water are both fluids and their dynamics can be described with the same physics. As in the ocean, there are waves in the air. They are invisible except from time to time when cloud formation turns parts of the airborne waves visible. The fast blowing wind and slow flowing ocean currents transport the air and water masses. When two distinct masses meet, fronts are formed. Fronts also exist in the oceans, even though they are not as familiar to people as the cold and warm fronts from TV weather maps. Cyclones or storms stir the atmosphere, and similarly there are storm-like structures in the sea known as eddies. In other words, there exists an ocean of air where the fishes are birds and vice versa!

The main difference between air and water is the large difference in density. At the ocean level, the density of the air is approximately 800 times less that of the ocean water. This density difference determines the speed and length scale of the energy transport, as the density can be seen as the ‘carrier’ of both momentum and heat. A storm in the North Sea lasts only a couple of days whereas a meso-scale eddy in the ocean can last from a few days to several months.

The mismatch in time and length scales between the air and ocean are challenging when trying to model the air-sea interaction. Nevertheless, great improvements have been made in the area of regional air-sea coupled models. Peng et al. (2012) have given an extensive review on the topic. They report that some of the critical problems imperative to be solved in air-sea modelling are the variation of the sea surface roughness caused by waves and the feedback to the lower boundary of the atmosphere.

2.1 Sea surface roughness

It takes a relatively long time before the wind manages to build up waves. A wind of 15 m/s is capable of raising a sea to four meters of significant wave height after 12 hours, and to five meters height after 24 hours (WMO, 1998). These locally generated waves are called wind waves. When such waves travel far from their place of origin into other areas of interest, they are called swell.

Locally generated wind sea consists of several different waves with different length, speed and amplitude. They superpose on each other and the result can be quite a confused looking sea surface. Longer waves travel faster than waves with shorter wave lengths and during the time of travelling there will be a systematic sorting of the waves. The faster waves travel away from the shorter waves which again makes the swell look different from the wind waves. Swells are smoother, with longer wave periods compared to wind waves. Wind waves can be considered young sea, whereas swell is characterized as old sea. The sea state is a mixture of different wind waves and swell. In order to characterize a sea state in relation to the local wind, it is useful to define a wave age parameter, χ_{10}. The wave age is the ratio between the phase speed of the peak of the wave spectrum (c_p) and the wind speed at 10 m (U_{10}):

$$\chi_{10} = \frac{c_p}{(U_{10} cos\theta)}, \quad (1)$$

where θ is the angle between the wave field and the wind field. A wind driven wave regime is characterized by $\chi_{10} < 1.2$ and a swell dominated wave field by $\chi_{10} > 1.2$ (Edson et al., 2007). In the open ocean, young wind waves are steeper and can often be higher than old sea or swell. Therefore, young wind waves generally represent a rougher sea surface than the older swells (Janssen, 2004). This sea state dependent roughness can be captured in the Charnock relation (Charnock, 1955), which expresses the dependence of the roughness length, z_0, on the surface stress, or friction velocity u_*, as

$$z_0 = \frac{A\, u_*^2}{g}, \quad (2)$$

where g is the acceleration due to gravity and A the sea state dependent Charnock parameter. The surface stress is the force per unit area exerted by the ground surface on the flow (Stull, 1988) given as

$$\tau = {u_*}^2 \rho, \quad (3)$$

where ρ is the density of the air. The total wind stress over a surface can be parameterized as

$$\tau = \rho C_D U^2, \quad (4)$$

where U is the wind speed and C_D is the surface drag coefficient at the same height. A good parameterization of the wind stress is very important in

atmospheric modelling and forms an important basis for both forecasts and hindcast. The Charnock relation is thus essential in coupled ocean and atmospheric forecasting models.

At The European Centre for Medium Range Forecast (ECMWF) the Charnock relation is used in their global operational coupled set up for wave and wind forecasts (ECMWF, 2006). Global forecast models can be nested with a regional model with better resolution than e.g. the ECMWF model. Such a model is the Weather Research and Forecasting (WRF) model. This model is increasingly being used in the field of wind energy. It is an open source code, which can be tuned and tailored in order to provide the wind energy industry with specialised services and high quality forecasts. NORCOWE and StormGeo both strive to couple WRF with regional wave models. Jenkins et al. (2012) have coupled WRF to the WAM wave model (Wambi Group, 1988) and Winther and Lisæter (2011) use the Simulating Waves Nearshore (SWAN) model (Booij et al. 1999) in their coupling work. Both projects are ongoing and preliminary results show improvements in forecast quality for the coupled system compared to the non-coupled systems (Krogsæter 2013, Jenkins et al. 2012).

In the coupled set up of Jenkins et al. the air-to-sea momentum flux associated with wave generation, as well as the total momentum flux and the friction velocity, are fed back into the atmospheric model. In the coupled set up of Winther and Lisæter, the Charnock parameter is expressed in terms of the inversed wave age. Practically speaking, this means that the roughness of the sea will change according to how much wind waves or swell are present. It will, however, not capture the effect the direction of the swell is known to have on the surface drag. When a swell is propagating aligned with, and faster than, the wind, the surface drag has been observed to be reduced (Drennan et al. 1999, Smedman et al. 1999). If a swell opposes the wind, the drag is increased (Doneland et al. 1997, Ocampo-Torres et al. 2011).

2.2 Wind profiles over the sea

As well as modifying the surface drag on the wind above, swells are also known for influencing the logarithmic wind profile shape. When a swell is propagating faster than the wind, a near surface wave driven wind increase is observed (Smedman et al. 1999, Drennan et al. 2005). When this near surface jet is present, the wind profile will no longer have a logarithmic shape. Since swells are waves that have travelled away from the generating storm, they can

travel into a wind park area and completely oppose the local wind field in the park. There exists few wind profile observations from swell opposing the wind, but it has been reported from several researchers that the drag from the sea surface increases in these situations (Doneland et al., 1997 and Ocampo-Torres et al., 2011). Measurement campaigns often focus on the overall sea surface drag, since this parameter is usually used in atmospheric forecast models and in coupled atmospheric and wave models, as well as in climate models. However, the shape of the wind profile is very important for wind turbine performance (Christakosa et al., 2013). Offshore wind turbines with large rotor sizes will have the lowest turbine blade positioned close to the sea surface, while the upper rotorblade extends over the surface layer into area where in fact the usual parameterization of the wind profile is no longer valid (Gryning, et al. 2007). It is important to investigate how waves will affect the wind shear in the swept area of the wind turbine rotor.

Monin-Obukhov (MO) similarity theory (Monin & Obukhov, 1954) is widely used within boundary layer meteorology, as well as in wind engineering and in the field of wind energy. This theory is applicable to the surface layer, which is the layer close to the surface where the fluxes vary less than 10% with the height (Stull, 1988). In the surface layer, MO assumes that the mean flow and the turbulence characteristics can be described only by the friction velocity, buoyancy flux and the height. The wind shear can then be expressed with a non-dimensional function, Φ_m, which scales with the atmospheric stability (Monin & Obukhov, 1954) as,

$$\frac{\partial U}{\partial z}\frac{\kappa z}{u_*} = \Phi_m(\frac{z}{L}), \tag{5}$$

where $\kappa = 0.4$ is the von Kármán's constant, z is the height and L is the Obukhov length. The Obukhov length is a scaling parameter and it expresses the relation between mechanical or shear turbulent production and buoyant turbulent production (Stull, 1988),

$$L = -\frac{\theta_v u_*^3}{\kappa g \overline{(w'\theta_v')_s}}, \tag{6}$$

where θ_v and θ_v' are the mean virtual potential temperature and the corresponding fluctuating component, respectively, and w' is the fluctuating component of the vertical wind. The integration of Equation (6) gives the following empirical expression for the surface layer wind profile (Foken, 2006)

$$U(z) = \frac{u_*}{\kappa}\left[ln\left(\frac{z}{z_0}\right) - \psi_m\left(\frac{z}{L}\right)\right], \quad (7)$$

where ψ_m is a non-dimensional function that is related to atmospheric stability. Both Φ_m and ψ_m are empirical relations and have been estimated from various field experiments (Högström, 1988). The sign of the ratio Obukhov length to height, z/L, is used to classify the atmospheric stability. A positive ratio corresponds to stable atmospheric stratification, and a negative ratio corresponds to unstable stratification. For near neutral condition z/L=0, and equation (7) is reduced to the well-used logarithmic wind profile,

$$U(z) = \left(\frac{u_*}{\kappa}\right) ln\left(\frac{z}{z_0}\right), \quad (8)$$

The logarithmic wind profile is widely used in offshore wind energy, even if the conditions are not neutral, if the sea surface is not stationary and even if parts of the turbine operate above the surface layer, where MO theory is no longer valid! In Paper 1, a brief review is given of how sea surface roughness and the wind profile are approximated in the governing standards in offshore wind energy.

There is a lack of information and knowledge of what happens in the lowest meters of the MABL with respect to the wind profile and the turbulence levels with changing sea states. The current parameterizations, based on the Charnock relation and modified drag coefficients, will not take into consideration that the direction of the waves relative to the wind is important. Larger wind turbines are now being built, and these are sensitive to the shape of the wind profile and turbulence levels in the rotor swept area. Therefore, the influence from the waves to the wind in the lowest 100 m of the atmosphere is of great importance. To study flow on this scale, CFD is suitable.

2.3 Numerical wave simulations

To model the effect of waves on the wind flow there was a need for a method that could resolve the individual waves, including the direction of the waves relative to the wind. For this purpose, CFD with a moving grid approach was chosen.

For both mesh generation and computations the open source CFD toolbox OpenFOAM (OpenFOAM, 2014) is used. The development commenced using a transient turbulent solver that could handle deforming mesh

(pimpleDyMFoam). With the help of both OpenCFD[1] and Acona Flow Technology, a new solver that models flow above a moving wave surface was developed. A turbine model was later integrated with the new solver and the combined set up was given the name Wave influenced Wind Turbine Simulations (WIWiTS). In this section, a brief description of the wave simulation part of WIWiTS will be given. For numerical turbine modelling, as well as turbulence modelling, reference is made to Chapter 3.

By using a moving mesh approach, several sinusoidal waves can be superposed on each other and implemented as a boundary condition on a patch in the CFD domain. The wavy boundary condition then writes:

$$\boldsymbol{\xi}(x,t) = a\left\{\boldsymbol{a_n}\, sin\left(2\pi(\frac{x-ct}{\lambda})\right) + \boldsymbol{w_n}\, cos\left(2\pi(\frac{x-ct}{\lambda})\right)\right\}, \quad (9)$$

where $\boldsymbol{\xi}$is the total wave surface displacement, $\boldsymbol{a_n}$ is a unit vector with a vertical direction (along the amplitude), $\boldsymbol{w_n}$ is a unit vector with a horizontal direction (along the wave direction), x is the horizontal position at a given time t, a is the wave amplitude, λ is the wavelength and c is the wave speed. In deep water the wave water particles moves in a circular pattern. The wave particles, here thought of as grid cells, sweep out a circle with a diameter equal the wave height as illustrated in Fig.2. The different grid cells will have different positions in different time increments according to a harmonic function. The numerical simulations performed for Paper 2 had only the first term in Eq. 9 implemented. Then each grid cell moved only in the vertical, up and down. Later, for the work with Paper 5 and 6, the horizontal movement represented with the last term of Eq. 9 was implemented and as a sum, the vertical movement and the horizontal movement are now prescribing circles for every grid cell. Testing with and without the horizontal wave movement was performed. The effect of the horizontal movement does not play a significant role on the type of waves that are the focus for this work – relatively long waves. Figure 3 shows difference in wind profiles with and without the horizontal wave motion for a wave with wave length of 56 meters and amplitude of 2 meters.

No deformation due to the wind force is allowed as the moving wave is seen as a solid wall. The investigations performed were mainly done with only one harmonic wave, but for demonstration purposes some tests with multiple waves

[1] OpenCFD Ltd is owned by ESI-OpenCFD and they produce the OpenFOAM® open source CFD toolbox and distribute it through the OpenFOAM Foundation.

were also carried out. Examples of the mesh over two different wave states can be seen in Figure 4.

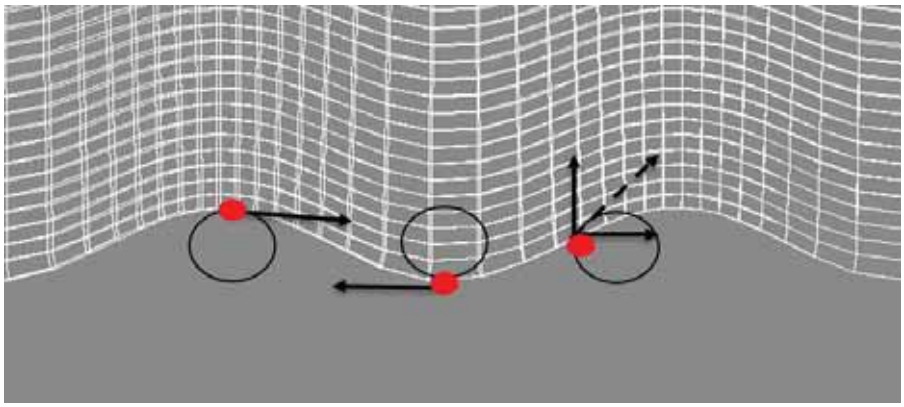

Figure 2: Illustration of grid cell movements. As for an real ocean waves each water particle (or grid cells) prescribing a circular movement.

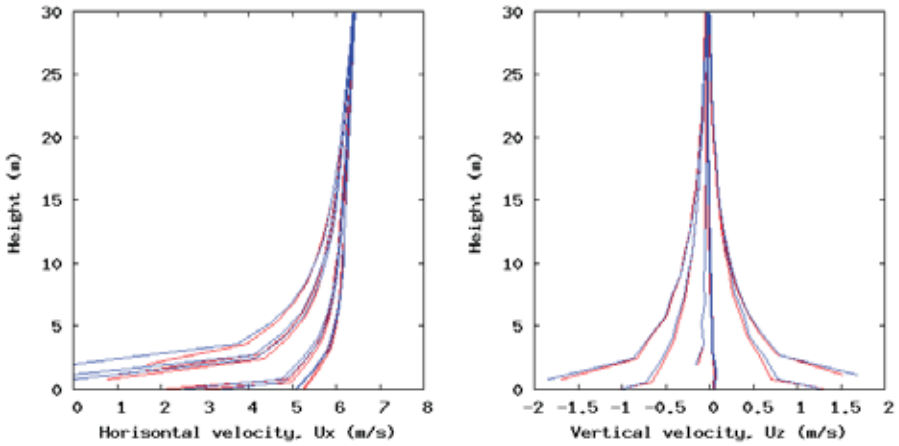

Figure 3: Wind profiles over a wave sampled over approximately a whole wavelength. Red lines are with circular grid cell movements and blue lines are with only vertical wave movements. Left: horizontal wind velocity Ux (m/s), Right: vertical wind velocity, Uz (m/s).

The mesh in the wave simulations domain consists of regular hexahedral cells and is refined close to the wave surface. Different refinements were tested, but most of the simulations performed, had gradually refined mesh where the

grid cells close to the wave surface were three times as small as those at the top of the domain.

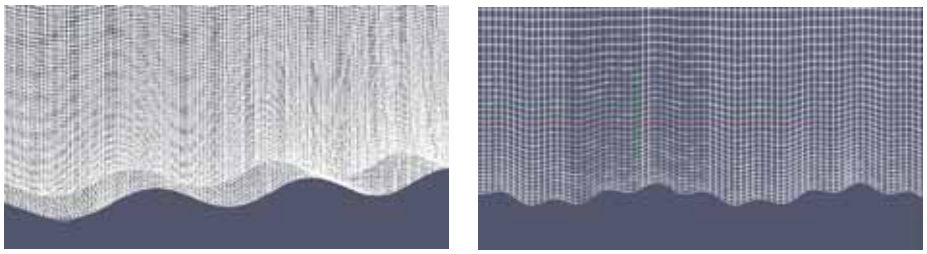

Figure 4: Illustration of the mesh over the wave surface. A single sinusoidal wave (left) and superposition of one wave with λ =100 m and a=4m, and one with λ =25 m and a=2 m length, travelling against each other (right).

Wave speed, wave amplitude and wavelength are input parameters to the wave generating model. The wave will gradually grow during the first seconds of simulations. The wave will also gradually develop some meters after the inlet and fade out some meters before the outlet. This gradually developing wave, both in time and space, was implemented in order to ensure that the inlet and outlet grid part of the domain did not change form and also to ensure stable simulations. Normally the first 10 seconds was used for this gradual time development, and the first and the last 10 meters of the domain for the gradually growing wave. This is input values to the model set up that can be changed according to simulations time, wave states and domain sizes.

The starting points of these CFD simulations are the Navier-Stokes equations and the continuity equation for an incompressible, Newtonian fluid. These can be expressed as (Veersteg & Malalasekera, 2007),

$$\rho\left(\frac{\partial \boldsymbol{U}}{\partial t} + \boldsymbol{U}\cdot\nabla\boldsymbol{U}\right) = -\nabla p + \mu\nabla^2\boldsymbol{U} \tag{10}$$

$$\nabla U = 0, \tag{11}$$

where **U** is the velocity vector, p is the pressure and μ is the dynamic viscosity. The simulations are only valid for a neutrally stratified atmosphere where no buoyancy effects are present. The Coriolis force is also neglected. Reynolds Averaging is used on the Navier-Stokes equation, and for turbulent closure the standard k-ε model (Launder & Spalding, 1974) is used. The turbulence modelling will be described in Chapter 3.2. Since this is a time dependent or transient problem unsteady RANS, denoted URANS, will be used.

Tests of the wave simulations were done using a two dimensional set up with and without cyclic boundary conditions for the inlet and outlet parts. Figure 3 to 5 illustrate some examples of flow responses for a wave propagating along with and against the wind. The flow response is clearly different in the two cases. Results from wave influenced wind simulations are presented in Papers 2, 5 and 6.

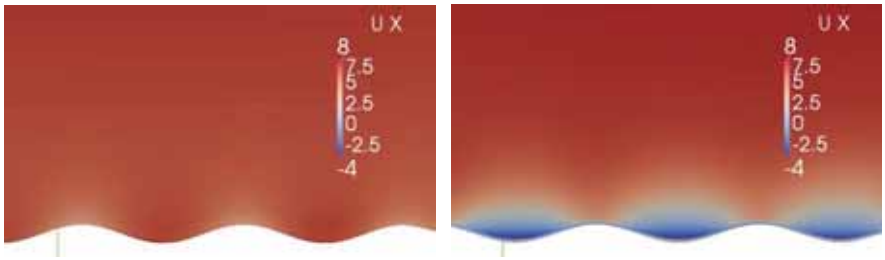

Figure 3

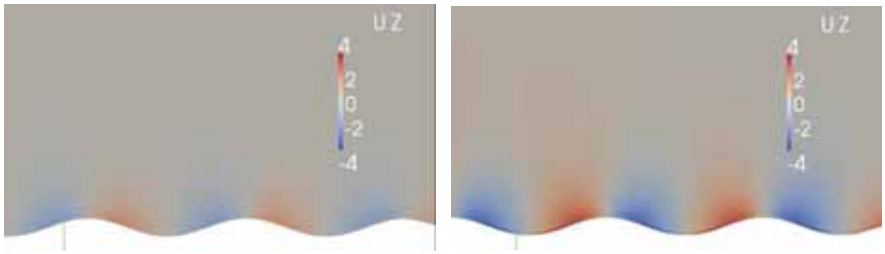

Figure 4

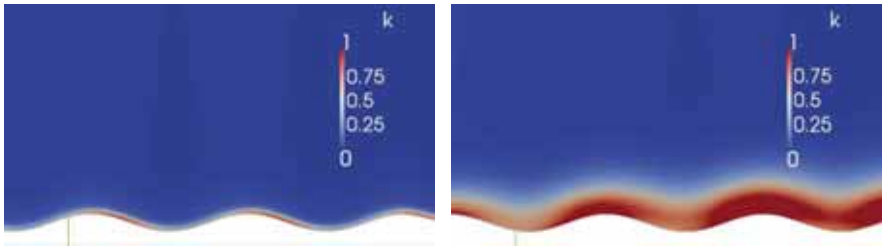

Figure 3-5: The horizontal component of the wind speed, m/s, (Figure 3), the vertical component of the wind speed, m/s, (Figure 4) and the turbulent kinetic energy, m^2/s^2 (Figure 5) over a wave (a=4 m, λ =70 m and c=10.5 m/s) aligned with the wind (left) and opposing the wind (right). The inlet wind speed is a logarithmic wind profile with 8 m/s in 400 m. The inlet turbulent kinetic energy was uniformly distributed with 0.5 m^2/s^2. The domain size was 450 m x 400 m, only a close up is shown her.

The crudest simplification in this wave influenced wind simulation method, is to look at the wave as a solid oscillating wall not allowing any influence from the wind onto the wave. In reality there is of course a constant interplay between the air and the sea surface. Nevertheless, for studying situations with calm wind and significant swell, the assumption is believed to be valid. Interestingly, those situations are also the ones that are observed to create intriguing flow responses. As stated in Chapter 2.1 and 2.2, swells will affect the wind profiles and the turbulence levels, and this results in different surface drag than the common parameterization used today implies.

3 Offshore wind turbines

Windmills or wind turbines – one could perhaps use these words interchangeably. Historically, wind energy was used to pump water or grind oats, amongst other things. There are records of windmills in Persia from the year 950 and in Normandy and England from 1180 (Baker, 2007). For modern ways of converting the energy in the wind into useful energy or electricity, the terminology wind turbine seems most appropriate. Wind turbines can be categorized in two ways: vertical axis turbines and horizontal axis turbines (Figure 6). The principal mechanism for converting the kinetic energy of the wind into electrical energy for the two different turbine types is the same. Using turbine blades, the energy in the wind is transferred into mechanical energy and converted to electrical energy via a generator. In offshore applications, wind turbines have mainly been horizontal axis turbines. Only horizontal wind turbine models have been used for this thesis work. For offshore energy, turbines can further be categorized into floating turbines and bottom fixed turbines. The large growth in offshore wind energy has so far been realized with bottom fixed turbines. Floating offshore wind parks, however, will soon be a reality as several players are in the phase of planning pilot parks in deep water (EWEA[c], 2013). In this thesis, the work has been limited to bottom fixed horizontal axis turbines, but the work with wave influenced wind will be interesting for other types of turbines. The method used here can be transferred with relative ease to vertical axis turbines and possible also for floating concepts.

Numerical modelling of a wind park or a single turbine is useful in various stages of the whole life cycle of a park. The different modelling approaches are determined by the intended use of the model. An operational set up designed to model the wind park's electricity production on a daily basis requires a different modelling approach and level of detail, than, for instance, design optimization for a specific airfoil. Since the objective of this research is to investigate if wave influenced wind affects the wind turbine, a turbine model that could provide information about the turbine wake, as well as forces along individual turbine rotor blades, was chosen. The actuator line model is such a model.

Figure 6: Two floating wind turbine concepts developed in Norway, Statoil's horizontal axis turbine, Hywind, photo: Lene Eliassen (left) and Gwind's vertical axis turbine, Spinwind, photo: Simen Malmin (right).

3.1 Actuator line method and SOWFA

The concept of the actuator line model is to consider the wind turbine rotor blades as span-wise sections with airfoil characteristics. In the actuator line methodology of Sørensen & Shen (2002), blade loading is implemented in these span-wise sections and introduced in the Navier-Stokes equations as a body force:

$$\rho\left(\frac{\partial \boldsymbol{U}}{\partial t} + \boldsymbol{U}\cdot\nabla\boldsymbol{U}\right) = -\nabla p + \mu\nabla^2\boldsymbol{U} + \boldsymbol{f}_{\epsilon_G}. \tag{12}$$

The body force $\boldsymbol{f}_{\epsilon_G}$ originates from the sum of lift and drag force (F_L, F_D) per unit span-wise section (dr),

$$\frac{d\boldsymbol{F_L}}{dr} = \frac{1}{2}\rho {U_{rel}}^2 c_{chord} C_L \boldsymbol{e}_L, \tag{13}$$

$$\frac{d\boldsymbol{F_D}}{dr} = \frac{1}{2}\rho {U_{rel}}^2 c_{chord} C_D \boldsymbol{e}_D, \tag{14}$$

where C_L and C_D are the lift and drag coefficients, c_{chord} is the chord length and $\mathbf{e}_L$and $\mathbf{e}_D$ denote unit vectors in the direction of the lift and drag. The lift and drag coefficients are dependent on the angle of attack (α) and the local Reynolds number (Re). These coefficients can be determined from measurements or from an airfoil development system such as, the freeware XFOIL (XFOIL, 2014), which has been used in this thesis. The lift and drag forces are calculated for each section and they need to be distributed smoothly around the whole span-wise section that resembles the rotor blade. This smoothing is done by the use of a regulation kernel η_ϵ and a Gaussian distribution function,

$$\eta_{\epsilon_G}(r) = \frac{F_i^A}{{\varepsilon_G}^3 \pi^{3/2}} exp\left[-\left(\frac{r}{\varepsilon_G}\right)^2\right], \tag{15}$$

where r is the distance between the CFD cell center and the actuator section point, and ε_G is the Gaussian width element. Then the convolution of the computed local load gives the force field, f_ϵ, projected as a body force onto the CFD grid;

$$f_{\epsilon_G} = f \otimes \eta_{\epsilon_G}, \tag{16}$$

Figure 7 illustrates the basic concept of the method. More details about the method can be found in Sørensen & Shen (2002). It is important to highlight that the actuator line simulations are sensitive to the size of the Gaussian width element.

The size of the Gaussian width element has been discussed, among others, in Shives & Crawford (2012), Troldborg (2008), Martinez et al. (2012) and Nodeland (2013). In the work with papers 3 and 4, a fitting procedure has been used in order to establish an appropriate Gaussian width element. For the work with the small scale turbine, in the wind tunnel blind test of NOWITECH and NORCOWE (Krogstad et al. 2011), this fitting procedure resulted in a Gaussian width element of approximately the same size as the length of the smallest grid cell (0.02 m). This is in contrast to the findings of Troldborg (2008) who recommended that the Gaussian width element should be at least twice the length of the smallest local grid cell. Nodeland (2013) did extensive testing of the actuator line model in her Master's thesis and recommended that the Gaussian width element should be $\epsilon_G = c_{chord}/4.3$. Our fitting procedure produced a Gaussian width element smaller than this ratio. The fitting procedure used is described in Paper 3. Up to now there is no solid generic way to establish the Gaussian width element and more investigations should be devoted to this.

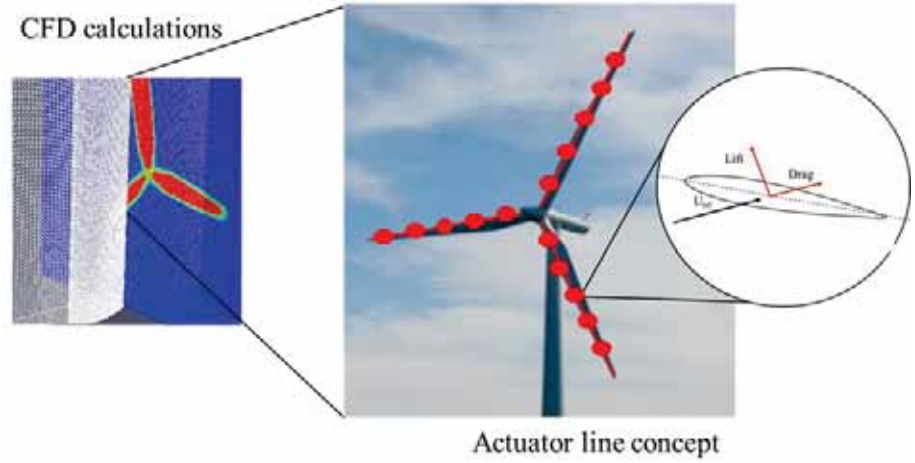

Figure 7: Illustration of the basic concept of actuator line CFD calculations. The lift and drag forces are calculated for each actuator line section and then distributed smoothly around the whole span-wise section that resembles the rotor blade. The force field is then projected as a body force onto the CFD grid.

Churchfield et al. (2012) has implemented the actuator line method in NREL's Simulator for Wind Farm Applications (SOWFA). SOWFA is a flexible open source tool that allows users to investigate wind turbine performance and wake development under different atmospheric conditions. SOWFA is based on the OpenFOAM tool box and has a dynamic two way coupling to FAST, an aero elastic code that can model the dynamic response of horizontal-axis wind turbines (Jonkman & Buhl, FAST User's Guide, NREL/EL-500-38230, 2005). It also consists of a 'precursor' simulator that creates a turbulent atmospheric boundary layer as an input to the wind turbine simulations. The FAST part of the SOWFA is used in Paper 6 and it is briefly introduced in Chapter 4.2.

Since a major goal in this work was to couple the actuator line model with the model for wave influenced wind, some modifications needed to be done to the original actuator line solver for SOWFA. Originally, SOWFA was set up for LES, but here a URANS approach has been utilized. The SOWFA-solver was also modified to include the new wave generating method (Chapter 2.3). These modifications resulted in the combined WIWiTS setup (Chapter 4.1). As turbulent closure, the standard k-ε model (Launder & Spalding, 1974) has been used. The turbulence model, will briefly be described in the next chapter.

3.2 Turbulence modelling

For more than a century turbulent flows have been studied and investigated, but it is still one of the great remaining fundamental challenges to scientists. In the attempts to describe turbulence, it always turns out to be more unknowns than equations. Consequently, the theory of turbulence relies on crude assumptions and modelling. Apparently, Albert Einstein once said, "Before I die, I hope someone will clarify quantum physics for me. After I die, I hope God will explain turbulence to me". With this in mind, the turbulence modelling part of this summary will be limited to a brief introduction of the two turbulence models that have been used in this work.

Turbulence modeling approaches in the field of CFD can be grouped into three: Turbulence models for Reynolds-averaged Navier-Stokes (RANS) equations, large eddy simulations (LES) and direct numerical simulations (DNS). The most computationally intensive of these approaches is DNS, as it resolves the turbulence on all scales. In LES, only the larger turbulent eddies are solved, but it is still computationally demanding. RANS, on the other hand, strives to model the effect of the turbulence, making the modeling of turbulence more accessible to those who do not have sufficiently large computational resources.

In the RANS approach, Reynold averaging – or time averaging – is used on the Navier-Stokes equation (Eq. 10), hence the acronym RANS. The averaging introduces the following nonlinear term,

$$\tau_{ij} = -\rho\overline{u_i' u_j'}\,, \tag{17}$$

where $u_i' u_j'$ is the product of the fluctuating part of the velocity vector **U**. This term is known as the troublesome Reynold's stresses. These cannot be explicitly solved, and in order to close the system of equations there is a need for a turbulence model – or a turbulent closure model. The k-ε model is such a model, and it has become a very popular and widely used one. Important quantities here are the turbulent kinetic energy (k) and the turbulent dissipation of kinetic energy (ε), defined respectively as:

$$\mathrm{k} = \frac{1}{2}\left(\overline{u_i' u_i'}\right) \text{ and} \tag{18}$$

$$\varepsilon = 2\nu\,\overline{\mathrm{S'_{ij}} \cdot \mathrm{S'_{ij}}}\,, \tag{19}$$

where u_i' denotes the x-, y- and z-component of the fluctuation part of the velocity vector **U** (by the use of Einstein notation), ν is the viscosity and S'_{ij} is the fluctuating deformation rate (Veersteg & Malalasekera, 2007). The quantities that define k and ε are not directly solved, instead they are modelled and an important step in this process is the use of the Boussinesq relationship. Boussinesq postulated in 1877 that the Reynold's stresses are isotropic and proportional to the mean rate of deformation, hence:

$$\tau_{ij} = \mu_t \left(\frac{\partial U_i}{\partial x_j} + \frac{\partial U_j}{\partial x_i} \right) - \frac{2}{3} \rho k \delta_{ij}, \tag{20}$$

where $\mu_t$is the turbulent eddy viscosity given by,

$$\mu_t = \rho C_\mu \frac{k^2}{\varepsilon}. \tag{21}$$

Two additional equations are now established and need to be solved along with the RANS equations; the transport equation for k and the transport equation for ε. Hence this turbulent closure approach is categorized as a two equation model. There are also zero (mixing length model), one (Spalart-Allmaras model) and seven (Reynold's stress model) equation models, but this will not be addressed here. In the URANS simulations performed in this work the standard k-ε turbulence model of Launder & Spalding (1974) is used and the transport equations for k and ε reads,

$$\frac{\partial(\rho k)}{\partial t} + \mathrm{div}(\rho k \mathbf{U}) = \mathrm{div}\left(\frac{\mu_t}{\sigma_k} \mathrm{grad}\, k \right) + 2\mu_t S_{ij} \cdot S_{ij} - \rho \epsilon, \tag{22}$$

$$\frac{\partial(\rho \varepsilon)}{\partial t} + \mathrm{div}(\rho \varepsilon \mathbf{U}) = \mathrm{div}\left(\frac{\mu_t}{\sigma_\epsilon} \mathrm{grad}\, \varepsilon \right) + C_{\varepsilon 1} \frac{\varepsilon}{k} 2\mu_t S_{ij} \cdot S_{ij} - C_{\varepsilon 2} \rho \frac{\epsilon^2}{k}. \tag{23}$$

Now five model constants have been introduced and these constants are usually assigned the following values;

$$\sigma_k = 1.0, \sigma_\varepsilon = 1.3, C_{\varepsilon 1} = 1.44, C_{\varepsilon 2} = 1.92 \text{ and } C_\mu = 0.09\,. \tag{24}$$

It is worth mentioning that Richards & Hoxey (1993) and Hargreaves & Wright (2007) suggested that for simulations in the atmospheric surface layer these constants should be adjusted and in particular recommended that $C_{\varepsilon 1}$=1.11. Richard & Norris (2011) stated that by adjusting model constants one might move away from a general turbulence model and thus caution should be taken. Hence, in the simulations presented in Papers 2-6 the k-ε model constants have

the values referenced above except from $C_{\varepsilon 1}$=1.11. Furthermore, these values have been standardized as the default constant in some of the tutorials available from openCFD that are based on k-ε turbulence model (e.g. the tutorial turbineSiting).

In the LES approach, the larger energy-containing eddies are directly resolved, but the smaller more isotropic ones are modelled. In RANS or URANS, the turbulent length scales are not determined by the CFD-grid, but in LES this is the case. The spatial filtering process determines which eddies should be modelled with the LES momentum equations derived from the unsteady Navier-Stokes equations (Eq.10), and which eddies that should be regarded as unresolved and described with a subgrid-scale (SGS) model. A Lagrangian-averaged dynamic Smagorinsky subgrid-scale turbulence model is used in Paper 4 (Meneveau et al. 1996) which, like the k-ε model, relies upon the Boussinesq hypothesis. The SGS viscosity that goes into the Boussinesq hypothesis is given by

$$\nu_t = (C_s\Delta)^2(2S_{ij}S_{ij})^{1/2}, \tag{25}$$

where C_s is the model constant, the filter width Δ is related to the grid cell size (the cube root volume of each cell), and S_{ij} is the filtered deformation-rate tensor. In Paper 4 more details regarding the LES simulations is given.

Different CFD discretization schemes can produce quite different results for turbulence calculations due to numerical diffusion. Two different discretization schemes for the calculation of the divergence term in Equations 10 and 12 were tested for wind turbine wake modelling. The results were compared with measurements from the NORCOWE and NOWITCH wind tunnel experiment (Krogstad et al. 2011). Results using the first order bounded upwind scheme and, according to Minkowycz et al. (2000), the more accurate QUICK scheme (quadratic upwind interpolation for convective kinematics), were also compared with the LES results. The upwind scheme was found to be far too dissipative and smeared out nearly all the turbulence, whereas the QUICK scheme improved the results. Figure 8 shows wake simulations with LES and URANS with the two different discretization schemes. URANS with the upwind scheme looks more like the steady state RANS.

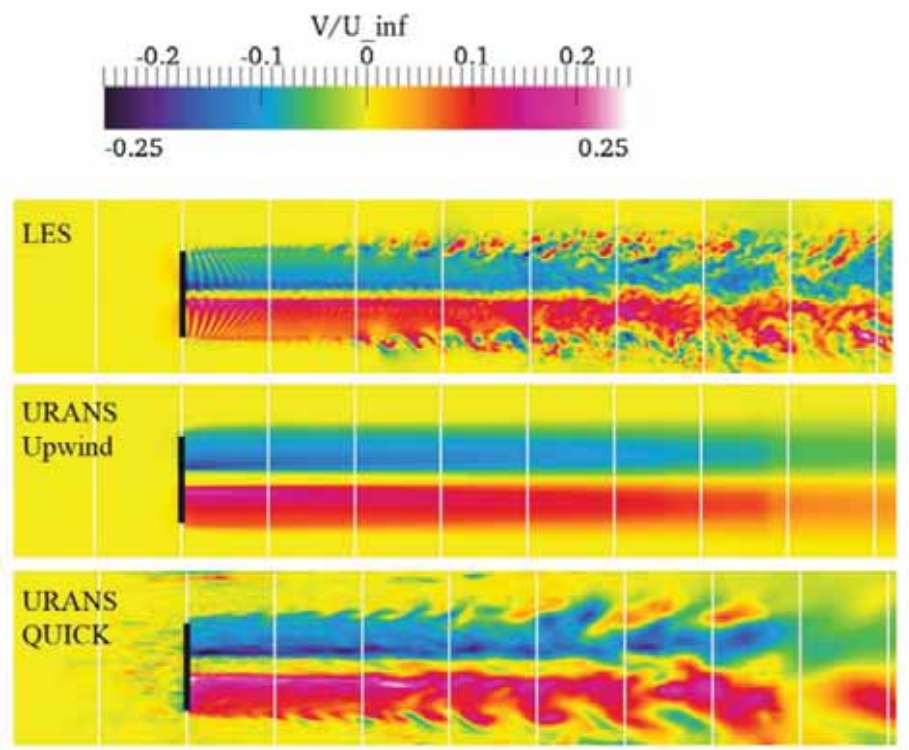

Figure 8: Two URANS calculations (with different discretization procedures) and LES calculation of the wind turbine wake. V is the velocity in the y-direction and normalized with the inlet velocity of 10 m/s. The black lines indicate the rotor plane and white lines are spaced one rotor diameter apart (LES performed by Churchfield, NREL).

For comparison of turbulent kinetic energy calculations from URANS with measurements, it is important to note that in the URANS approach one part of the turbulence is modelled, and one part is resolved. The k-values directly given from the k-ε turbulent model (Eq. 22) should be added together to the resolved larger scale turbulence before comparison with experimental data (Davidson, 2011). The velocity fluctuations can be found from the difference between the mean velocity and the instantaneous velocity, and then using Eq. 18 in order to get the resolved k contribution. Figure 9 shows the k contributions from the resolved k and the modeled k, as well as the total k values compared to measurements from the URANS QUICK simulation. The results shown are from the actuator line wake simulations of the NOWITECH and NORCOWE wind tunnel test (Krogstad et al., 2011).

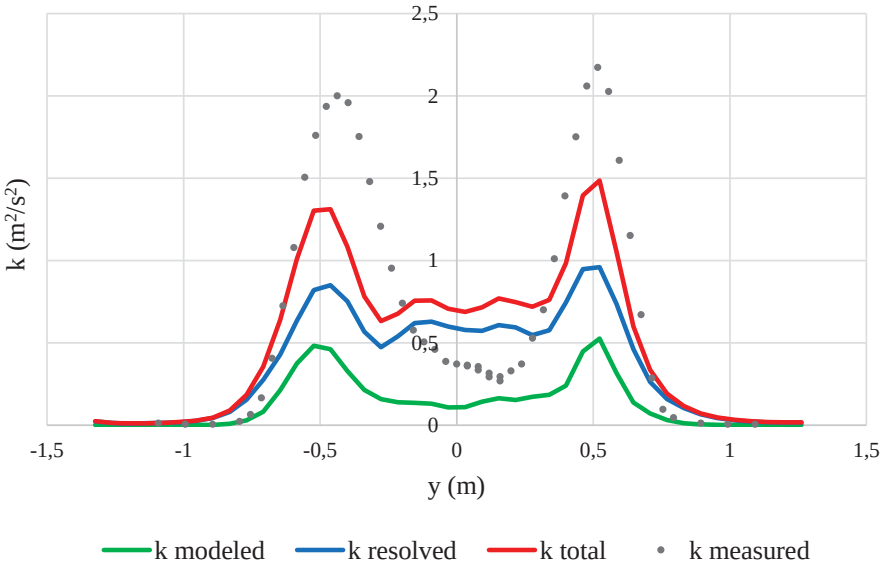

Figure 9: URANS Actuator line wake simulation of a test wind turbine five rotor diameter downwind. Turbulent kinetic energy k, (m^2/s^2) contributions from the resolved k and the modelled k, as well as the total k values. Measurements are from the first NORCOWE and NOWITECH wind tunnel blind test.

4 Wave influenced wind turbine performance

A direct study of the effect of wave influenced wind on the wind turbine was achieved by coupling the method for wave influenced wind (Chapter 2.3) with the actuator line simulations (Chapter 3.1). This combined set up of Wave-Influenced Wind Turbine Simulations (WIWiTS) is described in the following, first as a stand-alone set up (Chapter 4.1) and then linked to a structural response tool (Chapter 4.2). In this manner it is possible to seek answer to the 'effect' part of the research question put forward in Chapter 1.2.

4.1 Development of WIWiTS

OpenFOAM is a very flexible CFD toolbox. It is built with the generic and object-orientated language C++. The design of the toolbox is highly modular and its different functionalities are organized into shared libraries. The SOWFA solver is an important building block in WIWiTS. Since this was also based on OpenFOAM, it was fairly straightforward to extend parts of the SOWFA solvers to include the wave influenced wind model, and to be able to deal with moving mesh.

The original SOWFA solver used the PISO algorithm (Issa et al., 1986) for solving the time-dependent fluid flow equations. This was changed to use the PIMPLE algorithm in order to be compatible with the moving mesh solver used for the wave influenced wind simulations. PIMPLE is a more robust version of the PISO algorithm (OpenFOAM, 2014), where an additional loop is added within the PISO loop for enhanced stability.

While working with this PhD thesis, three Master's students have been engaged with studies that have contributed to the overall development of WIWiTS. The first Master's student, Richard Kverneland, tested the wave influenced wind method (Kverneland, 2012). Tommy Fredriksen (Fredriksen, 2013) and Anne Mette Nodeland (Nodeland, 2013) worked with the actuator line method and SOWFA. Nodeland did a thorough testing of the various input parameters to the actuator line model and Fredriksen experimented with inclusion of nacelle and tower in the model. Acona Flow Technology and Fredriksen improved the robustness of the actuator line solver by making the wind turbine forces calculations implicit. The original actuator line SOWFA

solver used as a starting point for WIWiTS was a beta version from 2012. This code had an explicit scheme for calculation of the wind turbine forces. This was changed to an implicit scheme where the wind turbine forces now are calculated and updated within the PIMPLE algorithm. This ensured a tighter coupling between the flow field and the turbine blades, and made the code more robust with respect to the time step sensitivity. Figure 10 (left) illustrates the actuator line structure with an implicit scheme.

All WIWiTS have been performed on realistic scales, and it has been technically challenging to work with the simulations. The MABL domain needs to be of a certain size for the wind field to properly develop over the waves. The simulations have usually been carried out on a scale of 500-1000 meters in the horizontal direction, and a vertical height from 100-800 meters. The wind turbine representation has a hub height of 90 meters height and a the rotor radius is 61 meters. This implies also a lateral extension of the domain to a minimum of 260 meters. The University of Stavanger exclusively made available extensive disk space and resources on their Linux machines and the simulations were run in parallel. However, the computations soon turned out to be too large, and compromises had to be made reducing the resolution of the grid. The mesh was constructed with a background-graded mesh having a refinement towards the wave surface and a refined area around the turbine rotor. In Figure 11 the WIWiTS domain is shown. The domain length and possibly the height is believed to be too short to avoid all boundary effects. These effects stem from the fact that the wave originates from one side of the domain and decays on the other side. Grid independency was not completely reached. The WIWiTS simulations, presented in Papers 5 and 6, will, nevertheless, give indications on the relative differences in wind turbine power output and fatigue for different wave conditions compared to a no-wave situation.

It would be interesting to study the turbine wake for different wave-wind regimes. Then the domain size needs to be further extended to several rotor diameter down wind. Because of the above mentioned compromise regarding the grid size, wake studies have not been a topic for investigation for the current work with WIWiTS.

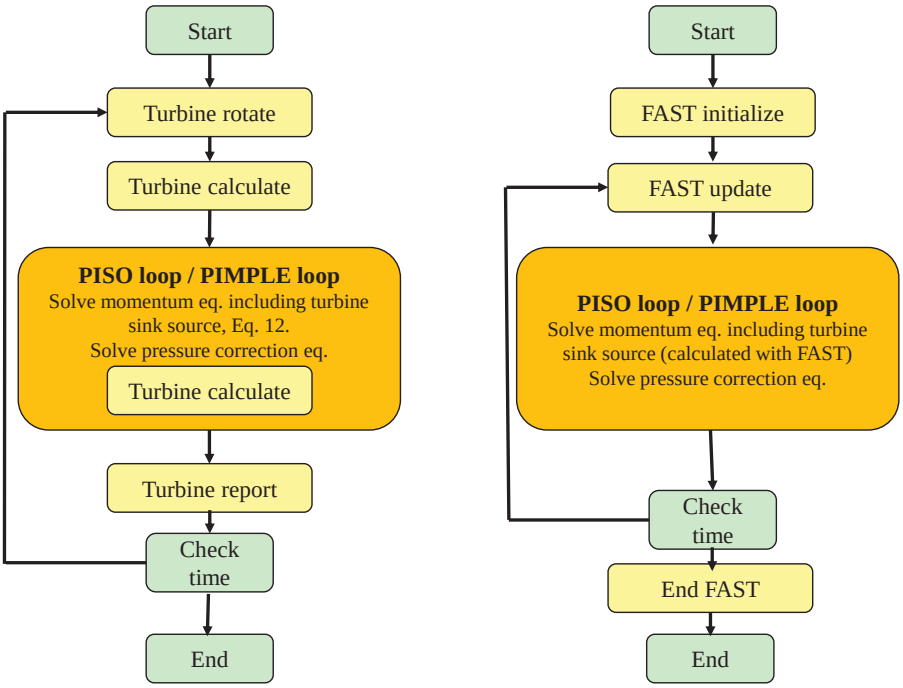

Figure 10: Turbine force calculations with and without the FAST link activated. If the actuator line is used within the WIWiTS solver the PIMPLE algorithm is utilized, and if it is used without the moving mesh, as a standalone actuator line model, the solver used the PISO algorithm.

Left: Actuator line structure with the implicit scheme, where the wind turbine forces are calculated and updated within the PIMPLE algorithm. The 'turbine rotate' function calculates the rotational speed (and take into consideration yaw and pitch if necessary) and rotates the blades. Within the 'turbine calculate' function, wind vectors are calculated and these are used when lift and drag are calculated for each span wise segments (Eq. 13 and 14). The pressure and wind fields are calculated within the PISO or PIMPLE loop. The 'turbine calculate' is again executed and the forces are distributed according to Eq. 15 and projected into the momentum equation by the use of Eq. 16. The 'turbine report' function reports and writes to file. If the simulation end time is not reached, the process starts over again with 'turbine rotate'.

Right: When FAST is coupled to WIWiTS the procedure is explicit, meaning that the calculation of the turbine forces is done outside the PISO/PIMPLE loop. The 'FAST update' function rotates the turbine, calculate the forces and reports and writes to file.

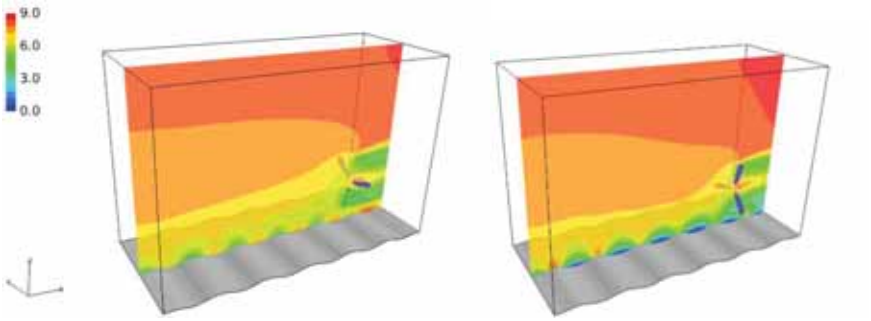

Figure 11. WIWiTS domain with wave aligned (left) with the wind direction and wave opposing the wind direction (right). The color contours showing the wind velocity in the x-direction.

Recently, Yang et al. (2014) published work about swell effects on a wind turbine park. Yang et al. used a LES approach for the wind simulations and simulated waves using a higher order spectral method where the discretization is done by use of Fourier-series. The wind park was represented with actuator disks. Only swell aligned with the wind was considered. The approach of Yang et al. is hence quite different from what is used for WIWiTS. Interestingly, the results from the WIWiTS simulations in Paper 5 are in line with Yang et al.'s. Both simulation methods show that the swell will induce oscillation in the extracted wind power at the swell frequency. Yang et al. also showed that the wind power extraction from the wind park increased as a total when downwind swell was present.

4.2 WIWiTS coupled to FAST

A wind turbine that is exposed to both wind and wave forces will, of course, respond with various movements. In the actuator line and WIWiTS presented in Papers 3, 4 and 5, these aerodynamical and hydrodynamical load responses have been ignored. To include such responses, one possibility is a full CFD analysis with fully resolved turbine. However, this is probably unrealistic because of the computational resources needed. Another possibility is to use different engineering tools for response investigation. SOWFA was already making use of such a tool; the Fatigue, Aerodynamics, Structures and Turbulent

code (FAST) (Jonkman & Buhl, 2005). FAST is a computer-aided engineering tool specially designed for analyzing horizontal axis wind turbines.

Since WIWiTS has been based on the SOWFA code it was also feasible to extend the simulations to the FAST coupled set up. In this manner it will be possible to investigate not only the wind turbine power output and forces, but also bending moments on the wind turbine structure. FAST provides various output parameters and from this it is possible to perform fatigue analyses and investigate fatigue that may result from a varying wind field influenced by wave movements. In Paper 6, results from nine different WIWiTS simulations coupled to FAST are presented. The co-author Lene Eliassen is a researcher at NTNU and she carried out fatigue calculations and generated the frequency spectrum for the bending moment.

WIWiTS will replace the blade element momentum (BEM) part that is usually used with FAST. FAST calculates the structural response and feeds this back into the CFD simulations. The wind field is then changed and new structural responses are calculated with FAST. Figure 10 (right) shows the structure of the turbine force calculation with the FAST link activated. The wind field is then influenced by the turbine structural response, whereas without FAST the WIWiTS just sees the turbine as a fixed structure. The resulting wind field will be slightly different with the FAST link activated compared to a simulation without FAST (all other conditions being the same), as is seen in Figure 12. The theoretical background for the structural response and fatigue calculations will not be discussed in this thesis summary. Reference is made to Almar-Næss (1985) for a good introduction to structural response and fatigue theory.

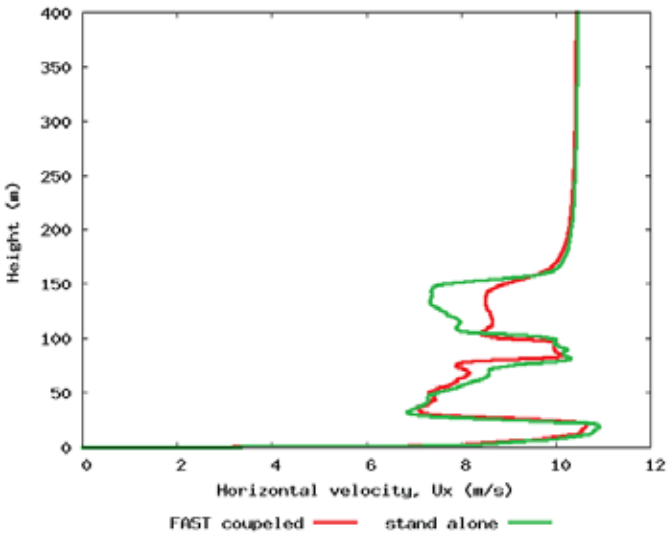

Figure 12. Example of a wind profiles sampled in the rotor plane for a WIWiTS turbine coupled with FAST (red) and one standalone without FAST.

Since WIWiTS coupled to FAST was the last part of the work in this PhD project, the full capacity of FAST to study structural response from the wave-influenced wind field was not utilized. As mentioned earlier, the tower of the wind turbine is not a part of the turbine representation in WIWiTS, but it is a part of FAST. The CFD generated wind field will therefore not be influenced by any tower, but FAST will calculate bending moment on the tower, based on the wind field that is influenced by the turbine rotor as well as the wave state. The simulations presented in Paper 6 are done by the use of the default tower in FAST, which is the tower of the NREL 5 MW reference turbine (Jonkman et al., 2009). It is possible to change the tower representation to a tower more representative for bottom-fixed offshore turbines, but this was not feasible within the time frame of the thesis. For fatigue considerations, it is necessary to use long time series. The simulation time ranged from 100 to 300 seconds, which is believed to be too short. It is recommended to use results from at least several cases with 10 min simulations time (Zwick & Muskulus, 2014).

5 Summary of appended papers

Papers one to six represent investigations in order to find an answer to the guiding research question put forward in Chapter 1. In this chapter, a summary of the findings in the papers will be given. Reference is made to Figure 1 where the overall structure of the work is visualized. Parts of the research question have been answered and the work has produced interesting findings. One major contribution of this PhD is the development of an open source CFD tool: the Wave Influenced Wind Turbine Simulation (WIWiTS) model. With WIWiTS, it is possible to directly study the effect of wave influenced wind on a wind turbine or a wind park. In this thesis simulations on one single wind turbine have been conducted, but the WIWiTS solver is set up for inclusion of multiple wind turbines as well as more complicated sea states than those used here.

A review of the governing offshore wind turbine standards and a literature study of marine boundary layer meteorology have revealed that there is a gap between best knowledge and best practice for boundary layer meteorology in the field of offshore wind energy. Findings and contributions of this review and the subsequent modelling work are presented in Papers 1 to 6. The Papers are indicated as numbers on the visualized structure of this PhD work in Figure 1.

Paper 1 – Exploring the gap between ‘best knowledge’ and ‘best practice’ in boundary layer meteorology for offshore wind energy

The governing standards in the field of offshore wind energy have been reviewed in the context of boundary layer meteorology. The objective was to identify the industry best practice and compare this with recent scientific developments. Possible implications of simplifications made in the governing standards were also indicated. In this manner the paper explores the gap between ‘best knowledge’ and ‘best practice’ in boundary layer meteorology for offshore wind energy.

Atmospheric stability considerations and wave effects are two major factors affecting wind conditions over sea versus land. Therefore the focus of the paper was to investigate how these effects were handled in the governing standards in the field of offshore wind energy.

The major findings of the paper are that neutral stratification and a flat, smooth sea surface are routinely used as assumptions in wind energy calculations. Literature shows that the assumption of a neutral atmospheric stratification is not necessarily a conservative approach. The paper also reveals that the sea surface is normally thought of as level and smooth in various phases of offshore wind site development, even if both field experiments and numerical simulations show that turbulence levels, heat exchange and momentum transfer all depend on the sea state. Long periodic waves can result in both higher and lower effective surface drag. It is likely that these waves can create different wind shear and turbulence characteristics, so that a wind turbine site will be exposed to other environmental conditions than those it was designed for. Stratification and a changing sea state are effects that can be modelled and accounted for and there is need for improvements in design calculations, energy assessments and power output predictions. The inclusion of stability effects in offshore wind park modelling is still a relatively new area of research, and investigations that takes into account the role of the ever-changing sea surface is even newer. To further clarify the possible impact that wave-induced wind has on offshore wind turbines, more detailed studies are required.

Paper 2 – A method for wave driven wind simulations with CFD

A new method of wave simulations with a moving mesh approach was presented and the effects of various sea states on the wind were studied. At this stage of the PhD the horizontal wave movements had not yet been implemented, so the method only described and used the vertical wave movements. A sensitivity analysis, based on changing different inlet winds and different wave states, was performed. These studies were done on a relatively small domain and experiences from these simulations were then used when investigating the MABL in a larger domain, with length of 500 m and height of 100 m. For these simulations, the method was further improved. A logarithmic wind profile was implemented for the inlet velocity and a gradually developing wave was utilized. Four different cases were presented and compared with each other and with the standard logarithmic wind profile.

The simulations clearly showed that the wind field is influenced by the wave high above the layer, usually referred to as the wave boundary layer (WBL). Results show that the influence depends on the inlet wind speed (thought of as the geostrophic wind), and wind direction relative to the wave direction and the

wave states. The influence will probably also depend on inlet turbulence levels (thought of as natural atmospheric turbulence) and atmospheric stratifications, but this was not tested.

Vertical profiles of wind velocity and turbulent kinetic energy show distinct differences for waves aligned with the wind versus waves opposing the wind. When the wave is opposing the wind, the wave effects are notable throughout the whole domain. A speed up near the wave surface is present when the wind is blowing over, and aligned with, a faster moving wave. When the wave opposes the wind, the wind velocity will be reduced in the lowest meters and sometimes even reverted. The turbulent kinetic energy will be higher in the opposed situations compared to the aligned situation

After the publication of this paper, it was revealed that the discretization schemes for the convective term in the momentum equation were too dissipative when used on transient RANS simulations. The discretization scheme Upwind was used, and later work with Paper 4 clearly showed that it would be better to use a more accurate scheme such as the Quick scheme. It should also be noted that in this paper we concluded that the overshoots of the inlet wind speeds in the opposed situations was probably due to mass conservation in a limited height computational domain. In later work the overshoot was present even if one extended the height of the domain (see Paper 5).

Paper 3 – Comparing CFD calculations of different wind turbine modelling approaches with measurements

Three different wind turbine modelling approaches were investigated with reference to measurements from model wind turbine tests in a wind tunnel. The focus was on wake velocity and turbine forces. In order to compare turbulence levels of the three different methods, more work and investigations had to be carried out and this topic was omitted from the study. Turbulence investigation was instead prepared for a later paper (Paper 4).

Three wind turbine rotor tip speeds were tested and, as expected, the performance of the models was best for the design tip speed. For this speed, both the fully resolved method and the actuator line method predicted power and thrust that was very close to the measured values. The actuator disk method was not a part of these computations, since this method required that correct

power and thrust coefficient was used as input values to the model before running it. The fully resolved method produced superior wake velocity results compared to the actuator disk and the actuator line method, and on average it also produced better results for the force predictions. The actuator line captured the variation pattern in the velocity wake, but was far off in the hub area since the rotor-nacelle was not modelled.

During the course of this study, valuable data was gathered with three different modelling techniques. The actuator line was particularly dependent on correct input values and setup. The method was found to be quite sensitive for the composition of the airfoil data. The Gaussian width parameter, which controls how the forces are distributed along the lines representing the rotors, had a great influence on both the wake velocity predictions and the calculation of the wind turbine forces. Currently there is no robust generic way of establishing appropriate Gaussian width parameters without model tuning. Nevertheless, the actuator line results were promising for wind turbine investigations, especially for the design tip speed.

Since the results with the fully resolved method were accurate they could serve as a way to benchmark the other models if one was interested in testing different inflow conditions other than those available in the experiments.

Paper 4 – URANS versus LES based simulations of wind turbine performance and wakes - comparison with wind tunnel measurements

In this paper, we investigated strengths and weaknesses of the two different turbulence closure methods that are often used in the field of wind energy, and gave some recommendations for further usages. The motivation for this work was to examine if unsteady Reynolds-Averaged Navier-Stokes (URANS) could be used instead of large eddy simulations (LES) together with the actuator line model. Results were compared with experimental data from the first NORCOWE and NOWITECH wind tunnel test. The set up with the URANS actuator line simulations was given to Matthew Churchfield, senior researcher at NREL, who also performed the LES calculations.

URANS and LES both qualitatively predict wake velocity and wake turbulent kinetic energy close to experimental values for the design tip speed. URANS and LES differs 13,12 and 5 percentage points from each other one,

three and five rotor diameter downwind respectively. The turbine tower and nacelle are not modelled and the simulations does not captures the asymmetry in the velocity wake and the velocity deficit in the hub area.

Two different discretization schemes for the convective term were tested, and the first order bounded Upwind scheme was far too dissipative and unsuitable to use for wake simulations. The results were significantly improved when changing to the more accurate QUICK scheme.

Paper 4 demonstrated that URANS could do a good job and serve as a substitute to the more computationally demanding LES, at least for studies of low turbulent inflow on a single turbine as tested here.

Paper 5 – Wave influenced wind and the effect on offshore wind turbine performance

The method for wave simulation and the method for wind turbine modeling was established and these two methods were now combined. This resulted in Paper 5 where simulation results from the combined Wave-Influenced Wind Turbine Simulations (WIWiTS) were presented. The wind turbine used in these simulations was NREL's 5 MW offshore baseline wind turbine, which has a rotor radius of 61 m and a hub height of 90 m.

Before introducing the wind turbine in the simulations, the wind field over the waves was studied, using a less computationally demanding set up in two-dimensions. The purpose was to examine the required domain size, resolutions and the wind conditions without wind turbine influences. The method presented in Paper 2 had been further developed by the inclusion of the horizontal wave particle movement as well as the vertical movement, and the discretization schemes for the convective terms was also changed according to findings in Paper 4.

Paper 5 shows that the wave motions from a large swell wave with amplitude of 4 m, gives oscillations in the power output. The oscillation frequency is equal to the wave frequency. The wave motions periodically modify the wind profiles up to approximately 100 meters above the sea surface. The wind turbine will experience these fluctuations and it will lead to slightly larger tangential forces than in comparable situations over a flat surface. Interestingly, the situation with the swell opposing the wind field gave slightly higher power output than the aligned case and the no-wave case. Intuitively this seems perhaps a bit strange. However, the fast moving swell that oppose the

wind generates an overshoot of the wind speed compared to the logarithmic inlet and compared to the aligned situation. For the cases studied, this happens over 20-30 meters over the sea surface. The increased turbulence levels in the opposed situations is believed to create a 'richer' wind profile that results in this overshoot and increased power output.

These results can only serve as an indication of the wind turbine performance in the wave influenced wind, because during the work with this paper it was revealed that the moving wave introduces some boundary effects close to the inlet and outlet parts of the simulation grid. Nevertheless, it is interesting to note the relative differences between conditions with swell aligned with the wind field, opposing the wind field and over a surface with low roughness (no waves).

After publication of Paper 5 (and submission of Paper 6) an interesting paper from Yang et al., (2014) appeared in the litterature. This paper investegates down wind swell effect on a wind park. Their method is based on LES and they concluded that the swell occilations can be found in the power output. This is in line with the findings in Paper 5. Yang et al. only investegated downwind swell and found that the wind power extraction from the wind park increased as a total when downwind swell was present. The results presented in Paper 5 show however that swell opposing a wind turbine generated slightly higher power output. There is need for more investigations and work in order to be able to more quantitatively compare results with Yang et al.'s.

Even if results from Paper 5 show that wave conditions will influence the wind turbine power output, it concerns a smooth flow at the inlet, and thus does not include possible influences of the natural turbulent structure of the atmosphere and the varying atmospheric stability.

Paper 6 – On offshore wind turbine fatigue caused by wave influenced wind

In order to examine the further impact of the results from Paper 5, there is need for more sophisticated calculation methods. Therefore, work has started in order to investigate the structural turbine response as a result from wave influenced wind. FAST is a computer-aided engineering tool, specially designed for analyzing horizontal axis wind turbines, and it was linked to the wave influenced wind turbine simulations.

In this paper, four different waves in combination with a wind field with a wind speed of 8 m/s at the reference height of 400 m height are studied, as well as a reference case with flow over a flat surface. The direction of the wave is changed, resulting in a total of nine simulations investigated. Since the WIWiTS is now linked to FAST, it was possible to extract more structural response relevant information. Stress at the blade root and the base of the tower due to the flapwise moment was investigated. The equivalent fatigue damage was estimated by the use of the damage load relative to the reference case with flow over a flat surface.

At the current stage of work it was not possible to include an offshore monopile, instead the study was conducted on the base of an onshore tower situated offshore. Wave loads on the tower were neglected.

Paper 6 demonstrates that waves will influence the wind field, which in turn affects the equivalent fatigue damage at both the blade root and the tower base. In a relatively low wind regime (reference wind of 8 m/s in 400 m height) the wave influenced wind increases the fatigue damage compared to a situation with no waves, especially for the cases where waves oppose the wind field. There is a need for longer stimulation time and more simulations in order to be able to conclude more specifically regarding the wave influenced wind impact on turbine performance and fatigue.

The simulations in this paper were all run with a too dissipative discretization scheme for the convective term in the moment equation. It was clear from the work with Papers 4 and 5, that a more accurate discretization scheme should be used, but it was not possible to transfer this finding to the work in Paper 6. We have worked in parallel with several papers and since WIWiTS's linked to FAST is quite computationally demanding, it was not feasible resource wise to run them over again.

6 Conclusions

Wave wind interaction and the implications this has for offshore wind turbines have been addressed, and specific numerical model experiments have been conducted for both wave influenced wind and wind turbine performance and wake development. A combined CFD set up that allows direct investigation of the impact of wave influenced wind on a wind turbine, or a wind park, has been developed.

It has been an important guideline in this PhD work to try to estimate the *effect* of wave influenced wind on an offshore wind turbine. Therefore, importance has been given to developing a set up that is suitable for studying these possible effects directly. This tool has been successfully developed. However, there is still a lot of work that needs to be done in order to give reliable answers to the "effect" part of the research question. Some of this work is suggested as improvements in Chapter 7.

The standards used in the design of offshore wind turbines, particularly for the rotor-nacelle assembly, are similar to those used for onshore wind turbines. As a result, simplifications with respect to the marine boundary layer are made. Two important assumptions frequently used are neutral atmospheric stratification, and treating the sea surface as a static level surface with low roughness. A gap between 'best knowledge' and 'best practice' in boundary layer meteorology for offshore wind energy has been identified. This thesis contributes in bridging part of this gap that is due to simplifications made for the sea surface.

The CFD model experiments with wave influenced wind show that swells will influence the above wind field. The effect is notable far up into the MABL and depends on the wave state and the direction of the waves and the wind. The swept wind turbine rotor area will be exposed to wind profiles and turbulent levels other than what is predicted with the usual assumption of a logarithmic wind profile and low turbulence levels over a flat surface.

Several individual cases have been studied to determine the effect of wave influence on wind. In situations where a swell moves faster than the wind, the simulations show that the swell will transfer momentum to the wind in the aligned situation. Another general observation from the model experiments is in a fast moving swell regime, a swell that oppose the wind field will create larger turbulence levels than if the swell was aligned with the wind or with no

wave present. In this situation the wind speed will be lower close to the sea surface. Above this field with reduced velocity an overshoot of the wind speed compared to the logarithmic inlet has also been observed. The reason for this is believed to be due to the extra generated turbulence, which in the opposed cases gives rise to a 'richer' velocity profile. More detailed simulation and turbulence analyses are required to investigate this phenomenon further.

Three different CFD wind turbine modelling approaches and two turbulent calculation techniques have been tested and compared with wind tunnel measurements. The fully resolved method was proven as the best performing technique of the three. This method required a very fine resolution of the mesh near the rotor blades. This was feasible for the small scale turbine modelled in this test, but it would be far too computationally demanding on a full scale turbine. In order to investigate the effect of waves, full-scale simulations are needed. Therefore, the actuator line model was chosen as a model suitable for both wind turbine performance and wake predictions. Two popular turbulent calculation techniques, based on URANS and LES, have been compared with each other and with the wind tunnel measurements. Even though LES gave more accurate predictions of the wake than the URANS simulations, it is believed that URANS can do a good job and serve as a substitute to the more computationally requiring LES.

Based on the above mentioned work, both with wave modelling and wind turbine modelling, a combined set up where one can directly study the possible effect of wave influenced wind on a wind turbine was developed. This tool for Wave-Influenced Wind Turbine Simulations (WIWiTS) is developed with the OpenFOAM tool kit and the SOWFA tool, both of which are open source codes. WIWiTS can be run in two modes, with and without a coupling to the structural dynamic response code FAST

Simulations with WIWiTS without the FAST mode enabled showed that swell will affect the power output. The swell movements periodically modified the wind profiles up to approximately 100 metres above the sea surface and this resulted in oscillations in the power output. The oscillation had the same frequency as the waves. The opposed case gave slightly larger power output than the aligned case. The tangential forces on the rotor blade were larger with the wave present compared to situations over a flat surface.

Simulations with WIWiTS coupled to FAST demonstrated that wave influenced wind increases the fatigue damage compared to a situation with no waves, especially for the cases where the wave field opposes the wind field. Of the four wave cases studied, the larger wave periods (8 and 10 seconds) gave

rise to the highest equivalent loads, and these cases also resulted in the highest peaks in the frequency spectrum of the bending moment.

After publication of Paper 5, and submission of Paper 6, an interesting paper from Yang et al. (2014) became available. Yang et al. use a LES approach to study the effect of down wind swell on a wind park. Their numerical method is quite different from the one presented in this thesis. Except from Yang et al.'s publication it has not been possible to find other published literature this work can be compared with. Suitable observational data set have neither been assessable. Thus, it has not been possible to properly validate the WIWiTS results. There are reasons to believe that the domain size might be too small, and it cannot be guaranteed that boundary effects from the CFD domain were not present. In addition, grid independency was not completely reached. Nevertheless, it is interesting to note the relative differences between conditions with waves aligned with the wind field, opposing the wind field and over a surface with low roughness (no waves).

In the ongoing work of coupling atmospheric meso scale models and wave models, directional wave information is not taken into consideration. This PhD work demonstrates that the direction of the wave field relative to the wind is important. Hopefully, the work in this thesis will encourage further research regarding finding a way to include directional information in this important meso scale coupling work.

It is possible to conclude qualitatively that wave influenced wind will affect the turbine performance, as well as the loads and fatigue. However, it has not been possible to conclude if this influence is significant in relation to the natural turbulent structure of the atmosphere and the varying atmospheric stability. As a part of this thesis, a flexible open source CFD setup suitable to directly study the possible effects of wave influenced wind has been developed and used. This WIWiTS setup is a potential powerful tool and development and further improvements are recommended. This PhD work has demonstrated that wave influenced wind is an area worth paying attention to, and hopefully these results will encourage further studies in this area.

7 Suggestions for improvements and future perspectives

Since it has been documented that there is a gap between 'best knowledge' and 'best practice' in boundary layer meteorology in the field of offshore wind energy, several actions should be taken to close this. For the wave wind interaction part of the gap, more idealized CFD simulations should be carried out. The method developed in this PhD work should be further improved, and some suggested improvements are given in the following paragraphs.

The wave influenced wind simulations are based on an incompressible solver. There are reasons to believe that compressible calculations could give slightly different results than incompressible calculations for the steepest waves. Work should be carried out to properly test the difference between incompressible and compressible approaches.

More detailed sensitivity tests looking at the wind flow response on the changing sea states are needed. One should aim at identifying some generic relationship regarding wind speed and sea state. URANS calculations of turbulence in the near wake of the turbine deviated significantly from LES and measurements. Deviation from real turbulence levels could also be the case for wave generated turbulence, and should be a topic for further investigations.

The sea surface is never purely monochromatic and harmonic; at least, not for a very long time. By superposition of multiple waves, a more realistic sea surface can be described. Since the method developed in this thesis can use several different harmonic waves as input to the moving wave surface, it will be possible to link the simulated wave movements to a wave spectrum representation of the sea surface. Then it would be simpler to compare simulations with field measurements, since the sea surface measurements are normally given as wave spectrum representation of the surface.

The inclusion of thermal effects would be interesting. As Paper 1 reports, atmospheric stability is of great importance, and it is feasible to simultaneously study wave effects and thermal effects. The SOWFA tool includes thermal effects and this part of the code could also be used for wave influenced wind modelling.

The NORCOWE and NOWITECH wind tunnel blind test experiments serve as an excellent base for more testing of appropriate turbine models. For the actuator line model, a thorough investigation of different discretization schemes and various input parameters should be conducted. Also, testing of different URANS models would be interesting.

If further studies in the field mentioned above were performed, they could be included in WIWiTS and improve the total set up. It was challenging to work with WIWiTS because a very large domain was required in order to eliminate boundary effects and to get grid independent results. The mesh generation can be done more effectively than what has been done for the simulated cases in this thesis. One recommendation is to work more with mesh construction, for instance, a mesh that is fine in the areas where one expects large gradients and coarser in others.

WIWiTS with the FAST mode activated needs further validation and testing. Turbine towers representative for offshore wind park installations should be implemented. The method is open to inclusions of various towers. Hydrodynamic loads from the wave state should also be included. In order to study fatigue, there is a need for longer stimulation times. Several sea states and wind regimes must be investigated, and more realistic atmospheric conditions need to be implemented with buoyancy effects present. The SOWFA code includes both buoyancy and Coriolis and therefore it should be feasible to incorporate this in WIWiTS.

Only bottom fixed horizontal axis turbines are studied here. It would be interesting to extend the method to include vertical axis turbines and floating concepts.

On a more general level it is recommended a study of the frequency of different wind-wave regimes at certain offshore wind locations in order to be able to indicate how often situations where one can expect notable wave influenced wind effects to occur. Investigations on how knowledge from idealized CFD studies of wind wave effects can be incorporated in operational meso scale models will also be an important area to explore.

Models with a scale down to one km is used for operational MetOcean forecast for offshore wind parks. On the other hand, CFD models with scales under one meter are used in order to understand how these external geophysical forces affect the offshore structures. However, it is not feasible to run CFD models in operational forecasting modus. How can these two ‘worlds’ of

modelling traditions best be joined together? One possibility is to create look up tables, that are based on precursor CFD calculations. These look up tables should then be possible to couple to operational forecasting models. In this manner we could develop far better decisions support tools for an offshore wind industry which is extremely sensitive to changes in the weather and the sea state. A useful decision support tool need to be able to both predict the external geophysical forces as well as the impact of these changing forces on the structure and for the energy harvest. This calls for a better link between the geophysical macro world and the micro world of the structures in questions. I believe that finding an optimal link will be an important area of research in the coming years.

References

Almar-Næss, A. (1985). *Fatigue Handbook.* Trondheim: Tapir Publishers.

Baker, C. J. (2007). Wind engineering – Past, present and future. *Journal of Wind Engineering and Industrial Aerodynamics*, 843-870.

Booij, N., Ris, R. C., & Holthuijsen, L. H. (1999). A third-generation wave model for coastal regions: 1. Model description and validation,. *Journal of Geophysical Research*, 7649–7666. doi:doi:10.1029/98JC02622

Charnock, H. (1955). Wind stress on a water surface. *Q. J. R. Meteorol. Soc.*, 639-640.

Christakosa, K., Reuder, J., & Furevik, B. R. (2013). Experimental characterization of the marine atmospheric boundary layer in the Havsul area, Norway. *Energy Procedia*, 121-127.

Churchfield, M. J., Lee, S., Moriarty, P. J., Martinez, L. A., Leonardi, S., Vijayakumar, G., & Brasseur, J. G. (2012). A large-eddy simulation of wind-plant aerodynamics. *AIAA paper, (2012-0537)*.

Davidson, L. (2011). *Fluid mechanics, turbulent flow and turbulence modeling.* Göteborg, Sweden: Chalmers University of Technology, Div. of Fluid Dynamics, Dep. of Applied Mechanics.

Doneland, M. A., Drennan, W. M., & Katsaros, K. B. (1997). The Air–Sea Momentum Flux in Conditions of Wind Sea and Swell. *J. Phys. Oceanogr., 27*, 2087–2099. doi:http://dx.doi.org/10.1175/1520-0485(1997)027<2087:TASMFI>2.0.CO;2

Drennan, W. M., Kahma, K. K., & Doneland, M. A. (1999). On momentum flux and energy spectrra over waves. *Boundary-Layer Meteorology, 92*, 489-515.

Drennan, W. M., Taylor, P. K., & Yelland, M. .. (2005). Parameterizing the Sea Surface Roughness. *J. Phys. Oceanogr., 35*, 835–848. doi:http://dx.doi.org/10.1175/JPO2704.1

ECMWF. (2006). *ECMWF WAVE MODEL*. Reading: European Centre for medium-Range Weather Forecast.

Edson, J., Crawford, T., Crescenti, J., Farrar, T., Frew, N., Gerbi, G., . . . Zappa , C. (2007). The coupled boundary layers and air-sea transfer experiment in low winds. *Bulletin of the American Meteorological Society, 88(3)*, 341-356.

EWEA[a]. (2014). *The European offshore wind industry - key trends and statistics 2013*. Brussels: European Wind Energy Association.

EWEA[b]. (2014). *Wind energy scenarios for 2020*. Brussels: European Wind Energy Association.

EWEA[c]. (2013). *Deep water*. Brussels: European Wind Energy Association.

Foken, T. (2006). 50 years of the Monin-Obukhov Similarity Theory. *Boundary Layer meteorology, 119*, 431-447. doi:10.1007/s10546-006-9048-6

Fredriksen, T. (2013). *Wind Energy; CFD simulation of wakes and wind turbine forces.* Porsgrunn: Telemark University College, Faculty of Technology.

Gryning, S. E., Batchvarova, E., Brümmer, B., Jørgensen, H., & Larsen, S. (2007). On the extension of the wind profile over homogeneous terrain beyond the surface boundary layer. *Boundary-Layer Meteorology, 124(2)* , 251-268. doi:DOI: 10.1007/s10546-007-9166-9

Hargreaves, D. M., & Wright, N. G. (2007). On the use of the k-[epsilon] model in commercial CFD software to model the neutral atmospheric boundary layer. *Journal of Wind Engineering and Industrial Aerodynamics,, 95*(5), 355-369. doi:10.1016/j.jweia.2006.08.002

Högström, U. L. (1988). Non-Dimensional Wind and Temperature Profiles in the Atmospheric Surface layer: A Re-Evaluation. *Topics in Micremeteorology*, 55-78. doi:dx.doi.org/10.1007/978-94-009-2935-7_6

Issa, R. I., Gosman, A. D., & Watkins, A. P. (1986). The computation of compressible and incompressible recirculating flows by a non-iterative implicit scheme. *Journal of Computational Physics, 62*(0021-9991), 66-82. doi:DOI: 10.1016/0021-9991(86)90100-2

Janssen, P. (2004). *The interaction of ocean waves and wind.* Cambridge University press: Cambridge.

Jenkins, A. D., Paskyabi, P. M., Fer, I., Gupta, A., & Adakudlu, M. (2012). Modelling the effect of ocean waves on the atmospheric and ocean boundary layers. *Energy Procedia, 24*, 166-175. doi:10.1016/j.egypro.2012.06.098

Jonkman, J., & Buhl, M. (2005). *FAST User's Guide.* Golden: National Renewable Energy Laboratory. Retrieved August 2014, from http://wind.nrel.gov/designcodes/simulators/fast/FAST.pdf

Jonkman, J., & Buhl, M. (2005). *FAST User's Guide, NREL/EL-500-38230.* Golden: NREL technical report,. Retrieved from Accessible at: http://wind.nrel.gov/designcodes/simulators/fast/FAST.pdf

Jonkman, J., Butterfield, S., Musial, W., & Scott, G. (2009). *Definition of a 5-MW Reference Wind Turbine for Offshore System Development.* Golden: National Renewable Energy Laboratory, Rept. NREL/TP-500-38060.

Krogstad, P. Å., & Eriksen, P. E. (2013). 'Blind test' calculations of the performance and wake development for a model wind turbine. *Renew. Energ, 50*, 325-333.

Krogstad, P., Eriksen, P., & Melheim, J. (2011). *Blind test' workshop.* Trondheim: Department of Energy and Process Engineering, NTNU.

Krogsæter, O. (2013). *The marine atmospheric boundary layer and ocean waves under the aspect of offshore wind energy applications, PhD thesis.* Bergen: University of Bergen.

Kverneland, R. (2012). *CFD-simulations of wave-wind interaction.* Stavanger: University of Stavanger, Norway.

Launder, B. E., & Spalding, D. B. (1974). The numerical computation of turbulent flows. *Computer Methods in Applied Mechanics and Engineering*.

London Array Ltd. (2014, August 24). *Harnessing the power of offshore wind*. Retrieved from London Array: http://www.londonarray.com/

Martinez, L. A., Leonardi, S., Churchfield, M. J., & Moriarty, P. J. (2012). A Comparison of Actuator Disk and Actuator Line Wind Turbine Models and Best Practices for Their Us. *AIAA Aerospace Sciences Meeting including the New Horizons Forum and Aerospace Exposition 09 - 12 January*. Nashville, Tennessee: AIAA 2012-0900.

Meneveau, C., Lund, T., & Cabot, W. (1996). A Lagrangian dynamic subgrid-scale model of turbulence. *J. Fluid Mech*, 353-385.

Minkowycz, W. J., Sparrow, E. M., & Murthy, J. Y. (2000). *Handbook of Numerical Heat Transfer*. John Wiley & Sons, Inc. doi:doi: 10.1002/9780470172599.fmatter

Monin, A. S., & Obukhov, A. (1954). Basic lawa of turbulent mixing in the surface layer ofthe atmosphere. *Tr. Akad. Nauk SSSR Geophiz. Inst., 24*(151), 163-187.

Nodeland, A. M. (2013). *Wake Modelling using an actuator disk model in OpenFOAM*. Trondheim: Norwegian University of Science and Technology.

Nodeland, A. M. (2013). *Wake modelling using an actuator disk model in openFOAM* . Trondheim: Norwegian University of Science and Technology.

Ocampo-Torres, F. J., García-Nava, , H., Durazo, R., Osuna, P., Diaz Méndez,, G. M., & Graber, H. C. (2011). The INTOA Experiment: A Study of Ocean-Atmosphere Interactions Under Moderate to Strong Offshore Winds and Opposing Swell Conditions in the Gulf of Tehuantepec, Mexico. *138*(3), 433-451.

OpenFOAM. (2014, August 21). *The open source CFD toolbox*. Retrieved from http://openfoam.com/

Peng, S. Q., Liu, D. L., Sun, Z. B., & Li, Y. N. (2012). Recent advances in regional air-sea coupled models. *Science China, Earth Sciences*, 1391-1405. doi:10.1007/s11430-012-4386-3

Richards, P. J., & E, N. S. (2011). Appropriate boundary conditions for computational wind engineering models revisited. *Journal of Wind Engineering and Industrial Aerodynamics,, 99*(4), 257-266. doi:10.1016/j.jweia.2010.12.008

Richards, P. J., & Hoxey, R. P. (1993). Appropriate boundary conditions for computational wind engineering models using the k-ϵ turbulence model. *Journal of Wind Engineering and Industrial Aerodynamics, 46–47*, 145-153. doi:10.1016/0167-6105(93)90124-7

Sathe, A., & Bierbooms, W. (2007). Influence of different wind profiles due to varying atmospheric stability on the fatigue life of wind turbines. *Journal of Physics, Conference Series 75, 75*. doi:10.1088/1742-6596/75/1/012056

Shives, M., & Crawford, C. (2012). Mesh and load distribution requirements for actuator line CFD simulations. *Wind Energy*. doi:DOI: 10.1002/we.1546

Smedman, A., Högström, U., Bergström, H., & Rutgersson, A. (1999). A case study of air-sea interaction during swell. *Journal of Geophysical Research, 104*, 25,833-25,851.

Smith, S. D., Anderson, R. J., Oost, W. A., Kraan, C., Maat, N., De Cosmo, J., . . . Chadwick, H. M. (1992). Sea surface wind stress and drag coefficient. The hexos results. *Boundary-Layer Meteorology*, 109-142.

Statoil. (2012). *Hywind - The floating wind turbine.* Stavanger: Statoil.

Stull, R. B. (1988). *An Introduction to Boundary Layer meteorology.* Vancouver: Springer.

Sørensen, J. N., & Shen, W. Z. (2002). Numerical modeling of wind turbine wakes. *Journal of Fluids Engineering, 124*(2), 393-399. doi:10.1115/1.1471361

Tennekes, H., & Lumley, J. L. (1972). *A first course in turbulence.* Massachusetts: MIT press.

The Wamdi Group. (1988). A third generation ocean wave prediction model. *Journal of Physical Oceanography*, 1775–1810. doi:http://dx.doi.org/10.1175/1520-0485(1988)018<1775:TWMTGO>2.0.CO;2

Troldborg, N. (2008). *Actuator LIne Modeling of Wind Turbine Wakes.* Lyngby: TechnicalUniversityofDenmark.

Veersteg, H. K., & Malalasekera, W. (2007). *An Introduction to Computational Fluid Dynamic.* Essex: Pearson Education Limited.

Winther, N., & Lisæter, K. (2011). *RFF project report. SWAN 9km model - North Sea verification - PART 2.* Bergen: StormGeo.

WMO. (1998). *Guid to wave analysis and forecasting.* Brussel.

XFOIL. (2014, August 21). *Subsonic Airfoil Development System*. Retrieved from http://web.mit.edu/drela/Public/web/xfoil/

Yang, D., Meneveau, C., & Shen, L. (2014). Effect of downwind swells on offshore wind energy harvesting – A large-eddy simulation study. *Renewable Energy*, *70*, 11-23. doi:http://dx.doi.org/10.1016/j.renene.2014.03.069.

Zwick, D., & Muskulus, M. (2014). The simulation error caused by input loading variability in offshore wind turbine structural analysis. *Wind energy*. doi:10.1002/we.1767

Part II – Papers

Appended papers

Paper 1 Kalvig, S., Gudmestad, O.T. and Winther, N. (2013) 'Exploring the gap between 'best knowledge' and 'best practice' in boundary layer meteorology for offshore wind energy'. *Wind Energy*, 17: 161–171. doi: 10.1002/we.1572

Paper 2 Kalvig. S., Manger, E. and Kverneland, R. (2013) 'A method for wave driven wind simulations with CFD', *Energy Procedia*, vol. 35, pages 148-156, ISSN 1876-6102, http://dx.doi.org/10.1016/j.egypro.2013.07.168.

Paper 3 Kalvig, S., Manger, E. and Hjertager, B. (2014) 'Comparing different CFD wind turbine modelling approaches with wind tunnel measurements', *Journal of Physics, Conference series.* 555.

Paper 4 Kalvig, S., Churchfield, M., Manger, E. and Hjertager, B. (In review), 'URANS versus LES based simulations of wind turbine performance and wakes - comparison with wind tunnel measurements', *Journal of Renewable and Sustainable Energy (JRSE), AIP.*

Paper 5 Kalvig, S., Manger, E., Hjertager, B. and Jakobsen, J.B. (2014) 'Wave influenced wind and the effect on offshore wind turbine performance', *Energy Procedia*, Volume 53, 2014, Pages 202-213, ISSN 1876-6102, http://dx.doi.org/10.1016/j.egypro.2014.07.229.

Paper 6 Kalvig, S., Eliassen, L. and Manger, E. (In review), 'On offshore wind turbine fatigue caused by wave influenced wind', 2nd Symposium on OpenFOAM in Wind Energy, May 2014, Boulder, Colorado, USA. *E3S Web of Conferences*

Paper 1

Kalvig, S., Gudmestad, O.T. and Winther, N. (2013) ‘Exploring the gap between ‘best knowledge’ and ‘best practice’ in boundary layer meteorology for offshore wind energy’. *Wind Energy*, 17: 161–171. doi: 10.1002/we.1572

Exploring the gap between 'best knowledge' and 'best practice' in boundary layer meteorology for offshore wind energy

Siri Kalvig[1,2], Ove Tobias Gudmestad[1] and Nina Winther[2]

[1]The Department of Mechanical and Structural Engineering and Materials Science, University of Stavanger, 4036 Stavanger, Norway

[2]StormGeo, Lagårdsveien 73, 4010 Stavanger, Norway

Abstract

Onshore wind turbine technology is moving offshore, and the offshore wind industry tends to use larger turbines than those used over land. This calls for an improved understanding of the marine boundary layer. The standards used in the design of offshore wind turbines, particularly the rotor-nacelle assembly, are similar to those used for onshore wind turbines. As a result, simplifications regarding the marine boundary layer are made. Atmospheric stability considerations and wave effects, including the dynamic sea surface roughness, are two major factors affecting flow over sea versus land. Neutral stratification and a flat, smooth sea surface are routinely used as assumptions in wind energy calculations. Newly published literature in the field reveals that the assumption of a neutral stratification is not necessarily a conservative approach. Design tests based on neutral stratification give the lowest fatigue damage on the rotors. Turbulence, heat exchange and momentum transfer depend on the sea state, but this is usually ignored and the sea surface is thought of as level and smooth. Field experiments and numerical simulations show that during swell conditions the wind profile will no longer exhibit a logarithmic shape and the surface drag relies on the sea state. Stratification and sea state are parameters that can be accounted for, and they should therefore be considered in design calculations, energy assessments and power output predictions.

Keywords:

Marine Atmospheric Boundary Layer, Atmospheric Stability, Sea Surface Roughness, Wind-Wave Interactions, Offshore Wind Turbine

1) Introduction

Offshore wind energy is a growing business and there will be vast investments in offshore wind technology in the near future [1]. Although offshore wind technology has many similarities with wind energy on land, it is still recognized as an immature industry and there are special challenges associated with the offshore environment.

The development of an offshore wind site can be divided into five different stages: financial decision and site selection, design and fabrication, installation, operation and maintenance, and decommission. Offshore wind resource assessments, as part of the first stage, are essential to exploit the economical potential and to choose the right technological solutions. Metocean

conditions[1] then need to be investigated in order to give guidance on the general metocean climate and hence the potential energy outcome for a planned park. The assessment process can be further divided into an evaluation of wind resources at a regional scale and a more detailed site-specific evaluation of local wind characteristics and turbulence [2]. For installation and decommission, the metocean conditions need to be forecast in order to find appropriate time windows for the different weather-sensitive installations or decommission operations. Also day-to-day metocean conditions need to be forecast with high accuracy and services must be tailored to specific operations, i.e. tuning the daily operation of the farm, planning maintenance work and reporting expected power output to the market.

The offshore wind industry therefore relies on accurate *assessments* of the site-specific metocean climate and also on *forecasts* of the same metocean conditions under installation and decommission as well as in the operational modus. The different stages of the wind industry are closely linked to each other. Forecast methods are sometimes used in the assessment and design phase (such as hindcast models), and the forecasting requirements are again highly influenced by the assessments and the design guidelines. As stated in the latest NEK IEC 61400-3 standard (Wind Turbines – Part 3: Design Requirements for Offshore Wind Turbines, hereafter named IEC 61400-3) [3], issued in 2009, it is also important to assess the wave climate and other oceanographic features. Hence extensive knowledge of the geophysical processes in the marine atmospheric boundary layer (MABL) is essential in all five stages.

The aims of this paper are to highlight the major simplifications made with regard to the MABL in the governing standards for the offshore wind industry, and to some extent indicate the implications of these simplifications. In doing so, the paper explores the gap between 'best knowledge' (science) and 'best practice' (codes, standards). A successful outcome from the major investment in the growing offshore wind industry requires a better understanding of geophysical processes in the MABL as well as an increased knowledge of how offshore wind turbines respond to changing atmospheric stratification and the sea state.

2) Boundary layer simplifications in the governing standards

The boundary layer over land and sea has different characteristics and the large heat capacity of the ocean is one important reason for the differences. When cold/warm air outbreaks from land take place over warmer/colder sea this can result in severe vertical atmospheric temperature gradients that are not common over land [4]. The sea surface can also be thought of as a 'dynamical roughness', where the changing sea state results in different levels of roughness. There has been significant investment in experimental work in the Baltic Sea to investigate how the sea state influences the atmospheric heat and momentum fluxes in the MABL; see e.g. [5, 6]. The wave boundary layer (WBL) is defined as the layer directly influenced by the waves and is of the order of one metre [7, 8]. A common assumption is that the same theories that are applied over land should also be valid over sea provided there is a shallow WBL. Rutgersson et al. [5] studied measurements from Östergarnsholm in the Baltic Sea and found that the atmospheric layer directly or indirectly influenced by the waves was considerably deeper than the WBL and that the atmospheric stability was influenced by swell. MABL research has demonstrated several cases where the much-used Monin-Obukhov

[1] The term 'metocean' is here used as an abbreviation for 'meteorological and oceanographic'.

similarity theory does not hold; see e.g. [5]. This is further highlighted in sections 3 and 4, but we first present a short summary on how the MABL processes are parameterized in the governing standards that are used in the offshore wind industry.

Det Norske Veritas (DNV), the Germanischer Lloyd (GL) and the International Electro-technical Commission (IEC) have each developed guidelines and standards for the offshore wind energy industry [9, 10], but there is no specific standard development on technology qualification for offshore wind farm technology, such as there is for the more mature oil and gas industries [11]. Until 2009 offshore wind turbines were designed according to national design rules in addition to international standards for the wind industry. The IEC 61400-3 wind turbine standard, which was released in 2009, specifically addressed the design requirements for fixed offshore wind turbines [3]. Waves, currents, sea ice and marine growth (surface layer caused by plants, animals and bacteria) were new features that needed to be addressed in design situations for an offshore wind turbine compared to an onshore turbine. In general the standards require that a structural dynamic model is used to determine the load effects for all relevant combinations of external conditions and the specified design load cases. External conditions that are particular to the offshore environment are only regarded as important for the supporting structure of the turbine. According to IEC 16400-3, the engineering integrity of the rotor-nacelle assembly is regarded as covered by the basis of IEC 16400-1 [12]. The same turbine classes used onshore are also used offshore, and these are defined in terms of wind speed and turbulence. Nevertheless, IEC 61400-3 states that it should be demonstrated that the offshore site-specific external conditions do not compromise the structural integrity.

In order to perform the analysis for the load cases specified by IEC 61400-3, the designer has to use data from a site-specific metocean database. Such a database can be established from site-specific measurements or by hindcasting (numerical simulations − forecast models run in historical modus). In IEC 64100-3, waves and sea currents are not regarded as important for the design of the rotor-nacelle assembly, and only the atmospheric condition is assessed in order to provide the design basis for this component. Both the normal and the extreme wind conditions need to be considered, and IEC 64100-3 refers to IEC 61400-1 for the estimation of the wind speed using the power law,

$$U(z) = U_{hub}\left(\frac{z}{z_{hub}}\right)^{\alpha}. \quad (1)$$

The average wind speed U(z) is expressed as a function of height, z, over the still water level[2], U_{hub} is the wind speed at the hub height z_{hub} and α is the power law exponent. Also the GL standard [13] refers to Equation (1) for wind speed estimations. The power law in Equation (1) has no explicit theoretical basis [14], and it is widely used in engineering applications because it is easy to work with. The DNV-OS-J101 [15] standards recommend using the logarithmic wind profile. The simplest expression of the wind profile in the surface layer is found in statically neutral conditions where atmospheric buoyancy effects are negligible. The surface layer is the bottom 10% of the boundary layer where the fluxes are assumed to vary

[2] For offshore purposes the inclination with the horizontal plane can be considered to be zero and U(z) is calculated over the still water level. According to the definition in NEK IEC 61400-3, the still water level is calculated by including the effects of tides and storm surge but excluding the height variations due to waves.

little with height [16]. Under neutral conditions the Monin-Obukhov similarity theory leads to the logarithmic wind profile [16],

$$U(z) = \left(\frac{u_*}{k}\right) \ln\left(\frac{z}{z_0}\right), \tag{2}$$

where k = 0.4 is the von Kármán's constant (see [17] for a evaluation of k) and z_0 is the roughness length. z_0 corresponds to the height above the surface where the mean velocity is zero. $u_*$is the friction velocity and this is defined as [14, 16],

$$u_*{}^2 = \frac{\tau_0}{\rho}, \tag{3}$$

where τ_0 is the force per unit area exerted by the ground surface on the flow and ρ is the density of the air. In DNV-OS-J101 [15] reference is made to DNV-RP-C205 [18] for inclusion of a stability correction of wind profiles (see section 3). Equations (1) and (2) are widely used in wind energy technology and often for heights beyond the surface layer where the Monin-Obukhov similarity theory does not hold. This may lead to inaccurate wind speed estimations [19]. The roughness length, z_0, can be derived from wind speed measurements, and the literature contains different recommendations for selection of z_0 for different surfaces [20].

The turbulent wind field can be approximated by the use of a turbulence model. Both the GL standard [13] and the IEC 16400-3 refers to IEC 16400-1 for descriptions of the turbulence models necessary for design load calculations. IEC 61400-1 and also the DNV guidelines' recommended turbulence models assume neutral atmospheric conditions and Gaussian statistics [9]. For the estimation of the turbulence intensity, I, the standards and guidelines recommend using measured de-trended data.

$$I = \sigma_1/U, \tag{4}$$

where σ_1 is the standard deviation of the mean wind speed U (the subscript 1 refers to the along-wind direction). In the absence of measurements, the different standards refer to different empirical relationships, and IEC 61400-3 recommends expressing the surface roughness by the use of the Charnock relation [21] and then employing this for the calculation of turbulence intensity. Coherent (or organized) turbulence structures can develop in stable atmospheric stratifications and impact the dynamic response of wind turbines [22]. These effects are currently not taken into consideration in the governing offshore wind standards [9]. A more detailed elaboration regarding measured turbulence intensity over the sea surface versus estimated values following the different guidelines can be found in [9, 23].

The Charnock relation expresses the dependence of roughness length on the surface stress,

$$z_0 = \frac{A_c u_*^2}{g}, \tag{5}$$

where g is the acceleration due to gravity and the empirical constant A_c is the Charnock parameter. Note that IEC 16400-3 refers to A_c as a constant; in open sea it is recommended to be 0.011 and for near coastal waters 0.034 [3]. Charnock himself regarded A_c as a constant, but later studies have revealed that A_c is dependent on the sea state; see e.g. [8, 24].

For selections of which turbine classes to use for a specific site, IEC 61400-3 refers to IEC 61400-1. The turbine classes are defined in terms of the U_{ref} (reference wind speed averaged over 10 min) and I_{ref} (expected turbulence intensity at 15 m/s) [12]. In order to choose the correct turbine classes, a designer has to estimate the appropriate $I_{ref.}$ This is, to a great extent, based on the same methods that are used to determine turbulence intensity over land. Again, the sea surface is regarded as smooth and level. The question is whether this gives the correct 'picture' of the turbulence to which an offshore wind turbine will be exposed.

To summarize: for a prediction of the vertical wind profile, the governing offshore wind industry standards rely on the power law or the logarithmic wind profile expression, and the form used in IEC 61400-3, DNV-OS-J101 and in the GL standard is only valid under neutral atmospheric stratification in the surface layer. The design requirement for offshore wind turbines uses wind turbine classes originally defined over land. The Charnock relation is used to some extent for the estimation of the sea roughness, but there is no consideration of how the sea state itself can affect the wind profile and the turbulence in the MABL. The differences in the momentum and heat fluxes over sea versus land and how these differences affect the rotor-nacelle assembly are not currently taken into account.

3) The role of atmospheric stability

Wind measurements are sparse and more expensive offshore compared to those onshore, and the use of wind calculations and wind models as substitutes for wind measurements is more frequent offshore than onshore. In stable and unstable atmospheric conditions, thermal effects influence the wind profile, and buoyancy and drag play an important role. According to the Monin-Obukhov similarity theory, the wind shear can be expressed with a non dimensional function, Φ_m, that scales with the atmospheric stability,

(6)

$$\frac{\partial U}{\partial z}\frac{kz}{u_*} = \Phi_m\left(\frac{z}{L}\right),$$

where L is the Obukhov length. The Obukhov length is a scaling parameter expressed as [16],

(7)

$$L = -\frac{\theta_v u_*^3}{kg\left(\overline{w'\theta_v'}\right)_s},$$

where θ_v and θ_v' are the mean virtual potential temperature and the corresponding fluctuating component, respectively, and w' is the fluctuating component of the vertical wind. L expresses the relation between mechanical or shear turbulent production and buoyant turbulent production. The ratio z/L can be described as a surface layer stability scaling parameter and its sign is related to static stability. $z/L > 0$ corresponds to stable atmospheric stratification, and $z/L < 0$ corresponds to unstable stratification. The integration of Equation (6) gives the following empirical expression for the non neutral wind profile (see i.e. [25, 26, 27]),

(8)

$$U(z) = \frac{u_*}{k}\left[\ln\left(\frac{z}{z_0}\right) - \psi_m\left(\frac{z}{L}\right)\right],$$

where ψ_m is the extension of the logarithmic wind profile to account for stability. Φ_m and ψ_m are empirical relations and have been estimated from various field experiments (see historical survey of Foken [27]). A table of original and modified empirical expressions for Φ_m and ψ_m can be found in Högström [17, 28]. For near neutral condition z/L=0, and Equation (8) is reduced to the logarithmic wind profile (Equation (2)).

Both energy yield and fatigue damage differ when atmospheric stability is taken into consideration. Lange et al. [29] and Motta et al. [30] concluded that power output estimations significantly improve if stability is taken into account. A study by Sathe and Bierbooms showed that using the log law or the power law as a basis for fatigue simulations is not a conservative approach [31]. Fatigue calculations for the blade root were carried out at two different sites, Vindeby and Rødsand, in coastal waters south-east of Denmark. Atmospheric stability distributions at Vindeby and Rødsand have also been studied by Motta et al. [30]. Fatigue load simulations using different atmospheric stability distributions were compared with simulations which assumed the logarithmic wind profile and power law. As an example: lifetime fatigue damage was calculated to be nearly 25 times higher when considering stability classes instead of only neutral stability. Sathe and Bierbooms [31] used only simulations for steady conditions and neglected turbulent winds. Their study indicated that stable conditions give rise to higher fatigue damage than neutral conditions, and they concluded that a full-scale fatigue damage study using turbulent winds and real data was therefore needed.

Eliassen et al. [32] recently performed similar studies to those of Sathe and Bierbooms, but they included the effect of turbulence and stability. They used data from the FINO3 platform in the North Sea and performed a time-domain analysis of the structural response of the wind turbine. They found that the inclusion of atmospheric stability resulted in increased fatigue loading. When the effect of atmospheric stability was accounted for, the damage equivalent load of the rotor blade increased by a factor of 1.4 [32].

The offshore wind industry tends to use larger wind turbines than are used over land, hence there is a need for accurate calculations of wind profiles over 60-100 m in height. The precision of wind calculations differs according to different stability classes and the height over the surface layer. Gryning et al. [19] proposed a model for the calculation of the wind profile for the entire boundary layer over homogeneous terrain. Later, Peña et al. developed the model for extension of the wind profile beyond the surface layer in the marine boundary layer [33]. This study concluded that for neutral and unstable atmospheric conditions the height of the boundary layer could be neglected. Therefore the wind profile expressions based on the Monin-Obukhov similarity theory hold, and the simplified wind profile expressions (Equations (2) and (8)) are in good agreement with observations for neutral and unstable conditions. For stable conditions the height of the boundary layer needs to be included. In these situations the simplified expressions based on the Monin-Obukhov theory tend to overestimate the wind speed at a height of over 30-40 metres; better estimations were achieved by using a correction to account for the height of the boundary layer [33]. Bathelmie et al. [34] looked at the role of humidity fluxes on offshore wind profiles at Anholt and Nysted. They found that including humidity in the calculation of L was highly relevant under moderately stable conditions.

The governing standards [3, 12, 13, 15, 18] for the offshore wind industry use simplified models for wind profile estimations, although the literature suggests different approaches to

account both for stability and for the influence of the height of the boundary layer; see i.e. [30, 33]. By using slightly more complex expressions, more realistic design tests and power estimations can be performed.

4) Wave-induced wind

In the MABL the wind influences the waves and vice versa. Wind-waves (characterized by short periods and relatively low phase speed) are aligned with the local wind. Swell (characterized by longer periods and faster phase speed) are waves that have propagated away from the source origin, and the local wind direction is not always correlated with the swell direction. Recent wave climate studies have shown that the wind and waves are often in a state of nonequilibrium with misaligned surface wind and waves [35] and that the global wave field is dominated by swell [36]. For a long time wave-driven wind has been thought of as a peculiarity, and the impact on the dynamics of the atmosphere is often neglected [37]. Several studies have now identified that the influence of wave-induced wind alters the overall energy exchange between the sea and the atmosphere; see e.g. [5, 37, 38, 39]. Perhaps wave-wind interactions are also worth considering in the field of the offshore wind industry?

Only sparse detailed height quality measurements of wind and waves exist, but different field campaigns show that swell generates a wave-driven wind component that affects the momentum flux well above the WBL and extends far up into the MABL. Rutgersson et al., Semedo et al. and Smedman et al. have all given good overviews of the most important historical field experiments in this area [5, 37, 39], making reference to different Soviet ocean campaigns in the 1960s and 1970s and later those from Lake Michigan, the Baltic Sea and the Pacific Ocean. In addition to this, it is worth mentioning the CBLAST (The Coupled Boundary Layers and Air–Sea Transfer) campaigns in the Atlantic Ocean south of Martha's Vineyard in 2001 and 2003 [40] and the INTOA experiment in the Gulf of Tehuantepec in Mexico [41]. In Baltic Sea observations of swell propagating faster than the wind, a near surface wave-driven wind increase (in later publications often referred to as a near surface jet) was noted, as well as low net surface shearing stress [42], which is also observed in later field campaigns. Very few campaigns focus on swell opposing the wind field, but in 2005 the Gulf of Tehuantepec air-sea interaction experiment (INTOA) especially emphasized the effect of waves on the momentum flux that occurs when strong Tehuano winds[3] blow offshore against the Pacific Ocean long period swell. In moderate to strong wind with opposing swell conditions, the observed wind stress was consistently higher than that reproduced from commonly used relations [41].

Different numerical simulations have been carried out in order to simulate the observed wave effect on the wind field from the above-mentioned field campaigns. In 2000 and 2005 Sullivan et al. and Rutgersson and Sullivan used direct numerical simulation (DNS) with a focus on the turbulent structure and kinetic energy budgets over idealized waves [43, 44]. Later Sullivan et al. developed a large-eddy simulation (LES) with a two-dimensional sinusoidal wave, and identified flow responses for three cases: wind opposing swell, wind following swell and wind over a swell surface with no movement (stationary bumps). The simulation results showed a good correlation with the CBLAST campaigns [38]. The flow responses in the different cases were very different and 'fingerprints' of the surface wave

[3] Strong and persistent offshore winds that periodically blow across the Isthmus of Tehuantepec in southern Mexico.

extended high up in the MABL. Recently they also broadened their simulation by including a spectrum of resolved moving waves [45]. They introduced a more realistic sea surface, and the results from these simulations were in line with those from the simulations of a sinusoidal wave surface performed in 2008. However, the latest simulations indicated that the influence of swell on the wind is sensitive to the composition of the wave spectrum. In 2012 Nilsson et al. further explored the effect of wind following swell for different atmospheric stabilities using the LES set up in [38], and the results showed an increase in upward momentum flux during slightly unstable or convective conditions compared with neutral conditions [46].

The wave-wind interaction can be understood by studying the pressure field near the surface. The total surface stress can be divided into two parts: one linked to viscous stress and the other to the resultant stress from the pressure field in association with the wave slope. This latter part is called the form drag or form stress [47]. The pressure field can be thought of as the 'signal' of the form stress between the wave and the atmosphere, and it is a part of the total surface drag [38, 48]. The total wind stress over a surface can be parameterized as [16],

$$\tau = \rho C_D U^2 , \tag{9}$$

where C_D is the surface drag coefficient for the same height. A good parameterization of the wind stress is very important in atmospheric modelling and forms an important basis for both forecast and hindcast. The Coupled Ocean-Atmosphere Response Experiment (COARE) in 1992, under the Tropical Ocean-Global Atmosphere (TOGA) program [49], brought about the most frequently used algorithms for estimation of air-sea turbulent and radiative fluxes and bulk expressions for C_D. These algorithms were updated and verified in 2002 [50].

Sullivan et al.'s LES results in 2008 showed that, with low winds following the waves, nearly all measurements of C_D were less than those found in the COARE parameterization [38]. Often the C_D was found to be only 50% of the standard parameterization value in cases where winds were following the swells. In cases were winds were opposing the swells, C_D increased by more than a factor of four compared to a flat surface. These findings were in accordance with wind profile and turbulent kinetic energy investigations that used data from the Baltic Sea Swell Experiment (BASE) [39, 48]. In 2009 Semedo et al. proposed a different approach, which produced results in line with those of Sullivan et al. [37]. The effect of wind following swell was quantified by the wave damping parameter, and the correspondence between observed and model wind profiles was very good.

Recently, new knowledge from measurements and different numerical simulations has resulted in improved wave-atmospheric climate models, and also to some extent in mesoscale forecasting models. Finding that swell has different impacts in different areas, Carlsson et al. and Rutgersson et al. concluded that the impact of swell is not insignificant and should be taken into account when developing wave-atmosphere coupled climate models [51, 52]. Jenkins et al. employed a mesoscale atmospheric model and a spectral wave model, and the coupling method that they used was to exchange data between the atmospheric model and the wave model, hence altering the Charnock parameter [53]. Results from simulations with climate models and mesoscale forecasting models imply that wave-induced winds probably

have an effect on offshore wind resource assessments. More specifically, target modelling experiments need to be assigned in order to estimate quantatively what the specific impact on assessment will be.

Discussion:

What possible impact will these results have for design requirements and power harvesting in the offshore wind industry? The following is a discussion in respect of two different scenarios (wind following swell and wind opposing swell), in which it is assumed that an imaginary offshore wind turbine with turbine blades of 70 m and hub height of 100 m is placed in an area with frequent swell situations (this corresponds to the planned wind turbine testing in the Blyth area in the UK [54]). An assumption of the discussion in both scenarios is that the wind estimations are based either on a standard forecasting model or the use of a hindcast archive that parameterizes the sea surface in accordance with the COARE parameterization. Wakes are believed to be more persistent offshore than onshore due to the lower turbulence regimes that often are present in offshore wind sites [55]. Therefore the wakes are of particular importance offshore, and power losses under unfavourable wind directions can be significant in large wind farms [56]. It is not clear how the wave-induced wind will affect the wake, and, in the following discussion, which is primarily based on the Rutgersson et al., Sullivan et al. and Carlsson et al. works [5, 38, 51], the wake effects are neglected.

Wind following swell:

The drag coefficients will be significantly smaller than values reported in non-swell situations [5, 38, 51]. Some studies indicate that C_D will be approximately half the value estimated using COARE parameterization of C_D [38, 51]. This implies the likelihood that the calculated mean wind (from a standard forecasting model or hindcast archive) is lower than it really is. If light winds following swell is a frequent occurrence, then the design of the wind turbine could be based on too low a mean wind speed. There will be a low level jet near the sea surface; hence the vertical wind profile will not exhibit a logarithmic shape. Over the jet there will be less wind shear compared to a flat surface. The maximum wind speed in the low level jet could even be slightly higher than that of the geostrophic wind (in [38] the maximum wind speed at 20 m height was 0.5 m/s more than that of the geostrophic wind). The wind shear between 30 m and 170 m (the swept area of the rotor) can be negative, and this corresponds to the fact that the wind will be stronger in the near surface level because of the formation of the low level jet. The shear between the surface and the top of the MABL will be reduced, and hence the turbulence-creating mechanism could be greatly suppressed, which could lead to a turbulence collapse in the overall MABL. The turbulent kinetic energy and the turbulence intensity will be smaller compared to those of wind opposing swell, or compared to those of wind over a flat surface (no waves). The low level jet could represent unharvested wind energy. If light winds following swell incidents are frequently occurring it is possible that the wind turbine will be exposed to larger mean wind and greater fatigue damage than it is designed for.

Wind opposing swell:

This scenario is less investigated in the literature than the case of wind following swell, but there are indications that C_D will increase [38, 41], sometimes by more than a factor of four compared to a flat surface [38]. This implies that the calculated mean wind will be higher than it really is. Since the wind is more 'effectively' retarded by the opposing swell, there will also be a higher wind shear than is the case with a flat surface. Swells opposing surface winds generate turbulence variances larger than those over a flat surface. If light wind opposing swell incidents occur frequently, the real energy harvesting will be less than was assumed to be the case in the assessment phase. An important question is whether the feature of increased wind shear and turbulence intensity under wind opposing swell incidences will exist during a higher wind regime. In [41], moderate to strong winds and opposing swell were observed in the Gulf of Tehuantepec in Mexico, and the observation shows that under 7 m/s the neutral drag coefficient at 10 m height, $C_{D10N,}$ tends to decrease with increasing winds. Over 7 m/s there is a reduced scatter and a linear increase in C_{D10N}, but overall the values for C_{D10N} were higher than those reproduced from commonly used relations. The Gulf of Tehuantepec in Mexico has a favourable climate for the formation of winds propagating against swell. Nevertheless, it is reasonable to think that strong winds can develop opposite a fast moving swell in other areas relevant for offshore wind energy, for example in a situation where a storm suddenly develops or in strong wind outbreaks from land. In these cases it is probable that there is strong wind (12-20 m/s) over fast moving waves (swell, with phase speed over 12 m/s). Sudden strong winds could appear in connection with a polar low[4], and the wind could rapidly, i.e. within less than half an hour, increase to gale force (20 m/s), allowing insufficient time to moderate the wave field. In situations like this it is likely that damaging forces on the rotor-nacelle assembly could occur, along with fatigue damage, potentially leading to damage and increased torque on gear boxes.

Some studies conclude that the effect of changing sea surface roughness is not important for wind resource assessment [29, 30]. These studies have been based on wind profiles in the Danish Baltic Seas, where the wave climate is not necessarily representative of the wave climate at more exposed offshore locations typical of proposed offshore wind parks in the North Sea. These sites are exposed to a rougher wave climate and more frequent swell situations [35, 36]. The dynamics of wind and current coupled to surface waves are reviewed in [57], in which it is stated that, although surface waves and turbulent boundary layers are mature scientific subjects, we do not fully understand their mutual relationships but are in the midst of rapid progress in the understanding. What impact the mutual relationship will have for offshore wind energy is even less understood. It is still too early to conclude what specific implications wave-induced wind will have on design considerations and energy harvesting for the offshore wind industry. This is especially true with regard to the impact of wind cross or counter to swell, as this is only briefly described in the literature. The importance of wave-induced wind for wind energy harvesting and for design considerations should be studied further; possible future studies in this field could be:

- A study of the frequency of different wind-swell regimes at certain offshore locations in order to be able to indicate whether the effect of wave-induced winds is relevant to and significant for the offshore wind industry. There is a need for studying real load cases and real production data from offshore wind farms.

[4] Polar low is small-scale intense low pressure. It normally forms in convective unstable air masses and is often associated with cold air outbreaks from ice-covered Arctic areas over warmer sea. Polar lows can rapidly propagate southwards and sometimes extend to the southern part of the North Sea.

- Numerical simulations should be carried out with different wave states and wind speeds in order to investigate which combinations could significantly influence design requirements and power output from offshore wind turbines.

- To discover whether the effects from swell opposing wind can exist in a higher wind regime and to perform detailed studies to determine whether the increased surface drag and the increased turbulence intensity in cases of wind opposing swell can be damaging to the turbine, in particular to bearings and gears.

- There are industry demands for high quality forecasts with better spatial and temporal resolution. One should clarify whether and how improved models including enhanced wave state effects can give better forecasts and hindcasts relevant to the offshore wind energy field. One should also further investigate whether it is worthwhile developing operational forecasts for wave-induced wind situations one to ten days ahead.

5) Summary

The boundary layer over the sea is quite different from that over land, particularly because of the difference in the exchange of momentum and heat fluxes. The governing standards used in the offshore wind industry rely heavily on experience and practice over land. In our opinion there is a gap between 'best knowledge' (science) and 'best practice' (codes, standards) and there is a need for improved guidance on the impact that atmospheric stability and wave-wind interaction in the MABL can have on the offshore wind industry.

An accurate estimation of the wind profile is important for design purposes, wind energy assessment, operational production and for day-to-day power output estimations. Today several simplifications are used regarding the calculation of the wind profile. The most common simplification is to assume neutral stratified atmosphere and a constant roughness length, representing a very smooth surface.

Recent studies have shown that stability needs to be accounted for in relation to improved energy estimation and also for structural design analysis; see [30, 31, 32]. The assumption of a neutral atmosphere is not always a conservative approach, and design considerations should, as a rule, be based on conservative approaches. Atmospheric stability can be accounted for in design calculations by the use of diabatic wind profile expressions, and there are also methods of extending the wind profile calculations beyond the surface boundary layer [33]. It might be worth conducting a survey regarding the occurrence of the different stability classes in the general assessment procedure when planning a new wind farm. Atmospheric stability is a parameter that weather forecasters can provide information about days ahead if they use a high-resolution forecast model. The ability to predict the atmospheric stability depends on the different planetary boundary layer schemes[5] used, but assuming that the recommended scheme is utilized, an atmospheric stability forecast could possibly give the wind farm operator more accurate power production estimates [58].

[5] In order to simulate the MABL, the different numerical weather forecast models use a variety of paramaterizations of the physical processes in the boundary layer. These different parameterizations, or schemes, are called planetary boundary layer schemes.

Stability considerations can be accounted for relatively easily in design calculations and energy output estimates, but it is perhaps more complicated to comprehend the fact that the wind profile, turbulence and the heat and momentum fluxes are dependent on the state of the wave field; see [5, 37, 38, 39]. Assessments are sometimes based on a site-specific metocean database, and this is often created by the use of numerical models (hindcasts). Normally the sea state dependent energy exchange in the atmosphere is not well captured in these models and the assessment can result in inaccurate estimates of mean wind and turbulence characteristics. Swell can result in both higher and lower effective surface drag. It is likely that swell can create different wind shear and turbulence characteristics so that a wind turbine site will be exposed to other external environmental conditions than those it was designed for. To further clarify the possible impact this wave-induced wind has on offshore wind turbines, more detailed studies are required, and it will be important to investigate whether even higher turbulence intensities will occur if a stronger wind is opposing swell.

An improved two-way coupling of the ocean and atmospheric models will give better estimates of the momentum and heat flux exchange, and such a forecasting set-up will be important for the growing offshore wind industry. In the future the governing international standards should also be improved by including a better representation of the actual geophysical processes that take place between the sea surface and the atmosphere to ensure the structural integrity of the wind turbine facilities.

Acknowledgements

This work was made possible partly by funding from the Regional Research Fund, the Industrial PhD-program (Norwegian Research Council) and StormGeo. The work is also a part of the Norwegian Centre for Offshore Wind Energy (NORCOWE) under grant 193821/S60 from the Research Council of Norway (RCN). NORCOWE is a consortium with partners from industry and science, hosted by Christian Michelsen Research. We would also like to thank the reviewers for their thoughtful comments and suggestions that extensively improved this publication.

References

1. European Commission. Press release, Commission welcomes adoption of climate and energy. 23 April 2009, Brussels.

2. Sempreviva A, Barthelmie R, Pryor S. Review of methodologies for offshore wind resource assessment in European seas. *Surveys in Geophysics* 2008; **29(6)** : 471-497. DOI: 10.1007/s10712-008-9050-2

3. NEK IEC 61400-3. Wind Turbines – Part 3: Design Requirements for Offshore Wind Turbines. 2009.

4. Kristjánsson JE, Barstad I, Aspelien T, Føre I, Godøy Ø, Hov Ø, Irvine E, Iversen T, Kolstad E, Nordeng TE, McInnes H, Randriamampianina R, Reuder J, Saetra Ø, Shapiro M, Spengler T, and Ólafsson H. The Norwegian IPY-THORPEX: Polar lows and Arctic

fronts during the 2008 Andøya campaign. *Bulletin of the American Meteorological Society* 2011; Preliminary accepted version.

5. Rutgersson A, Smedman A-S, Högström U. Use of conventional stability parameters during swell. *Journal of Geophysical Research* 2001; **106(C11)** : 27, 117-27, 134. DOI:10.1029/2000JC000543

6. Smedman A-S, Tjernström M, Högström U. The near-neutral marine atmospheric boundary layer with no surface shearing stress: A case study. *Journal of Atmospheric Sciences* 1994; **51** : 3399-3411. DOI:10.1175/15200469(1994)051<3399:TNNMAB>2.0.CO;2

7. Janssen PAEM. Wave-induced stress and the drag of air flow over sea waves. *Journal of Physical Oceanography* 1989; **19** : 745-754.

8. Janssen PAEM. *The Interaction of Ocean Waves and Wind*. Cambridge University Press: New York, 2004.

9. Obhrai C, Kalvig S, Gudmestad OT. A review of current guidelines and research on wind modeling for the design of offshore wind turbines. *The 22nd International Ocean and Polar Engineering Conference*, Rhodes, Greece, June 17-22, 2012.

10. Saiga RK, Dolan D. Comparison of design guidelines for offshore wind energy systems. Conference paper. *Offshore Technology Conference* 2007.

11. Samarakoon SMSMK, Gudmestad OT. On the necessity of technology qualification in the offshore wind energy industry. *Proceedings of the ASME 2011 30th International Conference on Ocean, Offshore and Arctic Engineering* 2011.

12. NEK IEC 61400-1. Wind Turbines – Part 1: Design Requirements. 2005.

13. Germansher Lloyds. Guideline for the Certification of Offshore Wind Turbines. Ed 2005.

14. Holmes JD. *Wind Loading of Structures*. Taylor & Francis: Oxon, New York, 2007.

15. DNV-OS-J101. Design of Offshore Wind Turbine Structures. September 2011.

16. Stull RB. *An Introduction to Boundary Layer Meteorology*. Atmospheric and Oceanographic Sciences Library, Springer: Vancouver, 1988.

17. Högström U. Review of some basic characteristics of the atmospheric surface layer. *Boundary-Layer Meteorology* 1996; **78** : 215-246. DOI: 10.1007/BF00120937

18. DNV-RP-C205. Environmental Conditions and Environmental Loads, 2010.

19. Gryning S-E, Batchvarova E, Brümmer B, Jørgensen H, Larsen S. On the extension of the wind profile over homogeneous terrain beyond the surface boundary layer. *Boundary-Layer Meteorology* 2007; **124(2)** : 251-268. DOI: 10.1007/s10546-007-9166-9

20. Barthelmie R J, Palutikof JP, Davies TD. Estimation of sector roughness lengths and the effect on prediction of the vertical wind speed profile. *Boundary-Layer Meteorology* 1993; **66 (1-2)** : 19-47. DOI: 10.1007/BF00705458

21. Charnock H. Wind stress on a water surface. *Quarterly Journal of the Royal Meteorological Society* 1958; **81** : 639-640.

22. Kelley ND, Jonkman BJ, Scott GN, Bialasiewicz JT, Redmond LS. The impact of coherent turbulence on wind turbine aeroelastic response and its simulation. *Conference paper,* NREL/CP-500-38074, August 2005.

23. Türk M, Emeis S. The dependence of offshore turbulence intensity on wind speed *Journal of Wind Engineering and Industrial Aerodynamics* 2010; **98**: 466-471.

24. Smedman A, Larsén X, Högström U, Kahma K, Petterson H. Effect of sea state on momentum exchange over the sea during neutral conditions. *Journal of Geophysical Research* 2003; **108(C11)** : 3367. DOI: 10.1029/2002JC001526

25. Businger JA, Wyngaard JC, Izumi Y, Bradley EF. Flux-profile relationships in the atmospheric surface layer. *Journal of the Atmospheric Sciences* 1971; **28**: 181-189.

26. Dyer AJ. A review of flux-profile relationships. *Boundary-Layer Meteorology* 1974; **7(3)** : 363-372.

27. Foken T. 50 Years of the Monin–Obukhov Similarity Theory. *Boundary-Layer Meteorology* 2006; **119**, 431-447. DOI 10.1007/s10546-006-9048-6

28. Högström U. Non-dimensional wind and temperature profiles in the atmospheric surface layer: A re-evaluation. *Boundary-Layer Meteorology* 1988; **42** : 55-78. DOI: 10.1007/BF00119875

29. Lange B, Larsen S, Hojstrup J, Barthelmie R. Importance of thermal effects and sea surface roughness for offshore wind resource assessment. *Journal of Wind Engineering and Industrial Aerodynamics* 2004; **92(11)** : 959-988. DOI:10.1016/j.jweia.2004.05.005

30. Motta M, Barthelmie RJ, Volund P. The influence of non-logarithmic wind speed profiles on potential power output at Danish offshore sites. *Wind Energy* 2005; **8(2)** : 219-236. DOI: 10.1002/we.146

31. Sathe A, Bierbooms W. Influence of different wind profiles due to varying atmospheric stability on the fatigue life of wind turbines. *Journal of Physics* 2007; Conference Series 75. DOI:10.1088/1742-6596/75/1/012056

32. Eliassen L, Jakobsen JB, Obhrai C. The effect of atmospheric stability on the fatigue life of offshore wind turbines. *The 22nd International Ocean and Polar Engineering Conference*, Rhodes, Greece, June 17-22, 2012.

33. Peña A, Gryning S-E, Hasager CB. Measurements and modelling of the wind speed profile in the marine atmospheric boundary layer. *Boundary-Layer Meteorology* 2008; **129(3)** : 479-495. DOI: 10.1007/s10546-008-9323-9

34. Barthelmie RJ, Sempreviva AM, Pryor SC. The influence of humidity fluxes on offshore wind speed profiles. *Annales Geophysicae* 2010; **28** : 1043-1052. DOI:10.5194/angeo-28-1043-2010

35. Hanley KE, Belcher SE, Sullivan PP. A global climatology of wind-wave interaction. *Journal of Physical Oceanography* 2010; **40(6)** : 1263-1282.

36. Semedo A, Sušelj K, Rutgersson A, Sterl A. A global view on the wind sea and swell climate and variability from era-40. *Journal of Climate* 2011; **24** : 1461-1479. DOI: 10.1175/2010JCLI3718.1

37. Semedo A, Saetra Ø, Rutgersson A, Kahma KK, Pettersson H. Wave-induced wind in the marine boundary layer. *Journal of the Atmospheric Sciences* 2009; **66** : 2256-2271.

38. Sullivan PP, Edson JB, Hristov T, McWilliams JC. Large-eddy simulations and observations of atmospheric marine boundary layers above nonequilibrium surface waves. *Journal of the Atmospheric Sciences* 2008; **65(4)** : 1225-1245.

39. Smedman A, Högström U, Sahlee E, Drennan WM, Kahma KK, Pettersson H, Zhang F. Observational study of marine atmospheric boundary layer characteristics during swell. *Journal of the Atmospheric Sciences* 2009; **66(9)** : 2747-2763. DOI: 10.1175/2009JAS2952.1

40. Edson J, Crawford T, Crescenti J, Farrar T, Frew N, Gerbi G, Helmis C, Hristov T, Khelif D, Jessup A, Jonsson H, Li M, Mahrt L, McGillis W, Plueddemann A, Shen L, Skyllingstad E, Stanton T, Sullivan P, Sun J, Trowbridge J, Vickers D, Wang S, Wang Q, Weller R, Wilkin J, Williams AJ, Yue DKP, Zappa C. The coupled boundary layers and air-sea transfer experiment in low winds. *Bulletin of the American Meteorological Society* 2007; **88(3)** : 341-356.

41. Ocampo-Torres F, García-Nava H, Durazo R, Osuna P, Díaz Méndez G, Graber H. The INTOA Experiment: A study of ocean-atmosphere interactions under moderate to strong offshore winds and opposing swell conditions in the Gulf of Tehuantepec, Mexico. *Boundary-Layer Meteorology* 2011; **138(3)** : 433-451. DOI: 10.1007/s10546-010-9561-5

42. Smedman A, Högström U, Bergström H, Rutgersson A, Kahma KK, Pettersson H. A case study of air-sea interaction during swell conditions. *Journal of Geophysical Research* 1999; 1**04(C11)** : 25,833-25,851. DOI:10.1029/1999JC900213

43. Sullivan P, McWilliams JC, Moeng CH. Simulation of turbulent flow over idealized water waves. *Journal of Fluid Mechanics* 2000; **404** : 47-85. DOI:10.1017/S0022112099006965

44. Rutgersson A-S, Sullivan PP. The effect of idealized water waves on the turbulence structure and kinetic energy budgets in the overlying airflow. *Dynamics of Atmospheres and Oceans* 2005; **38** : Issues 3-4. DOI:10.1016/j.dynatmoce.2004.11.001

45. Sullivan PP, McWilliams JC, Hristov T. Large eddy simulation of high wind marine boundary layers above a spectrum of resolved moving waves. *AMS 19th Symposium on Boundary Layers and Turbulence* 2010.

46. Nilsson EO, Rutgersson A, Smedman AS, Sullivan PP. Convective boundary-layer structure in the presence of wind-following swell. *Quarterly Journal of the Royal Meteorological Society* 2012. ; **138(667)**:1476-1489. DOI: 10.1002/qj.1898

47. Makin VK. A note on a parameterization of the sea drag. *Boundary-Layer Meteorology* 2003; **3** : 593-600. DOI: 10.1023/A:1021267703298

48. Högström U, Smedman A, Sahleé E, Drennan WM, Kahma KK, Pettersson H, Zhang F. The atmospheric boundary layer during swell: A field study and interpretation of the turbulent kinetic energy budget for high wave ages. *Journal of Atmospheric Science* 2009; **66** : 2764-2779. DOI: 10.1175/2009JAS2973.1

49. Webster PJ, Lukas R. TOGA COARE: The coupled ocean & atmosphere response experiment. *Bulletin of the American Meteorological Society* 1992; **73(9)** : 1377-1416.

50. Fairall CW, Bradley EF, Hare JE, Grachev AA, Edson JB. Bulk parameterization of air-sea fluxes: updates and verification for the COARE algorithm. *Journal of Climate* 2003; **16(4)** : 571-591. DOI: 10.1175/1520-0442(2003)016<0571:BPOASF>2.0.CO;2

51. Carlsson B, Rutgersson A, Smedman A-S. Impact of swell on simulations using a regional atmospheric climate model. *Tellus* 2009; **61A**: 527-538. DOI: 10.1111/j.1600-0870.2009.00403.x

52. Rutgersson A, Nilsson EO, Kumar R. Introducing surface waves in a coupled wave-atmosphere regional climate model: Impact on atmospheric mixing length. *Journal of Geophysical Research* 2012; **117**: C00J15. DOI:10.1029/2012JC007940.

53. Jenkins AD, Paskyabi MB, Fer I, Gupta A, Adakudlu M. Modelling the effect of ocean waves on the atmospheric and ocean boundary layers. *DeepWind*, Trondheim, NORWAY, 19-20 January 2012.

54. Wind Power Engineering. *Britannia Breaks the 9 MW Barrier*. http://www.windpowerengineering.com/construction/projects/britannia-breaks-the-9-mw-barrier/, 14 May, 2010.

55. Barthelmie R, Larsen G, Pryor S, Jørgensen H, Bergström H, Schlez W, Rados K, Lange B, Vølund P, Neckelmann S, Mogensen S, Schepers G, Hegberg T, Folkerts L, Magnusson M. ENDOW (efficient development of offshore wind farms): modelling wake and boundary layer interactions. *Wind Energy* 2004; **7(3)**: 225-245.

56. Barthelmie RJ, Hansen K, Frandsen ST, Rathmann O, Schepers JG, Schlez W, Phillips J, Rados K, Zervos A, Politis ES, Chaviaropoulos PK. Modelling and measuring flow and wind turbine wakes in large wind farms offshore. *Wind Energy* 2009; **12** : 431-444. doi: 10.1002/we.348

57. Sullivan PP, McWilliams JC. Dynamics of winds and currents coupled to surface waves. *Annual Review of Fluid Mechanics* 2010. DOI: 10.1146/annurev-fluid-121108-145541

58. Krogsæter O, Reuder J. Validation of boundary layer parameterization schemes in the weather research and forecasting model (WRF) under the aspect of offshore wind energy applications. *Boundary-Layer Meteorology* 2012; in review.

Paper 2

Kalvig. S., Manger, E. and Kverneland, R. (2013) ‘A method for wave driven wind simulations with CFD’, *Energy Procedia*, vol. 35, pages 148-156, ISSN 1876-6102, http://dx.doi.org/10.1016/j.egypro.2013.07.168.

DeepWind'2013, 24-25 January, Trondheim, Norway

A method for wave driven wind simulations with CFD

Siri M. Kalvig[ab*], Eirik Manger[c], Richard Kverneland[a]

[a] *University of Stavanger,4036 Stavanger, Norway*
[b] *StormGeo AS, Nordre Nøstekaien 1, 5011 Bergen, Norway*
[c] *Acona Flow technology AS, Uniongt. 18, 3732 Skien, Norway*

Abstract

A flexible open source based CFD method is developed in order to directly study the effects of the wave movement on the wind field in a neutral stratified atmosphere. Sea surface waves modify the wind field in the marine atmospheric boundary layer (MABL) in different ways. Long periodic waves (swell) resemble a sinusoidal wave. The flow responses over this sinusoidal wave are studied in detail by the use of a moving grid approach. Waves aligned with the wind and opposed the wind are studied. Simulations show that a fast moving swell aligned with the wind will speed up the wind in the lowest meters of the MABL, whereas a fast moving swell opposed to the wind field will reduce and even revert the wind speed in the lowest meters. Swell opposing the wind field will also generate more turbulence in the lowest meters of the MABL than when waves and wind are aligned with each other. The simulations are compared with a logarithmic wind profile and wave influence causes the wave induced wind profiles to deviate from the logarithmic shape, especially in the case where swell is opposing the wind.

Offshore wind energy; Marine atmospheric boundary layer; Wind wave interaction; CFD

1. Introduction

The ocean surface can be seen as a surface with a dynamical roughness. Different wave states give rise to different roughnesses and the associated effect of the wind field will be different according to different wave regimes. For a long time wave driven wind was looked upon as a peculiarity. It was commonly assumed that the wave influenced layer was limited to the lowest meter over the sea surface, the wave boundary layer (WBL), and its effect often neglected [1]. Different measurement campaigns have however revealed that under certain conditions the wave influence extends far beyond the WBL and affects the whole depth of the marine atmospheric boundary layer (MABL) [2]. These wave driven wind effects have also been simulated with various computational fluid dynamics (CFD) methods, ranging from early work in 2000 with direct numerical simulations (DNS) [3] to large eddy simulations (LES), including buoyancy effects, in 2012 [4].

* Corresponding author. Tel.: +47 91604181.
E-mail address: siri.m.kalvig@uis.no.

Through examination of the governing design standards in the field of offshore wind industry it is clear that the industry to a large extent relies on experience and practice over land, and does not take into consideration how the ever-changing waves affect the wind field [5, 6]. Even if it is well documented that the wave state affects the wind field several tens and also hundreds of meters over the sea level, it is still not clear if the effects of wave driven wind will be of any significance to the offshore wind industry.

This work is part of a project aimed at revealing if wave driven wind should be accounted for in wind turbine power estimates and wind turbine design. The objective of this paper is to develop a flexible model for testing how different wave states affect the MABL by the use of computational fluid dynamics (CFD). Once this has been established, wind turbine models can be introduced in the CFD domain over the moving wave surface, thereby allowing studies of wave influence on both wind turbine wake and on wind turbine performance.

2. Wave wind interactions

For both design calculations and power production estimates it is important to get an accurate estimate of the average wind, U(z), as a function of height z over the ground or the sea surface. Expression for this wind profile can be found by the use of Monin-Obukhov similarity theory (MOST). MOST is valid in the constant flux layer (where the fluxes are assumed to vary little with height). Under atmospheric neutral conditions MOST theory leads to the logarithmic wind profile [7];

$$U(z) = \left(\frac{u_*}{k}\right) ln\left(\frac{z}{z_0}\right), \tag{1}$$

where k = 0.4 is the von Kármán's constant, z_0 is the roughness length (defined as the height where the wind speed equals zero) and $u_*$is the friction velocity. The friction velocity is defined as [7],

$$u_*^2 = \frac{\tau_0}{\rho}, \tag{2}$$

where τ_0 is the force per unit area exerted by the ground surface on the flow and ρ is the density of the air. The roughness length, z_0, can be derived from wind speed measurements. The literature contains different recommendations for selection of z_0 for different surfaces. In the field of offshore wind industry the sea surface is generally considered as levelled and smooth, and therefore a low z_0 value of 0.0002 m is often chosen [8].

Wind waves and swells influence the wind field differently and the angle between the wind field and the ocean waves is also of great importance when studying the wave wind interactions. The wave age, χ_{10}, is a parameter that can be used to characterize the wind-wave regime. The wave age is the ratio between the phase speed of the peak of the wave spectrum (c_p) and the wind speed at 10 m (U_{10});

$$\chi_{10} = \frac{c_p}{(U_{10} cos\theta)}, \tag{3}$$

where θ is the angle between the wave field and the wind field. The wave height is here assumed to be relatively small compared with the water depth, and according to the dispersion relation the wave speed depends on the wave length. When χ_{10} is 1.2 the wave field is believed to be fully developed. A wind driven wave regime is characterised by $\chi_{10} < 1.2$ and a swell dominated wave field by $\chi_{10} > 1.2$ [9]. Several sea states are studied in [10] and in this paper more detailed studies are performed for a sea with $\chi_{10} = 2$ and $\chi_{10} = 1$.

3. Method and models

The open source CFD toolbox OpenFOAM [11] is used for both mesh generation and CFD computations. By using a moving grid approach, a swell like (sinusoidal) wave was implemented on the form;

$$z(x) = a\sin(\omega t - kx), \tag{4}$$

where a is wave amplitude, ω is angular frequency, t is time and k is the wave number. Each grid cell moves up and down, reaching their maximum elevation in different time increments according to a sinusoidal signal, and the movement looks like a wave propagating - much like the different particles in a real ocean wave. The wave will gradually fade in during 10 seconds of simulations. The wave will also gradually fade in 10 meter after the inlet and fade out 10 m before the outlet. This gradually developing wave (both in time and space) was implemented in order to ensure that the inlet and outlet grid part of the domain did not change form and also to ensure stable simulations. Wave speed (c), wave amplitude (a), wave length (L) are input parameters to the model. Since the wave is an idealised sinusoidal wave surface, with no variation in the y-direction, only two-dimensional effects are studied. Nevertheless the CFD set up is three dimensional, but with only few cells in the y-direction. This is partly done in order to easily extend the work to include a wind flow angle to the wave direction. Currently only waves propagating along with the wind flow and directly opposing the wind flow are examined (θ=0).

The starting points of these CFD simulations are the Navier-Stokes equations and the continuity equation for an incompressible, Newtonian fluid [12];

$$\rho\left(\frac{\partial U}{\partial t} + U\cdot\nabla U\right) = -\nabla \mathrm{p} + \mu\nabla^2 \mathrm{U} \tag{5}$$

$$\nabla U = 0, \tag{6}$$

where U is the velocity vector, p is the pressure and μ is the dynamic viscosity.The simulations are only valid for a neutrally stratified atmosphere where no buoyancy effects are present. The Corioles force is also neglected.

Reynold Averaging is used on the Navier-Stokes equation and for turbulent closure the standard k-epsilon model [13] is used. This model includes two transport equations, one for turbulent kinetic energy (k) and one for the turbulent dissipation (ε). These are respectively defined as;

$$\mathrm{k} = \frac{1}{2}\left(\overline{\mathrm{u'^2}} + \overline{\mathrm{v'^2}} + \overline{\mathrm{w'^2}}\right), \tag{7}$$

$$\varepsilon = 2\nu\,\overline{\mathrm{S'_{ij}}\cdot\mathrm{S'_{ij}}}, \tag{8}$$

where u', v' and w' denotes the x-, y- and z-component of the fluctuation part of the velocity vector U and ν is the viscosity and $\mathrm{S'_{ij}}$ is the fluctuating deformation rate [12]. By introducing four model constants ($\sigma_k, \sigma_\epsilon, C_{1\epsilon}, C_{2\epsilon}$) the standard k-epsilon model reads [13];

$$\frac{\partial(\rho k)}{\partial t} + \nabla(\rho k U) = \nabla\left(\frac{\mu_t}{\sigma_k}\nabla k\right) + 2\mu_t S_{ij}\cdot S_{ij} - \rho\epsilon \tag{9}$$

$$\frac{\partial(\rho \varepsilon)}{\partial t} + \nabla(\rho \varepsilon U) = \nabla\left(\frac{\mu_t}{\sigma_\epsilon}\nabla \varepsilon\right) + C_{1\epsilon}\frac{\varepsilon}{k}2\mu_t S_{ij}\cdot S_{ij} - C_{2\epsilon}\rho\frac{\epsilon^2}{k} \tag{10}$$

This is a transient (time varying) simulation that uses the Reynold Averaging Navier Stoke approach so in short the method can be denoted unsteady RANS (or URANS).

4. Simulations and boundary conditions

First various sensitivity analyses were performed on a relatively small domain (length of 250 m, height of 50 m) where different wind velocities and sea states were studied. Only uniform wind was used as the inlet wind condition and detailed descriptions are given in [10].

Experiences from these simulations are then used when investigating the MABL in a larger domain, with length of 500 m and height of 100 m. For these simulations the method was further improved. A logarithmic wind profile was implemented as the inlet velocity (eq. 1) and the gradually developing wave was utilized. Four different cases are here presented and compared with each other and with the standard logarithmic wind profile used at the inlet.

The boundary conditions for velocity at the inlet and the parameters for the wavy ground patch are summarized in table 1. For the velocity on the ground patch (on the moving wave surface) the openFOAM specific boundary condition "movingWallVelocity" was used and at the top the movement was fixed to zero. This ensured that the pumping wave movements were transferred to the air flow. At the inlet the turbulent kinetic energy and the turbulent dissipation was uniformly distributed and fixed. All four simulation had starting value of k=0.5 and ε=0.015. This is a simplification of the reality where the turbulent kinetic energy will vary according to the wind velocity and height. During the computational time the simulations build up their own turbulent field (and the accompanying dissipation rates) and far downstream from the inlet, the boundary values are thought of as less important. Nevertheless a inlet k value of 0.5, together with a reference wind speed of 5 m/s, correlates to a turbulent intensity of approximately 11% [12] and this is believed to be within a realistic range for an offshore wind farm [5]. The rest of the boundary conditions were the same for all cases; at the top, the lateral sides and at the outlet of the computational domain the boundary conditions was "zeroGradient". Then the top and side walls did not influence the computations (the normal gradient of the field is zero at the boundary) and there was no change in the flow parameters on the outlet boundary. OpenFOAM specific wall-functions for turbulent kinetic energy, turbulent dissipation and turbulent viscosity where used with a roughness of the "wave-wall" that corresponds to a z_0 of 0.0002 m.

Table 1: Boundary conditions for velocity at the inlet and parameters for the wavy ground

Case	Logarithmic inlet conditions				Wave surface at ground patch		
χ_{10}	U_{Href} (m/s)	H_{ref} (m)	z_0 (m)	u_* (m/s)	a (m)	L (m)	c (m/s)
2 (aligned)	5	100	0.0002	0.15	3	40	8
2 (opposed)	5	100	0.0002	0.15	3	40	-8
1 (aligned)	10	100	0.0002	0.30	3	40	8
1 (opposed)	10	100	0.0002	0.30	3	40	-8

Since the wave is seen as a solid ground naturally no deformation of the wave surface due to wind forcing is captured. This is a major simplification of the reality and it is hence only possible to study wave induced wind and not wind wave interactions.

Changes in the resolution of the grid should not influence the results and grid independency tests were performed in [10] and the simulations are believed to be grid independent for velocity and nearly grid independent for turbulent kinetic energy for 12500 cells. A grid refinement towards the ground was used and this resulted in y+ (the non dimensional wall distance for wall bounded flows) values between 200 and 500. In order to calculate the boundary layer it is recommended to have $30 < y^+ < 500$ to model the

boundary layer properly [12]. The domain with length of 500 m and height of 100 m had 50 000 cells. Simulation periods of 500 seconds are believed to be sufficient to reach a “quasi”-steady state.

A simulation test, with a logarithmic inlet profile on an empty domain with a flat surface was performed, before executing the four cases in table 1. This was done in order to investigate if the code could sustain the logarithmic profile downwind the domain and this was the case.

5. Results

5.1. Sensitivity analyses

In [10] the wind at the inlet, U_{inlet}, were uniformly distributed and ranged from 5 m/s to 30 m/s. Simulations with waves aligned and opposed the wind field were performed and results are shown in figure 1 and 2. The wave had amplitude a = 3 m, wavelength L = 40 m, and wave speed c = +/- 8 m/s. The shape of the vertical profiles changes whether the flow is aligned with the waves or opposed to the waves. Note that only mean values of the horizontal component, Ux, are shown. Mean profiles were calculated over a simulation period of 25 sec (which corresponds to approximately one wave period) with the openFoam utility “fieldAverage”. This utility computes averages of each cell value for every time step. Since the applied inlet velocity was uniform and the “fieldAverage” utility unifies the profiles, the resulting simulated profiles are nearly constant over 20-30 meters. When comparing flow aligned with the wave and opposed to the wave the case with lightest wind propagating opposite to the wave deviates the most from a logarithmic shape. The opposed situation also generate higher turbulent kinetic energy levels than the aligned situations. Figure 3 shows different flow responses for four different wave states when the wind and wave oppose each other. The flow is clearly wave state dependent and the steepest wave seems to affect the flow field the most.

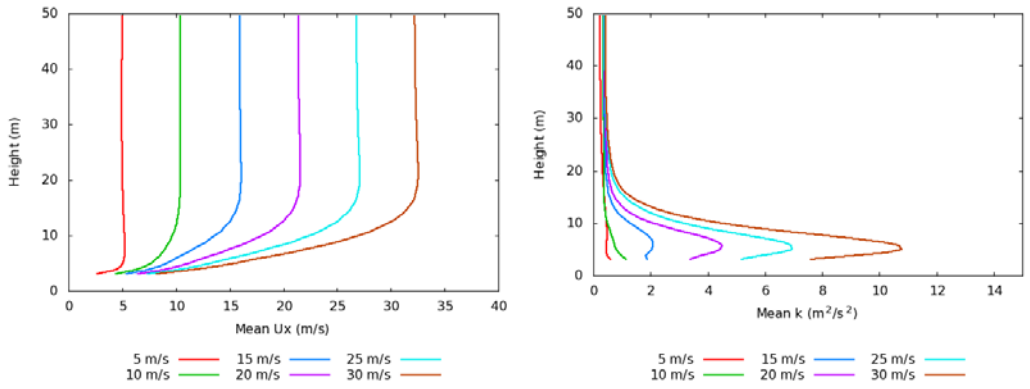

Figure 1: Wind aligned with waves: Vertical profile of mean values of the horizontal component of the wind flow and profiles of mean turbulent kinetic energy for six cases with different uniform inlet velocity.

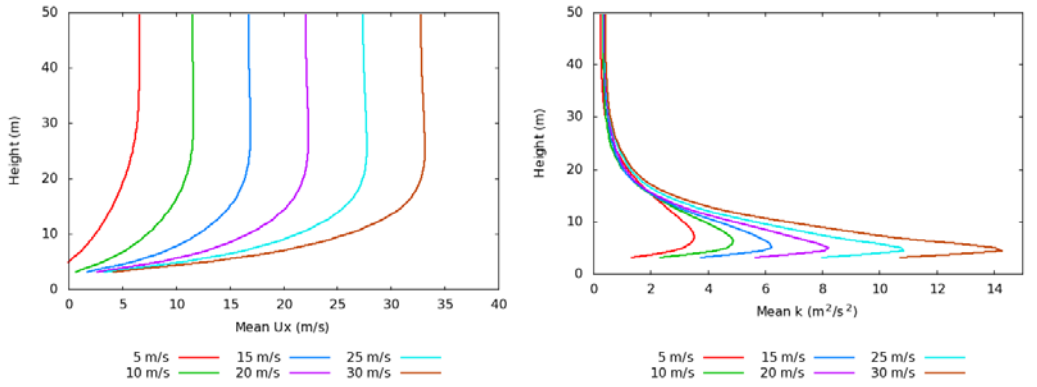

Figure 2: Wind opposed waves: Vertical profile of mean values of the horizontal component of the wind flow and profiles of man turbulent kinetic energy for six cases with different uniform inlet velocity.

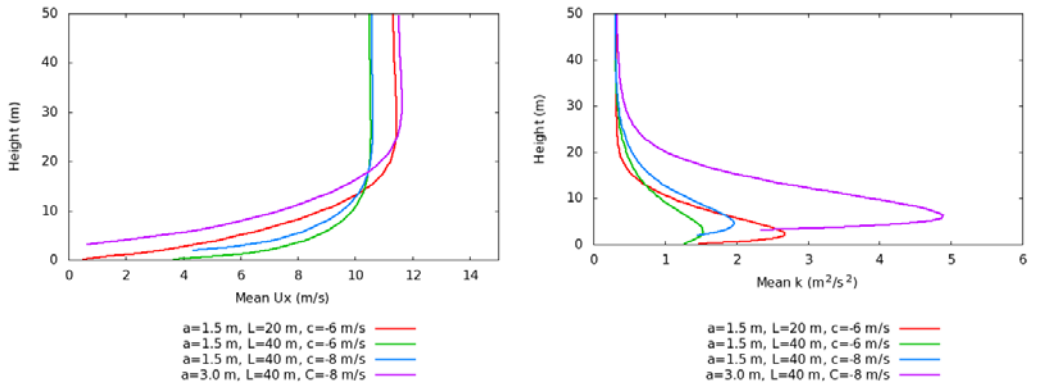

Figure 3: Wave opposed the wind field for various wave states. Uniform wind speed of 10 m/s at the inlet. Vertical profile of mean horizontal wind speed (left) and vertical profiles of mean turbulent kinetic energy (right).

5.2. Wind and wave aligned versus opposed

Based on the experience from the sensitivity study in 5.1, four cases were chosen to be investigated in more detail; in figure 4 wind profiles and turbulent kinetic energy profiles over waves with wave speed of +/- 8 m/s and wind flow at the inlet with U_{100m} of 5 m/s and 10 m/s are shown. This corresponds to absolute values of the wave age close to 2 and 1 (see table 1) because U_{10m} is 4.5 m/s and 8.1 m/s at the inlet. In the former case the wave is propagating faster than the wind, and in the latter case slower or equal to the wind. The resulting wind profiles are compared with the logarithmic velocity profile applied at the inlet. Only instantaneous velocity and turbulent kinetic energy profiles are shown. The profile will change according to where the profiles are located above the wave, but the pattern is repeatable for every wave length. In figure 4 profiles are plotted over 450-490 meters. This represents one wave length and curves are plotted for every 5 meter.

In the 2 wave age case the aligned situations shows a speed-up of the wind velocity up to a height of 25 meters. This is due to the fact that the high speed of the wave transfers momentum to the slower moving wind flow above the wave. Comparing the wind in the aligned situation with the inlet velocity, maximum speed up of 2.5 m/s occurred in approximately 2 meters height (occurring over the wave

trough, 470 meter downstream) and at 10 meter height this speed up was reduced to 1 m/s. At the same height the inlet velocity was 3.5 m/s. The wind velocity under the height of 37 meters is reduced in the case where wind and wave are opposing each other. Over this level the wind velocity exceeds the velocity of the logarithmic wind profile. In both the aligned and opposed situation the wind profile deviates from the logarithmic profile. The opposed situation deviates all the way up to the top of the domain. For heights less than 70 meters there is notably more turbulent kinetic energy when the wind and wave are opposed compared to the aligned case. Maximum turbulent kinetic energy levels occur in approximately 10 meters height with around 10 times more turbulent kinetic energy than in the same height for the aligned situation.

In the 1 wave age case the wind profile for the aligned situation seems to match quite well the logarithmic inlet profile, but with a slight deviation above 32 meter height. The speed up in the lowest meters was not as prominent as for the 2 wave age case. This illustrates that the relative difference in wave speed and wind speed is of importance. For the opposed situation the wind profiles have the same shape as in the 2 wave age case. Also the kinetic turbulent profiles show the same response as in the 2 wave age case. Maximum turbulent kinetic energy levels occur in approximately 5 meters height with around 30 times more turbulent kinetic energy than in the same height for the aligned situation. Compared to the 2 wave age case more turbulent kinetic energy is generated in the lowest meters due to the higher relative velocity – as a wave with speed of 12,5 m/s is now opposing the wind field of U_{100}=10 m/s.

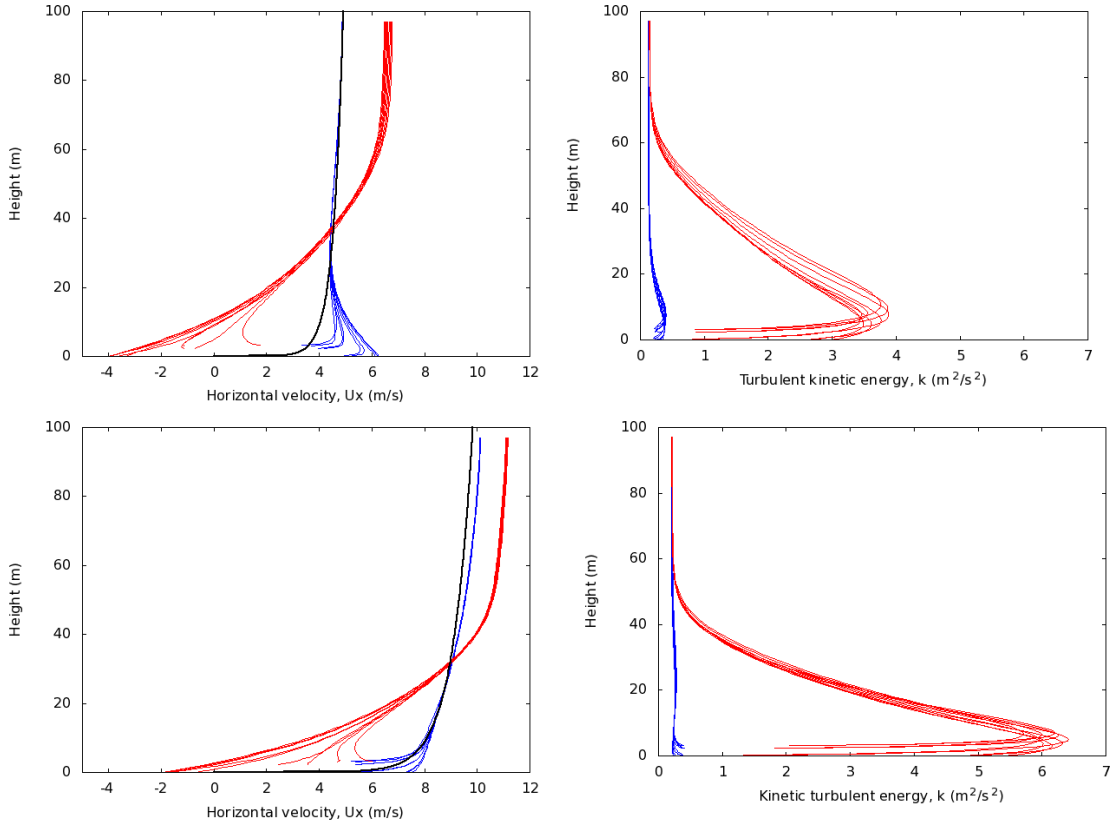

Figure 4: Turbulent kinetic energy profiles in the case of wind aligned with the wave (blue curves) and wind opposed with the wave (red curve) for simulations with U_{100m}=5 m/s at inlet and wave age 2 (top pictures) and U_{100m} =10 m/s at inlet with wave age 1 (bottom). The applied logarithmic inlet profile (black) is also shown. See table 1 for more details on boundary conditions.

The overshoots of the inlet wind speeds, seen clearly for the opposed situations in both the 2 and 1 wave age cases, are due to mass conservation in a limited height computational domain. This effect will diminish if the height of the computational domain is increased. For more realistic MABL the height of the domain should be increased.

Both speed up of the wind and increased turbulent levels over a fast moving swell have been observed in real life [14,15].

6. Conclusions

By the use of URANS computations with a moving grid approach it is possible to directly study the effects of the wave movement on the wind field. Vertical profiles of wind velocity and turbulent kinetic energy show distinct differences for waves aligned with the wind versus waves opposing the wind. When the wave is opposing the wind the wave effects are notable throughout the whole domain. A speed up near the wave surface is present when the wind is blowing over and aligned with a faster moving wave surface. When the wave is opposing the wind, the wind velocity will be reduced in the lowest meters and sometimes even reverted. With a wind in 100 meters of 5 m/s and 10 m/s over an opposing wave with phase speed of 8 m/s and amplitude of 3 meters, the wind will be reduced under the height of approximately 37 and 32 meters. The turbulent kinetic energy will also be 10 to 30 times higher under the height of approximately 70 and 55 meters compared to the aligned situation. These URANS simulations with moving wave surfaces will be further developed. More simulation results need to be compared with each other, and preferably also to real measurements. Even if it is clear that the effects from the wave surface extend far above the WBL, and possibly in the height of a wind turbine rotor, it is still unclear which effects this can have on wind turbine design and wind turbine yield. Since this work is based on highly flexible and freely available open source software and since it is a set up that uses URANS the simulations are less computational demanding than previous direct simulations of wave induced winds as DNS and LES**.** The method presented herein is believed to be suitable for further studies of more complex sea states and to be coupled with turbine performance models.

Acknowledgements

This work was made possible partly by funding from the Regional Research Fund, the Industrial PhD-program (Norwegian Research Council) and StormGeo. The work is also a part of the Norwegian Centre for Offshore Wind Energy (NORCOWE) under grant 193821/S60 from the Research Council of Norway (RCN). NORCOWE is a consortium with partners from industry and science, hosted by Christian Michelsen Research. We would also like to thank the OpenFOAM foundation for their support.

References

[1] Semedo A, Saetra Ø, Rutgersson A, Kahma KK, Pettersson H. Wave-induced wind in the marine boundary layer. Journal of the Atmospheric Sciences 2009; **66** : 2256-2271..

[2] Smedman A, Larsén X, Högström U, Kahma K, Petterson H. Effect of sea state on momentum exchange over the sea during neutral conditions. Journal of Geophysical Research 2003; **108**.

[3] Sullivan P, McWilliams JC, Moeng CH. Simulation of turbulent flow over idealized water waves. Journal of Fluid Mechanics 2000; **404** : 47-85. DOI:10.1017/S0022112099006965

[4] Nilsson EO, Rutgersson A, Smedman AS, Sullivan PP. Convective boundary-layer structure in the presence of wind-following swell. Quarterly Journal of the Royal Meteorological Society 2012. ; **138**(667):1476-1489. DOI: 10.1002/qj.1898

[5] Obhrai C, Kalvig S, Gudmestad OT. A review of current guidelines and research on wind modeling for the design of offshore wind turbines. The 22nd International Ocean and Polar Engineering Conference, Rhodes, Greece, June 17-22, 2012

[6] Kalvig, Gudmestad & Winther: Exploring the gap between 'best knowledge' and 'best practice' in boundary layer meteorology for offshore wind energy, Wind Energy, published online: 30 JAN 2013, doi: 10.1002/we.1572

[7] Stull RB. An Introduction to Boundary Layer Meteorology. Atmospheric and Oceanographic Sciences Library, Springer: Vancouver, 1988.

[8] Barthelmie R J, Palutikof JP, Davies TD. Estimation of sector roughness lengths and the effect on prediction of the vertical wind speed profile. Boundary-Layer Meteorology 1993; **66** (1-2) : 19-47. DOI: 10.1007/BF00705458

[9] Edson J, Crawford T, Crescenti J, Farrar T, Frew N, Gerbi G, Helmis C, Hristov T, Khelif D, Jessup A, Jonsson H, Li M, Mahrt L, McGillis W, Plueddemann A, Shen L, Skyllingstad E, Stanton T, Sullivan P, Sun J, Trowbridge J, Vickers D, Wang S, Wang Q, Weller R, Wilkin J, Williams AJ, Yue DKP, Zappa C. The coupled boundary layers and air-sea transfer experiment in low winds. Bulletin of the American Meteorological Society 2007; **88**(3) : 341-356.

[10] Kverneland R. CFD-simulations of wave-wind interaction. Master Thises, University of Stavanger, June 2012

[11] OpenFOAM; http://www.openfoam.com/ (retrieved 07.01.2013)

[12] Veersteg HK, Malalasekera W, An Introduction to Computational Fluid Dynamics, Essex, England: Pearson Education Limited, Second edition, 2007.

[13] Launder BE, Spalding DB, "The numerical computation of turbulent flows", "The numerical computation of turbulent flows." Computer Methods in Applied Mechanics and Engineering, 1974

[14] Sullivan PP, Edson JB, Hristov T, McWilliams JC. Large-eddy simulations and observations of atmospheric marine boundary layers above nonequilibrium surface waves. Journal of the Atmospheric Sciences 2008; **65**(4) : 1225-1245.

[15] Smedman A, Högström U, Bergström H, Rutgersson A, Kahma KK, Pettersson H. A case study of air-sea interaction during swell conditions. Journal of Geophysical Research 1999; **104**(C11) : 25,833-25,851. DOI:10.1029/1999JC900213

Paper 3

Kalvig, S., Manger, E. and Hjertager, B. (2014) ‘Comparing different CFD wind turbine modelling approaches with wind tunnel measurements’, *Journal of Physics, Conference series.* 555.

Comparing different CFD wind turbine modelling approaches with wind tunnel measurements

Siri Kalvig[1,2], Eirik Manger[3], Bjørn Hjertager[1]

[1]University of Stavanger, Norway

[2]StormGeo, Stavanger, Norway

[3]Acona Flow Technology, Skien, Norway

E-mail: siri.m.kalvig@uis.no

Abstract. The performance of a model wind turbine is simulated with three different CFD methods: actuator disk, actuator line and a fully resolved rotor. The simulations are compared with each other and with measurements from a wind tunnel experiment. The actuator disk is the least accurate and most cost-efficient, and the fully resolved rotor is the most accurate and least cost-efficient. The actuator line method is believed to lie in between the two ends of the scale. The fully resolved rotor produces superior wake velocity results compared to the actuator models. On average it also produces better results for the force predictions, although the actuator line method had a slightly better match for the design tip speed. The open source CFD tool box, OpenFOAM, was used for the actuator disk and actuator line calculations, whereas the market leading commercial CFD code, ANSYS/FLUENT, was used for the fully resolved rotor approach.

1. Introduction

In a cluster of wind turbines, wake effects will result in areas with lower wind velocity than the ambient undisturbed wind, and often higher turbulence levels. Wind farm wake effects will hence result in power losses and increased loading. As there are currently vast investments in offshore wind technology [1], wakes offshore are of particular interest. Due to the lower turbulence regimes that often are present in offshore wind sites, wakes are believed to be more persistent offshore than onshore [2]. Barthelmie et al. [3] showed that wind turbine wakes in large offshore wind farms resulted in average power losses of the order of 10 to 20% of total power output.

Modelling wind turbine performance and wakes is an important but challenging task which can be done using several numerical methods. Sanderse et al. [4] classified the different methods in six groups, with the simplest method, the so-called kinematic method, based on an analytical approach that exploits the far wake to obtain expressions for the velocity deficit and the turbulence intensity. Second in the list is blade element momentum (BEM), followed by vortex methods and panel methods. The final two methods are generalized actuator (which includes the actuator disk, actuator line and actuator surface methods) and what Sanderse calls direct methods. The direct methods include all computational fluid dynamic (CFD) methods that use complete or full modelling of the rotor by the use of body-fitted grids. These two last groups of methods are newer than the first four and quite computationally demanding.

In this paper we perform simulations of a small-scale model wind turbine in a wind tunnel with CFD methods in line with Sanderse's two last groups, i.e. generalized actuator methods and direct methods. More specifically, the model wind turbine is simulated using the actuator disk method (ADM), the actuator line method (ALM) and a fully resolved method (FRM). The PhD theses of Mikkelsen [5], Réthoré [6] and Troldborg [7] all provide valuable background information on the ADM and the ALM. The FRM has been studied by Zahle et al., [8] amongst others.

Our three different modelling approaches can be organized in terms of accuracy and cost efficiency, with the ADM believed to be the least accurate and most cost-efficient, and the FRM believed to be the most accurate and least cost-efficient. The ALM can be categorized in between the two ends of the scale. The open source CFD tool box OpenFOAM [9] was used for the ADM and the ALM calculations, whereas the market leading commercial CFD code ANSYS/FLUENT [10] was used for the FRM simulations. For all three simulations, Reynolds-averaged Navier-Stokes (RANS) methods were used, but the ALM and FRM simulations are transient and hence unsteady RANS (URANS) was used.

This paper focuses on wake velocity profiles and wind turbine torque and thrust. Results from the ADM, ALM and FRM are compared with each other, as well as with experimental results. The motivation for this is to gain knowledge on the different CFD methods available for wind turbine performance simulations and to provide recommendations for further usage.

2. Wind tunnel experiment and general simulation characteristics

In October 2011, the authors participated in blind test predictions of a model wind turbine organized by Nowitech[1] and Norcowe[2]in Bergen, Norway. Eight independent modelling groups submitted 11 sets of simulations, and the results from the blind test calculations are presented by Krogstad et al. [11]. In this current paper, the blind test contributions of Kalvig (ADM) and Manger (FRM) are further described and analyzed, and we have performed additional simulations and included the ALM in the comparison.

The length of the wind tunnel is 11.15 metres. The wind tunnel height increases slightly downstream. The height at the inlet is 1.80 metres and at the outlet 1.85 metres. This increasing tunnel height will limit the effect of the walls when the wake expands.

The turbine was located 3.66 m away from the inlet. The model wind turbine, with the National Renewable Energy Laboratory (NREL) s826 airfoil, had a rotor diameter of 0.89 m, and the centre of the rotor was located 0.82 m above the wind tunnel floor (see Figure 1). The rotor speed for the design tip speed ratio was 1282 rpm, giving a rotor tip Reynolds number of 103600. A grid at the tunnel inlet is used to create a turbulent field.

Both thrust and torque, as well as wake velocity, were measured in the wind tunnel. The velocity was measured using a hot-wire anemometer with an x-probe. The sampling rate was 14 kHz in 60 seconds. More information about the experiment can be found in [12, 13].

The ADM and FRM were performed as a part of the blind test in October 2011, but the ALM simulations were done later. In this study we have left the "blind-test principle". In order to run the ALM code, several input parameters need to be determined and in this process one of the input parameters has been tuned to the known turbine power output.

All three methods use the same boundary conditions. The given inlet condition for the blind test experiment was uniform inflow with a reference wind speed of 10.0 m/s and a turbulence intensity of 0.3%. These were used as boundary conditions at the inlet. The inlet boundary condition for dissipation was calculated based on the information given about the hydraulic diameter of 2.19 m. No slip conditions were used for the walls. The outlet boundary condition was zero gradient. All three methods use a two-equation turbulent closure. ADM and ALM use the standard k-ε model [14] and the FRM uses the SST k-ω model [15]. ADM is steady state, and ADL and FRM are transient simulations. Further simulation details are summarized below.

---

[1] Norwegian Research Center for Offshore Wind Technology, http://www.sintef.no/projectweb/nowitech/

[2] Norwegian Centre for Offshore Wind Energy, http://www.norcowe.no/

Figure 1: The model wind turbine in the wind tunnel, NTNU.

3. Actuator disk simulations

The actuator disk method (ADM) is based on momentum theory – the model turbine rotor is represented by a "disk" extracting momentum from the flow. Disk area (D), power coefficient (C_P) and thrust coefficient (C_T) are all input values to the model. Values for C_P and C_T were obtained from a performance test which Krogstad et al. [15] carried out in 2010. Here, C_P and C_T were measured for the model wind turbine. The simulations were performed for tip speed ratios (λ) 3, 6 and 10, with OpenFOAM using a steady state solver for incompressible, turbulent flow. Turbulence was modelled utilizing the standard k-ε model [14].

OpenFOAM is an open source computational toolbox containing various applications and utilities for finite volume simulations. A main advantage of OpenFOAM is that the program is open and free of charge, with a flexible structure, allowing the user to access and modify the code. Parallel runs on multiple processors can be performed without additional license costs. In OpenFOAM version 1.7.0, released in June 2010, the solver "simpleWindFoam" was distributed by the OpenFOAM Foundation [17]. This solver and setup formed the basis for the actuator disk simulations. The OpenFOAM tool "snappyHexMesh" was used to create the grid. The grid was refined in a region near the disk, see Figure 2, but not near the walls. The turbine tower was not modelled. Grid dependency tests were performed, and the solution is believed to be grid independent for velocity calculations. The final grid size used was 1.7 million cells, and the results presented are from 500 iterations; then the convergence criterion of 10^{-4} was reached.

4. Actuator line simulations

As for the ADM, the actuator line method (ALM) also relies on an actuator device extracting momentum from the flow. However, instead of having a disk with uniform distributed force, the rotor blades are now represented as span wise sections with airfoil characteristics. In the actuator line methodology of Sørensen and Shen [18], blade loading is implemented in these span wise sections and introduced in the Navier-Stokes equations as a body force. Churchfield [19] implemented the ALM of Sørensen and Shen in the toolbox OpenFOAM, and this is the basis for our ALM simulations. We have used the setup with the transient solver "pisoFoamTurbine". This was originally intended for large eddy simulations (LES), but we have changed the setup to use unsteady RANS (URANS).

The method requires airfoil look-up tables, i.e. an airfoil file containing a list of lift and drag coefficients versus angle of attack. The freeware airfoil development system XFOIL [20] was used to generate the required airfoil data, and the S826 airfoil geometry was found in the article by Somers

[21]. The airfoil data used here was created by John Amund Lund at Meventus[3], and a closer description of the XFOIL generated airfoil data can be found in [22]. The local blade Reynolds number, calculated on the basis of rotational speed and representative cord length, will vary along the blade, and in [22] a wide range of XFOIL calculations were made in order to account for Reynolds number sensitivity. These simulations were made by considering the blade as different airfoils, with the one closest to the rotor being simply a cylinder, and drag/lift coefficients for the four others being determined on the basis of different Reynolds numbers, in the range of 10000-150000. The simulations were performed for tip speed ratios (λ) 3, 6 and 10.

Unlike the ADM, ALM allows us to study wind turbine forces and information along the blade radius. Thus, thrust and torque are calculated for the model wind turbine. Several input parameters needed to be established in order to perform the ALM simulations and these are summarized in 4.1.

The grid was generated with the OpenFOAM tool "blockMesh". It is refined in a region around the rotor, but not near the walls. The method does not include the turbine tower and this is not modelled. Grid independency tests were performed, and the solution is believed to be grid independent for velocity calculations. The final grid size used was 2.4 million cells.

While Fredriksen [23] worked with the ALM code during his master thesis, the code was changed from explicit scheme to implicit scheme, and we have used this modification to the original code as well in the result presented here. By including the calculation of the wind turbine forces within the PISO algorithm [24], a tighter coupling between the flow field and the turbine blades was ensured. This change also made the code more robust regarding the time step size.

Martínez et al. [25] recommended that the time increments should be small enough so that the tip only passes through one local grid cell during each time step. For all simulations the time increment has been $2.5 \cdot 10^{-4}$ seconds, and this ensures that the blade tip will not pass through more than one local grid cell for the different simulations that were used in the grid independency test (from 350 thousand to 4 million cells) as well as the final simulations that are used later in this study.

The simulation time was 5 seconds. Since the rotor speed is very high for this small model wind turbine, this simulation time is believed to be enough in order to establish a quasi-steady result.

4.1. Input parameters in the actuator line method

ALM relies on various input values. Among others, the Gaussian width parameter and the number of the actuator line elements need to be chosen. It is also possible to use a correction term in order to allow the lift to approach zero more gradually at the tip and root of the blade. Martinez et al. [25] found that using Glauert tip- and root-loss correction terms decreased the predicted power. The result presented here is with the tip- and root-loss correction term (Table 1).

An important input parameter in the OpenFOAM setup by Churchfield [19] is the Gaussian width parameter that controls how the forces are distributed along the lines representing the rotors. Some publications exist regarding how to establish a representative Gaussian width parameter. Troldborg [7] recommends that the parameter should be larger than twice the local grid cell length. In Martinez et al.'s [25] experience, this was also good guidance in order to avoid numerical instabilities in the solver. The latest work of Churchfield [26] states, however, that the Gaussian width parameter should also correspond to a representative blade cord length. The master thesis of Nodeland in 2013 [27] also reaches the same conclusion after extensive testing of the ALM. It is still difficult to establish a physically appropriate value of the Gaussian width parameter, and this is ongoing research.

Based on the guidance [26], we have performed the following procedure to establish an appropriate Gaussian width parameter for the simulations presented here: grid independency tests were performed. Thereafter we ran three simulations with different Gaussian width parameters. A cubic spline interpolation was used to fit the Gaussian width parameter to the known power of 172 W. Then a Gaussian width parameter of 0.0214 was used as input to the new simulations presented here.

[3] Meventus is a Norwegian and Denmark based wind energy company, www.meventus.com

The ALM also requires an input parameter that states the number of actuator line elements, into which one blade should be divided. [25] recommended that for each grid cell across the blade, there should be at least 1.5 actuator line elements. In the following we have chosen the actuator line elements to be 46, which is twice the number of grid cells across one blade, in line with the suggestion in [27].

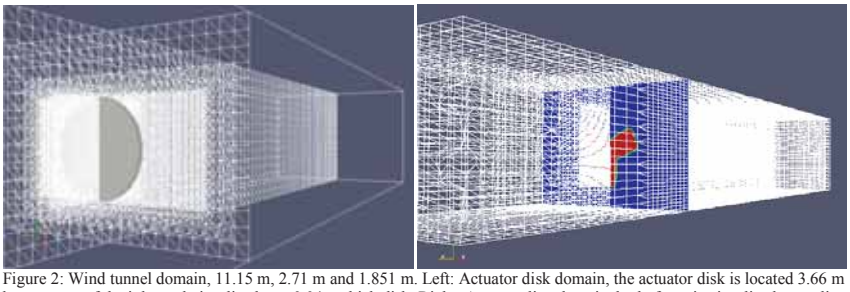

Figure 2: Wind tunnel domain, 11.15 m, 2.71 m and 1.851 m. Left: Actuator disk domain, the actuator disk is located 3.66 m downstream of the inlet and visualized as a 0.04 m thick disk. Right: Actuator line domain, body force is visualized on a slice.

5. Fully resolved rotor method

The fully resolved rotor (FRM) calculations were performed using ANSYS/FLUENT. In these calculations, the exact layout of the wind turbine is modelled geometrically and simulated using a sliding mesh technique. The method requires a fine resolution near the blade to obtain accurate predictions, which again means many computational cells. The mesh used here has approximately 5.3 million cells. In addition, the calculations must be performed using a transient solver, since the actual motion of the rotor is modelled directly during the simulations. Therefore, substantial computer resources are required to perform these calculations.

Figure 3 shows parts of the mesh used in the simulations, focusing around the turbine rotor. The blades of the turbine are meshed using squares and a mapped face mesh, ensuring the best possible mesh quality in this region. The left part of the figure shows the boundary layer, which is resolved down to $y^+ \sim 5$ for best possible accuracy.

Accurate results are highly dependent on the capability of predicting separation and re-attachment on the blade correctly – a few percent off here can give large deviations from measurements. The k-ε model, as used for the ADM and the ALM, is known to have poor properties with respect to correct prediction of recirculation, separation and re-attachment. The SST k-ω model by Menter [28] has, however, proved to predict flow around airfoils quite accurately. The model is a blend between the standard k-ω model near the wall and a transformed k-ω model in the free stream. The SST k-ω model is thus selected as turbulence model for the FRM calculations.

Typical time steps for the FRM model were around 10^{-3} seconds, somewhat depending on the tip speed ratios. The simulations were run until a quasi-steady state solution was achieved, typically some 2-3 seconds, before obtaining averaged quantities that are reported here.

To save computational time, the transient simulations are started from a solution computed with a moving reference frame (MRF) model. In this approach, the motion sources from the rotating parts are accounted for, but the mesh itself is static. This allows steady state simulations, and an average velocity field can be found and used as a starting point for the more accurate transient calculations.

Compared with the actuator disk and the actuator line modelling approaches, the fully resolved rotor simulations do not require any input constants; drag and lift are calculated directly by the code, as well as the velocity patterns in the wake.

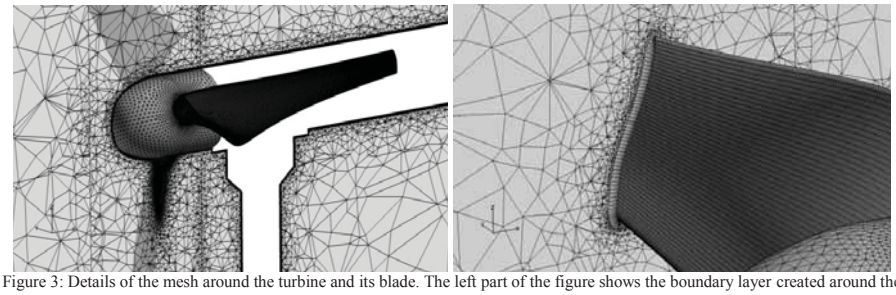

Figure 3: Details of the mesh around the turbine and its blade. The left part of the figure shows the boundary layer created around the blade profile.

6. Results

The wake velocity profiles' results from the different methods are presented first and compared with measurements and then compared with each other. Only the results from the design tip speed are used in the presentation of the wake velocity. Thereafter wind turbine forces are compared between ALM and the FRM for three different tip speeds.

6.1. Actuator disk wake velocity profiles

The ADM simulations of the velocity profiles exhibit the characteristic "top hat" shapes; see Figure 4. Since the rotor is represented as a disk with uniform momentum extraction, the variation in the wake velocity from tip to rotor is not captured. The velocity levels in the far wake[4] (X/D=5) are best captured. The asymmetry in the measurement is believed to be a result of the interaction between the rotor blades and the tower. The tower would normally produce a lower velocity in the shadow with corresponding velocity increase in its vicinity. The turbine blades, however, set up a rotation so that the tower shadow is skewed with a larger velocity increase on one side of the tower. In the ADM simulations the tower is not modelled, and this asymmetry is thus not captured. Close to the tip of the rotor, the wind speeds up and exceeds the reference velocity. This speed-up is less than the measurements. These results indicate that the ADM can to some extent predict the far wakes by the use of a steady state simulation, and this can be a very attractive and computationally effective approach for wake studies in wind farms.

[4] The wake region is divided into near and far wake, with the near wake being the region just behind the rotor to approximately one rotor diameter downwind and the far wake being the area after the near wake [21].

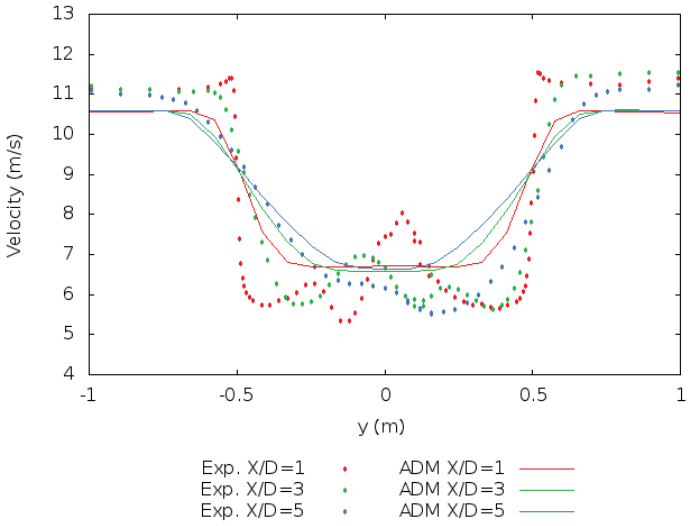

Figure 4: Horizontal wake velocity profiles simulated with ADM (design tip speed) and compared with measurements (Exp.) for different positions downwind, x/D=1, x/D=3 and x/D=5, where D is the diameter of the rotor.

6.2. Actuator line wake velocity profiles

The ALM calculations capture the relative variation of the velocity levels in the wake, but as seen in Figure 5, the velocity at the hub is seriously over estimated. The nacelle is not modelled, and too much wind passes by the centre of the nacelle. The tip velocity wake is best captured for the near wake, i.e. at X/D=1. Also the wake in the region outside the rotor is best captured for the near wake.

The Gaussian width parameter used here corresponds to 1.0899 of the local grid cell of 0.0196 m. This is in contrast to [7] and [25], which recommended that the lower limit for the Gaussian width parameter should be no smaller than twice the local grid cell length. They experienced numerically unstable solutions for too small Gaussian width parameters. We did not experience numerical instability, even though our Gaussian width parameter values were less than this limit. The fact that we have changed the code from explicit scheme to implicit scheme can imply that the codes are not comparable. Also, while the previous work was based on LES, we used URANS and this could also be part of the reason for this inconsistency in the Gaussian width parameter settings.

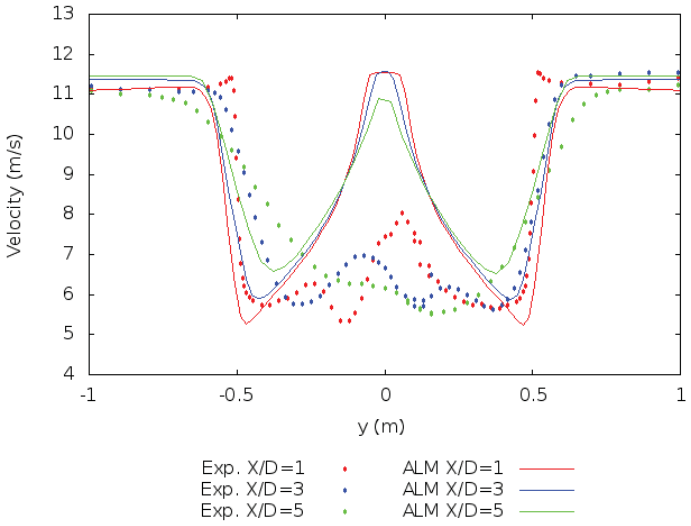

Figure 5: Horizontal wake velocity profiles simulated with ALM (design tip speed) and compared with measurements (Exp.) for different positions downwind, x/D=1, x/D=3 and x/D=5, where D is the diameter of the rotor.

6.3. Fully resolved rotor wake velocity profiles

The FRM simulation captures well the variation in the wake. The agreement with experiments is good for all positions, but best for the near wake, as seen in Figure 6. Part of the reason for the increasing deviation with increasing distance is believed to be too short calculation time and thereby insufficient averaging. As stated earlier, the FRM calculations are time-consuming, and the lack of available computer resources limited the simulation time. Note the asymmetry, present both in the experiments and in the simulations. This feature, also quite well captured in the predictions, is caused by the interaction between the turbine tower and the rotor blades, commented on earlier. Velocity contours behind the wind turbine are visualised in Figure 7.

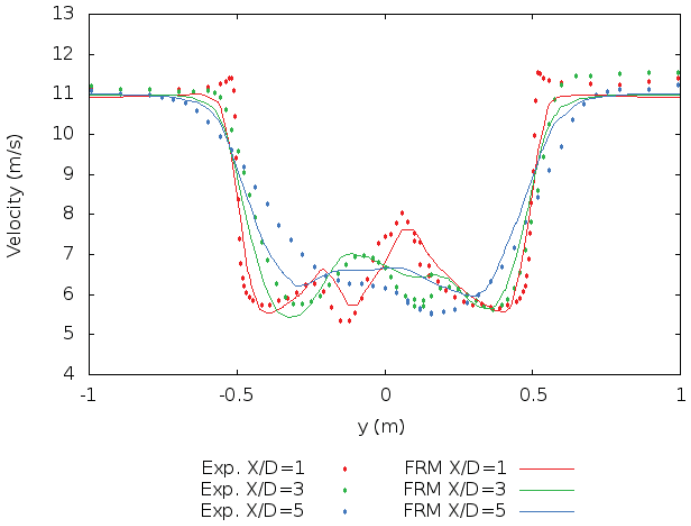

Figure 6: Left: Horizontal wake velocity profiles simulated using FRM (design tip speed) and compared with measurements (Exp.) for different positions downwind, x/D=1, x/D=3 and x/D=5, where D is the diameter of the rotor.

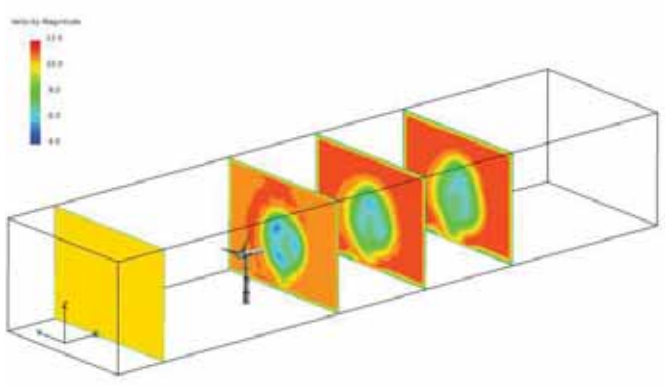

Figure 7: In the fully resolved rotor method, the whole wind turbine with the tower was modelled. Here predicted velocity pattern behind the wind turbine is displayed for position x/D=1, x/D=3 and x/D=5. Blue indicates areas with low wind, whereas the red areas indicate higher wind.

6.4. Simulations compared with each other

In Figure 8 simulations' results from near wake (X/D=1) and far wake (X/D=5) are compared with each other and with experiment values. The FRM stands out as the most accurate model and produces wake velocity values that are close to the experiment values, especially for the near wake. The ADM results for the far wake fit better to the experimental values than those for the near wake. The ALM results, on the other hand, show larger deviation for the far wake than for the near wake.

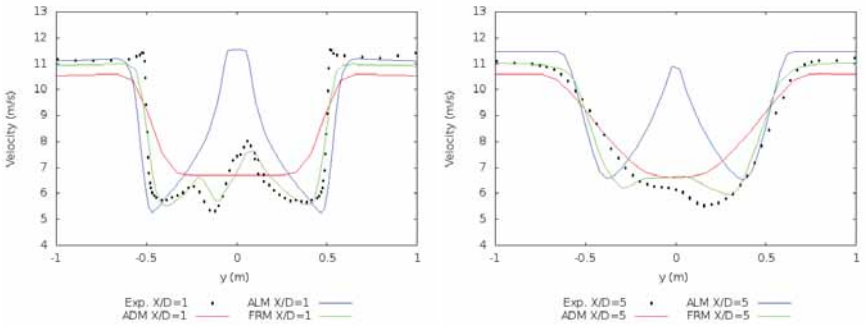

Figure 8: ADM, ALM and FRM compared with each other and with measurements for one and five rotor diameter downwind for tip speed ratio 6.

6.5. Wind turbine forces' calculations from ALM and FRM

This version of ADM does not give information about wind turbine forces, and only results from ALM and FRM can be compared against the experimental data. Table 1 lists the experimental values of C_P and C_T, and the measured values are compared with the estimated values from the two different simulation approaches.

As expected the design tip speed is easiest to model, and the simulated power and thrust compare best with the experiment values for the design speed. The FRM predicts values close to the experimental values, slightly overestimating C_P by 2% and underestimating C_T by 8 %. The simulation performed with ALM gives practically the same values for C_P as in the experiment and approximately 7% underestimation on the thrust.

For tip speed ratios 10 and 3, both the FRM and ALM results are far off. The largest deviations from the experiment values for FRM are for tip speed 3 and for ALM are for tip speed 10.

Tip speed ratios		Experiment	FRM	Deviation	ALM	Deviation
3	C_P	0.12	0.23	91.6 %	0.17	43.3 %
	C_T	0.40	0.46	15.0 %	0.34	- 15.3 %
6	C_P	0.45	0.46	2.2 %	0.45	0.8 %
	C_T	0.92	0.85	- 7.6 %	0.86	- 6.7 %
10	C_P	0.20	0.16	- 20.0 %	0.04	- 80.1 %
	C_T	1.17	1.03	- 12.0 %	0.88	- 24.4 %

Table 1: Power coefficient (Cp) and thrust coefficient (C_T) from FRM and ALM simulations for different tip speed ratios (λ) are compared with experimental values.

7. Discussion and conclusions

Wake velocity profiles, torque and thrust are fairly well predicted using a fully resolved rotor approach for the design tip speed ratio 6. For the wake simulations there are, however, larger discrepancies in the results from the ADM and the ALM approaches. Both the FRM and the ALM predicted power and thrust are very close to the measured values for the design tip speed; for the other tip speed ratios, the deviations were somewhat larger.

The ADM performs best on far wakes, where the magnitudes of the wake velocity deficit are in line with measurements. It would be interesting to study the performance of this model for positions further downwind, as the results are promising for far-wake predictions. The actuator disk method does not capture any variation over the rotor blade since the method used is a simple uniform actuator disk model.

The ALM, on the other hand, captures the variation pattern, but it is far off in magnitude for both near and far wake for the hub area. For a realistic turbine, the nacelle is believed to be of relatively less importance then for this down-scaled version of an operational wind turbine.
Réthoré et al. [6] report that the standard k-ε model is known to under-predict the wake effects and suggest LES instead. This could be an explanation, but in order to investigate this, we need to perform the same simulations with LES and compare the results. In this study we have focused on wake velocity and turbine forces, but turbulence characteristics in the wake are of course also of great interest. In order to compare turbulence levels between these three different methods, more work and investigations have to be carried out. Churchfield et al. simulated wake losses for Lillgrund wind farm [26], and the simulated time-averaged power production of the wind farm agrees well with Lillgrund field observations. There is reason to believe that the large discrepancies in the wake prediction for this small-scale model wind turbine are greater than would be the case for a full-scale wind turbine. Both the high rotational speed of the small-scale turbine and the relative large size of the nacelle (that the ALM does not model) complicate the calculations compared to a large scale wind turbine. Detailed field measurement in the wind turbine wake is sparse, and further study of the ALM must be performed in order to conclude on this matter.

The ALM is dependent on correct input values and setup. The method is also found to be quite sensitive for the composition of the airfoil data. The Gaussian width parameter has, in particular, a great influence on both the wake velocity predictions and the calculation of the wind turbine forces. Currently there is no uniform way of establishing appropriate Gaussian width parameters without model tuning. Nevertheless, the ALM results are promising for wind turbine force investigations, especially for the design tip speed.

In this study the FRM produces superior wake velocity results compared to the ADM and ALM and on average it also produces better results for the force predictions, although the ALM had a slightly better match for the design tip speed.

The good results, close to the measured values for both wake velocity profiles and forces' calculations with the FRM simulation, suggest that this setup can be further utilized in model tuning and in an examination of both the ADM and the ALM approaches. Measurements from both real wind farms and wind tunnels are sparse and often costly, whereas the FRM setup, on the other hand, can easily be modified and hopefully serve as a way to benchmark the other models.

Acknowledgements

We would like to acknowledge Mr John Amund Lund at Meventus for the use of his xFOIL generated airfoildata.

This work was made possible by funding from the Norwegian Research Council Industrial PhD-program (198257) and from StormGeo. The work is also a part of the Norwegian Centre for Offshore Wind Energy (NORCOWE) under grant 193821/S60 from the Research Council of Norway (RCN). NORCOWE is a consortium with partners from industry and science, hosted by Christian Michelsen Research.

References

[1] European Commission 2009 Press release: Commission welcomes adoption of climate and energy. Brussels, 23 April 2009

[2] Barthelmie R, Larsen G, Pryor S, Jørgensen H, Bergström H, Schlez W, Rados K, Lange B, Vølund P, Neckelmann S, Mogensen S, Schepers G, Hegberg T, Folkerts L and Magnusson M 2004 ENDOW (efficient development of offshore wind farms): modelling wake and boundary layer interactions. *Wind Energy* **7** (3): 225-245

[3] Barthelmie RJ, Hansen K, Frandsen ST, Rathmann O, Schepers JG, Schlez W, Phillips J, Rados

K, Zervos A, Politis ES and Chaviaropoulos PK 2009 Modelling and measuring flow and wind turbine wakes in large wind farms offshore. *Wind Energy* **12**: 431-444 doi: 10.1002/we.348
[4] Sanderse B, van der Pijl SP and Koren B 2011 Review of computational fluid dynamics for wind turbine wake aerodynamics. *Wind Energy* **14**: 799-819 doi: 10.1002/we.458
[5] Mikkelsen R 2003 Actuator disc methods applied to wind turbines. PhD Thesis, Department of Mechanical Engineering Technical University of Denmark, June 2003
[6] Réthoré P-E 2009 Wind turbine wake in atmospheric turbulence. PhD Thesis, Ålborg University, October 2009
[7] Troldborg N 2008 Actuator line modeling of wind turbine wakes. PhD Thesis, Technical University of Denmark, Lyngby, Denmark
[8] Zahle F and Sørensen NN 2007 On the influence of far-wake resolution on wind turbine flow simulations. *J. Phys.*: *Conf Series* **75** 012042
[9] OpenFOAM http://www.openfoam.com/ accessed September 2012
[10] ANSYS/FLUENT http://www.ansys.com/ accessed September 2012
[11] Krogstad PÅ and Eriksen PE 2013 'Blind test' calculations of the performance and wake development for a model wind turbine. *Renew. Energ.* **50** 325-333 ISSN 0960-1481, 10.1016/j.renene.2012.06.044
[12] Krogstad PÅ, Eriksen P and Melheim J 2011 'Blind test' workshop. Department of Energy and Process Engineering, NTNU, 30 March 2011
[13] Krogstad PÅ and Eriksen PE 2013 'Blind test' calculations of the performance and wake development for a model wind turbine. *Renew. Energ.* **50** February 2013, 325-333, ISSN 0960-1481, http://dx.doi.org/10.1016/j.renene.2012.06.044
[14] Launder BE and Spalding DB 1974 The numerical computation of turbulent flows. *Comput. Meth. Appl. M.* **3** March 1974, 269–289
[15] Menter FR, Kuntz M and Langtry R 2003 Ten years of experience with the SST turbulence model *Turbulence, Heat and Mass Transfer* **4** 625-632 (Begell House Inc.)
[16] Krogstad PÅ, Karlsen J and Adaramola M 2010 Performance of a model wind turbine *17th Australian Fluid Mechanics Conf.* New Zealand
[17] OpenFOAM Foundation release June 2010 http://www.openfoam.org/download/version1.7.0.php accessed August 2012
[18] Sørensen JN and Shen WZ 2002 Numerical modeling of wind turbine wakes. *J. Fluid Eng.* **124** 393-399 DOI: 10.1115/1.1471361
[19] Churchfield MJ, Lee S and Moriarty P 2012 Overview of the simulator for offshore wind farm application (SOWFA) National Renewable Energy Laboratory, Golden, CO, USA 03 May 2012 http://wind.nrel.gov/designcodes/simulators/sowfa/ accessed June 2013
[20] Xfoil http://web.mit.edu/drela/Public/web/xfoil/ accessed August 2012
[21] Somers DM 2005 The S825 and S826 airfoils. National Renewable Energy Laboratory, NREL/SR-500-3634
[22] Krogstad PÅ and Amund JA 2011 An experimental and numerical study of the performance of a model turbine. *Wind Energy* Wiley Online Library 13 June 2011 DOI: 10.1002/we.482
[23] Fredriksen T 2013 Wind energy; CFD simulation of wakes and wind turbine forces. Master's thesis spring 2013, Telemark University College, Faculty of Technology, Porsgrunn, Norway
[24] Issa RI 1985 Solution of the implicitly discretized fluid flow equations by operator-splitting. *J. Comput. Phys.* **62** 40-65 ISSN 0021-9991
[25] Martínez LA, Leonardi S, Churchfield MJ and Moriarty PJ 2012 A comparison of actuator disc and actuator line wind turbine models and best practices for their use. *50th AIAA Aerospace Sciences Meeting and Exhibit*, Nashville, TN, Jan. 9–12, AIAA, Washington D.C., 2012.
[26] Churchfield MJ, Lee S, Michalakes J and Moriarty PJ A numerical study of the effects of atmospheric and wake turbulence on wind turbine dynamics. *J. Turbul*. Available online: 02 May 2012
[27] Nodeland AM 2013 Wake modelling using an actuator disk model in openFOAM. Master's thesis

spring 2013, Norwegian University of Science and Technology, Department of Energy and Process Engineering, EPT-M-2013-85, Trondheim, Norway
[28] Menter FR 1994 Two-equation eddy-viscosity turbulence models for engineering applications. *AIAA Journal*, **32**(8):1598-1605 August 1994

Paper 4

Kalvig S., Churchfield M., Manger E. and Hjertager B. (In review) “URANS versus LES based simulations of wind turbine performance and wakes - comparison with wind tunnel measurements”

Submitted to: Journal of Renewable and Sustainable Energy (JRSE), AIP.

Paper 5

Kalvig S., Manger E., Hjertager B. and Jakobsen J.B. (2014) “Wave influenced wind and the effect on offshore wind turbine performance”, *Energy Procedia,* Volume 53, 2014, Pages 202-213, ISSN 1876-6102, http://dx.doi.org/10.1016/j.egypro.2014.07.229.

Available online at www.sciencedirect.com

ScienceDirect

Energy Procedia 53 (2014) 202 – 213

Energy Procedia

EERA DeepWind'2014, 11th Deep Sea Offshore Wind R&D Conference

Wave influenced wind and the effect on offshore wind turbine performance

Siri Kalvig[a,c]*, Eirik Manger[b], Bjørn H. Hjertager[a], Jasna B. Jakobsen[a]

[a] *University of Stavanger,4036 Stavanger, Norway*
[b] *Acona Flow technology AS, Uniongt. 18, 3732 Skien, Norway*
[c] *StormGeo AS, Nordre Nøstekaien 1, 5011 Bergen, Norway*

Abstract

In this paper the effect of wave influenced wind on offshore wind turbines is studied numerically.The wave is seen as a dynamical roughness that influences the wind flow and hence the wind turbine performance. An actuator line representation of the NREL's 5 MW offshore baseline wind turbine is placed in a simulation domain with a moving mesh that resolves the ocean waves. These wave influenced wind turbine simulations, WIWiTS, show that the wave will influence the wind field at the turbine rotor height. Both the produced power and the tangential forces on the rotor blades will vary according to the three different cases studied: wind aligned with a swell, wind opposing the swell and wind over a surface with low roughness (no waves).

Selection and peer-review under responsibility of SINTEF Energi AS

Keywords: Wave wind interactions, Offshore wind energy, Actuator line, CFD

* Corresponding author. Tel.: +47 91604181
E-mail address: siri.kalvig@uis.no / siri.kalvig@stormgeo.com

Selection and peer-review under responsibility of SINTEF Energi AS
doi:10.1016/j.egypro.2014.07.229

1. Introduction

Ocean surface waves develop due to the frictional drag over the water's surface. Momentum from the air is transported to the ocean during the wave development, but the waves themselves will also influence the wind field. This process is often ignored, both in weather forecasting and in the field of offshore wind energy [1]. Different sea states affect the wind field in various ways. Wave shape, wave age and wave direction are important for upward momentum transfer in the marine atmospheric boundary layer (MABL) [2]. It is common to divide the wave regime into two parts: wind-waves are locally generated by the wind and swells are waves that have propagated away from the source origin. While wind-waves are often aligned with the wind, the swell direction is not necessarily correlated with the wind direction. Occasionally, swells will oppose the wind field, and this is known to give rise to interesting situations with increased turbulence levels over the sea surface [3]. Although it is known that fast moving waves in a low wind regime will influence the whole depth of the MABL, it is still uncertain to what extent the wave induced wind field will affect an offshore wind turbine or a wind farm [1].

In this paper, we present a numerical study of the possible effects wave states may have on the wind field and the following indirect effect on an offshore wind turbine. This is done by using computational fluid dynamics (CFD). In these CFD simulations the air flow does not influence the waves themselves. The wave is prescribed as a solid moving ground. Therefore this is a study of the wave *influenced* wind and the possible effect on offshore wind turbine performance.

2. Wave influenced wind

The wind profile over a surface is influenced by the roughness of the surface and the atmospheric stability. Wind observations at different heights are limited in offshore environments. Therefore wind speed profile models are frequently used to extrapolate the wind speed observations at lower levels to the wind turbine hub height or the swept rotor area. Small deviations from the real wind speed will significantly influence the anticipated wind power levels which are proportional to the cube of the wind speed. Different wind profiles will also give rise to different loads on the blade and the rotor nacelle assembly [4]. Therefore a correct description of the wind profile is of outmost importance for both for wind turbine design, wind assessment and wind energy harvest.

Expression for the wind profile can be found by using Monin-Obukhov similarity theory (MOST). MOST is valid in the constant flux layer (where the fluxes are assumed to vary little with height). Under neutral atmospheric stability conditions MOST theory leads to the logarithmic wind profile [5]:

$$U(z) = \left(\frac{u_*}{k}\right) ln\left(\frac{z}{z_0}\right) \quad (1)$$

where k = 0.4 is the von Kármán's constant, z_0 is the roughness length (defined as the height where the wind speed equals zero) and u_* is the friction velocity. The friction velocity is defined as [5],

$$u_*^2 = \frac{\tau_0}{\rho}, \quad (2)$$

where τ_0 is the force per unit area exerted by the ground surface on the flow and ρ is the density of the air. The roughness length, z_0 , can be derived from wind speed measurements. The literature contains different recommendations for selection of z_0 for different surfaces. In the field of offshore wind industry the sea surface is generally considered as levelled and smooth, and, therefore, a low z_0 value of 0.0002 m is often chosen [6]. This is also the value of the roughness used in the simulations described later in this paper.

Atmospheric stability is of importance when studying the wind profiles and it has also been documented that both energy yield and fatigue damage on a wind turbine differ when atmospheric stability is taken into consideration [7,8]. Nevertheless, in this study, we have assumed neutral atmospheric stratification; hence there will be no heat exchange between the sea surface and the overlying air.

The waves can be seen as a dynamical roughness of the sea surface. Different sea states and different directions of the waves, relative to the wind direction, will give rise to different perceived sea surface roughness. The ratio between the phase speed (c_p) of the waves at the peak of the wave spectrum and the wind speed at 10 m, adjusted to neutral conditions (U_{10N}), is called the wave age (χ_{10}) [9];

$$\chi_{10} = \frac{c_p}{U_{10N}}, \tag{3}$$

This can be a useful parameter when classifying different wave regimes because wave ages for young seas (associated with locally generated wind waves and developing seas) are smaller than those for old seas (associated with faster moving swell and decaying seas). When χ_{10} is 1.2 the wave field is believed to be fully developed. Young wind seas have a wave age that is characterised by $\chi_{10} < 1.2$ and a swell dominated wave field by $\chi_{10} > 1.2$ [9]. In this paper, two different swells with wave age of 1.5 and 2.1 are investigated and coupled with wind turbine performance modelling.

3. Wind turbine performance modelling

Wave loads, corrosion and marine organic growth affect the offshore wind turbines and this is covered in the governing standards for offshore wind turbines. There are however, no considerations of how the sea state itself can affect the wind profile and the turbulence in the MABL and the following possible indirect effect of waves on the rotor-nacelle assembly [1].

The basis for the wind turbine performance in this paper is the actuator line methodology of Sørensen and Shen [10]. Here the rotor blades are represented as span-wise sections with airfoil characteristics, and the blade loading is implemented in the spanwise sections and introduced in the Navier-Stokes equations as a body force. Data and description of the National Renewable Energy Laboratory's (NREL) offshore baseline wind turbine, the NREL 5 MW turbine [11], which is easily accessible and well documented, has been chosen as the test turbine.

Power output and blade loading are examined in order to reveal whether the oscillating waves will change the performance of the wind turbine. This could have consequences for both power harvest and fatigue considerations.

4. Methods and calculations

In [12] a method for wave simulations with the help of deforming mesh was established. This method is further developed by the inclusion of the horizontal wave particle movement as well as the vertical movement, and the discretization schemes for the numerical simulations are also slightly changed. Subsequently the Simulator for Offshore Wind farm Application (SOWFA) [13], developed at NREL, was modified in order to be integrated with the method for wave simulations. The result is a CFD set up that is suitable to study implications of wave movements on the wind flow and directly study the effect on a wind turbine or a wind farm. Hereafter, this set up will be referred to as the wave influenced wind turbine simulations (WIWiTS).The simulations are incompressible and transient with an unsteady Reynolds-averaged Navier-Stokes (URANS) approach. As turbulent closure, we have used the standard k-epsilon model [14].

4.1. Wave generation by the use of moving mesh

The method allows a description of a single sinusoidal wave on the ground patch in the simulation domain or a multiple of sinusoidal waves. Different waves can have different properties as well as different angles to each other and hence it is possible to describe a real wave spectrum on the surface. In this paper, only single sinusoidal waves are studied. This is of cause a simplification of a realistic sea. At the current stage of this study, we need to simplify the problem and focus on the swell conditions - primarily because this is the case when wind and waves can occur with different angels to each other, but also because this wave state is fairly well approximated with a pure sinusoidal form. Others have studied wave influenced wind by the use of coordinate transformation [15], but the method simulating wave influenced wind by the use of a moving mesh approach is believed to be unique in the context of offshore wind energy.

The open source CFD toolbox OpenFOAM [15] is used for both mesh generation and computations. By using a moving mesh approach, several sinusoidal waves can be implemented on the form;

$$\eta(x,t) = a\left\{\sin\left(2\pi(\frac{t}{T}-\frac{x}{L})\right) + \cos\left(2\pi(\frac{t}{T}-\frac{x}{L})\right)\right\} \quad (4)$$

where η is the sea surface elevation at a horizontal distance x at a given time t. a is the wave amplitude, T the wave period and L the wave length. Each grid cell moves up and down, reaching its maximum elevation in different time increments according to a sinusoidal function, and the movement looks like a wave propagating - much like the surface particles in a real ocean wave. A new solver was developed in the OpenFOAM tool box and named 'pimpleDyWFoam'. No deformation due to the wind force is allowed as the moving wave is seen as a solid wall. The wave properties and boundary conditions are listed in table 1 and 2. For more details regarding the moving wave method, reference is made to [12].

Before introducing the wind turbine in the simulations, the wind field over the waves was studied, using a less computationally demanding set up in two-dimensions. The purpose was to examine the required domain size, resolutions and the flow responses without wind turbine influences. The moving wave introduces some boundary effects close to the inlet and outlet part of the simulation grid. Even if the wave develops gradually after 10 sec of simulations and grows gradually to the prescribed amplitude size after 50 meters, these boundary effects are detectable. These effects come from the fact that the wave originates from one side of the domain and decays on the other side. In a large horizontal domain these boundary effects will not influence the core area of the domain.

Several domain sizes and wave states were tested and here we present results with a domain size of 1200 meters length and 400 meters height for four different cases. In order to ensure that the waves were properly resolved without too much computational resources a graded mesh was used where the cells near the surface are three times as small as the cells near the top. The smallest cells width close to the wave surface was approximately 1.5 meters. The mesh was generated with the openFOAM specific tool 'blockMesh'.

A logarithmic wind profile with the wind speed of 8 m/s at a reference height of 400 m is used as the inlet wind speed for all cases.

Table 1. The four different simulation cases without wind turbine representation

case	Decription	Wave parameters	Wave age
1a	wind and swell in the same direction	a = 4 m, L = 50 m, c = 8.8 m/s	1.5
1b	wind and swell in the opposite direction	a = 4 m, L = 50 m, c = -8.8 m/s	1.5
2a	wind and swell in the same direction	a = 4 m, L = 100 m, c = 12.5 m/s	2.1
2b	wind and swell in the opposite direction	a = 4 m, L = 100 m, c = -12.5 m/s	2.1

4.2. Actuator line method in SOWFA

SOWFA is a powerful tool for offshore wind power plant simulations, which includes both a model to run precursor atmospheric simulations and an actuator line turbine model, as well as an integration to the aeroelastic computer-aided engineering tool for horizontal axis wind turbines, FAST. This work uses only the actuator line part of SOWFA (which includes the 'pisoFoamTurbine' solver). Originally SOWFA was based on large scale eddy simulations (LES). The code is here changed to URANS in order to be compatible with the moving wave simulations.

The actuator line model in SOWFA relies on various input parameters. The Gaussian width parameter is an input parameter that controls how the forces are distributed along the lines representing the rotors. The number of the actuator line elements on a rotor blade need also to be chosen. Both these two parameters rely on the mesh and on the rotor characteristics. In [17] various testing of best suitable input parameters was performed. In this way the model was "tuned" to given results. This is not possible in the present study and the value of the input parameters is chosen based on best practice. The NREL 5 MW turbine is assumed to produce power close to 2 MW with a reference wind

speed of 8 m/s and a rotation speed of approximately 9 RPM [18]. The turbine rotational speed is set to 9 RPM. The wind speed at the hub height will be influenced by the wave and the resulting wind speed at hub height will be lower than 8 m/s and the simulated power should be less than 2MW. A variable-speed controller is incorporated in the SOWFA actuator line model. In these simulations the turbine will operate in underrated wind and try to optimize the power capture. In this region the generator torque should be proportional to the square of the filtered generator speed [11].

The turbine properties and input parameters are listed in table 1. For more details regarding the actuator line method in SOWFA, reference is made to [13, 17, 18 and 19].

4.3. Combined simulations; wave influenced wind turbine simulations - WIWiTS

The wave simulations described in 4.1 were coupled with the turbine simulations described in 4.2. Hence, a new combined CFD simulation was developed. This new solver embedded in the WIWiTS was named 'pimpleDyWTurbineFoam'.

Grid dependency studies performed on the two dimensional set up (without turbine representation) showed that in order to have grid independent solutions a very fine mesh is preferable. Also the domain needs to be large to minimize boundary effects. This resulted in hundreds of millions of cells when used on an equivalent three dimensional case. Simulations on such a mesh were not feasible. The mesh was instead constructed with a background graded mesh of same resolutions as in the wave simulations without wind turbine (described in section 4.1) and a refined area around the turbine rotor as a necessary compromise between the domain size and the resolution of the grid (see figure 1). The simulation domain was 600 m long, 260 m wide and 400 m high. This is believed to be too short to avoid all boundary effects, but the simulations will nevertheless give indications on the relative differences in power generation for different wave conditions compared to a no-wave situation.

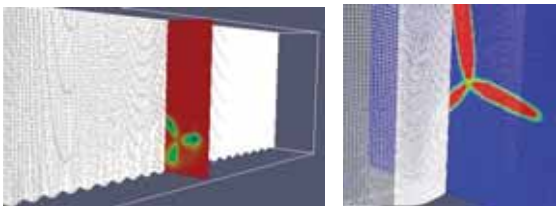

Fig.1. Illustration of the WIWiTS domain, turbine size is exaggerated (left). The WIWTS mesh is graded near the surface and refined in a region around the turbine (right).

The turbine will rotate in a mesh with changing grid cell size. The input parameters should be a ratio of the grid cell size. Troldborg [20] recommends that the Gaussian width parameter should be larger than twice the local grid cell length. In all three cases the Gaussian width parameter is 2.85 times larger than the smallest local grid cell length and 0,98 times larger than the largest grid cell length. The largest grid cell length is located in the very top of the domain and the rotor will not experience the largest grid cells. [19] recommended that for each grid cell across the blade, there should be at least 1.5 actuator line elements. In these cases the airfoil is divided into 40 elements. The implication is that for every local grid cell there are between 0.78 and 2.24 actuator line elements depending on what part of the grid the rotor experiences. Thus the vertically graded grid resolution gives problems in estimating the right input values for the turbine simulations. It will nevertheless be interesting to compare the results since this will be discussed in light of a control run over a flat surface that is performed on the same grid as the simulations with the wave movements. The results of the WIWTS simulations should serve as a demonstration of the relative influence the wave modified wind profiles could have on the wind turbine performance.

Only the wave with wave age 2.5 is used together with the wind turbine. The reason for this choice is that this is a

more realistic swell condition although the wave amplitude will be higher than what can normally be expected. Wind turbine performance for three different cases are presented as listed in table 2: wind and swell in the same direction, wind and swell in the opposite direction and wind over surface with low roughness (no waves).

The WIWiTS input parameters and boundary conditions are presented in table 2 and 3. In section 5, we emphasize on the wind velocity and the turbulent kinetic energy because this is the most important flow parameters when studying turbine performance. Tests have been made to find the minimum simulation time required for the flow to reach a quasi-stationary stage and, based on the tests, a simulation time of 300 seconds should be enough.

Table 2. The three different simulation cases with wind turbine representation

case	Description	Wave parameters	Wind at inlet
a	wind and swell in the same direction	a=4 m, L=100m, c=12,5 m/s	8 m/s
b	wind and swell in the opposite direction	a=4 m, L=100m, c= -12,5 m/s	8 m/s
c	wind over a surface with low roughness	No wave, z_0 = 0,0002 m	8 m/s

Table 3. Boundary conditions on the different patches for the WIWTS, with OpenFoam specific naming. On the ground patch the boundary conditions for U will be different in the case of a flat surface (fixedValue) compared to a moving wave surface (movingWallVelocity).

field		Inlet	outlet	top	sides	Ground
U	wind velocity	ABLvelocity*	zeroGradient	slip	slip	movingWallVelocity fixedValue
p	pressure	zeroGradient	fixedValue	slip	slip	zeroGradient
k	turbulent kinetic energy	fixedValue	zeroGradient	slip	slip	kqRWallFunction
epsilon	turbulent dissipation of energy	fixedValue	zeroGradient	slip	slip	epsilonWallFunction;
nut	viscosity	fixedValue	zeroGradient	slip	slip	nutkRoughWallFunction

*Full openFOAM specific name: atmBoundaryLayerInletVelocity

5. Results and discussion

First, an examination of two different wave states with the same inlet wind is presented in section 5.1. Thereafter the turbine is introduced in the domain and power generation and some examples of blade loading are presented in 5.2.

5.1. Wind velocity and turbulence profiles without turbine representation

Both the wind profile and the turbulent kinetic energy profiles will depend on the direction of the wave relative to the incoming wind field. In Figure 2 and 3 results from simulations with wave ages, 1.5 and 2.1 (listed in table 1) are shown. The figures show the sampling of instant horizontal and vertical wind velocity profiles for every second between 251-300 seconds of simulations. During this runtime, the simulations have reached a quasi-steady state. Figure 4 shows the corresponding turbulent kinetic energy profiles. The sampled data are from the middle of the domain (x=600 m) where boundary affects are negligible.

The wave movement periodically modifies the wind profiles up to approximately 100 metres over the sea surface. The waves with wave age 1.5 are the shortest and steepest wave generating more turbulence, and variations in the lowest meters compared to the wave with wave age 2.1. The latter moves faster with longer wave lengths and this wave state induce variations at the highest levels. The vertical velocity fluctuations are identifiable up to 100 metres.

For both cases the wind profile in the opposed situation shows an ‘overshoot’ of the wind speed compared to the logarithmic inlet and also compared to the aligned situation. This is believed to be due to the fact that the extra generated turbulence in the opposed case gives rise to a ‘richer’ profile near the surface and further up in the MABL. In other words The short and steep wave (case 1a and 1b in table 1) gives higher turbulence values and the overshoot is more pronounced than in the longer wave case (case 2a and 2b, table 1).

It should be noted that the turbulence profiles indicate little or no vertical mixing from approximately 75 m and upwards, whereas the velocity profiles show slight variations above this level. The true turbulence level is a combination of the large-scale motion generated by the waves as well as the turbulence predicted by the k-epsilon model. In Figure 4 only the filtered k values directly obtained from the k-epsilon model is shown. One should also account for the large-scale variances and calculate the turbulent kinetic energy contribution from this. In order to do so, time averaging must be enabled in the CFD simulations and this has not been done. The turbulence result presented in Figure 4 should thus be interpreted with care.

Since the gradient of both the horizontal and vertical velocity profiles is close to zero at the top of the domain, it is a valid assumption that the domain height is high enough and that the overshoot represent a physical sound flow response in the cases where a wave opposes the wind field.

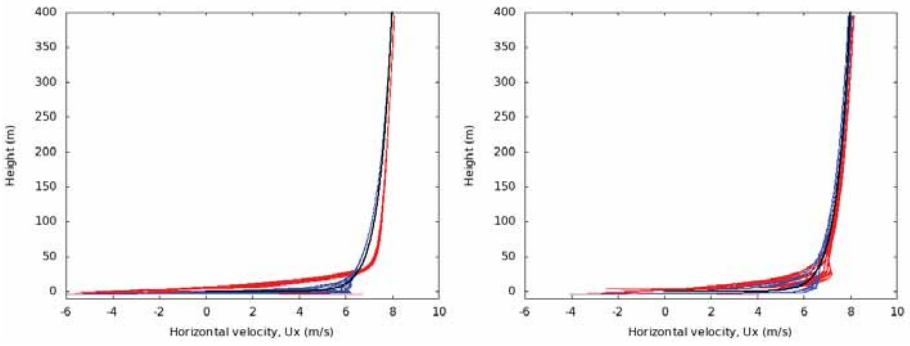

Fig. 2. Profile of horizontal wind (m/s). Wind and wave in the same direction (blue), wind and wave in the opposite direction (red) and the logarithmic inlet wind velocity (black). Profiles are sampled from the middle of the domain (x=600 m) for every second between 251-300 seconds of simulations. Case 1a and 1b, see table 1 (left) and case 2a and 2b, see table 1 (right).

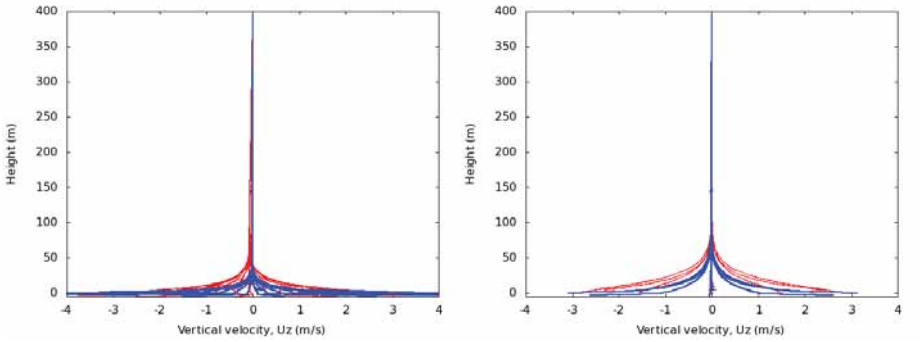

Fig. 3. Profile of vertical wind (m/s). Wind and wave in the same direction (blue), wind and wave in the opposite direction (red). Profiles are sampled from the middle of the domain (x=600 m) for every second between 251-300 seconds of simulations. Case 1a and 1b, see table 1 (left) and case 2a and 2b, see table 1 (right).

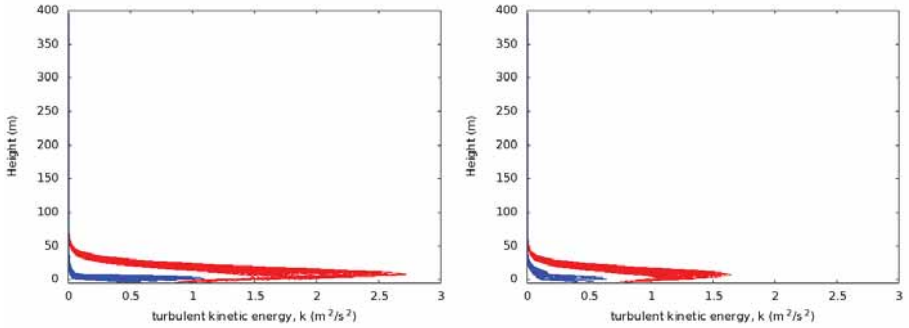

Fig. 4. Profile of turbulent kinetic energy, k (m^2/s^2), directly obtained from the k-epsilon model. Wind and wave in the same direction (blue), wind and wave in the opposite direction (red). Profiles are sampled from the middle of the domain (x=600 m) for every second between 251-300 seconds of simulations. Case 1a and 1b, see table 1 (left) and case 2a and 2b, see table 1 (right).

5.2. Power generation and blade loading

For every simulations time step "global" turbine quantities i.e. rotor power (W), thrust (N), and "local" blade quantities, i.e. axial force (N), tangential force (N), will be calculated and stored. In Figure 5 produced power are shown for the three cases a, b and c. The power will oscillate for cases a and b where the swell is present, but for case c where the wind flow is over a flat surface, the same oscillations are not present. There will always be some minor variations in the power curve and this is believed to be code specific and dependent on how the user defines the parameters mentioned in section 4.3 [18]. The oscillations in cases a and b have the same frequency as the wave. The simulation for case c, over the flat surface, is performed on the same grid as for cases a and b. Therefore it seems that these oscillations are a consequence of the wave movements.

In Figure 5 the generated power is higher in case b that in case a and c. This is linked to the fact that the fast moving swell generates a "richer" profile in case b, as mentioned in 5.1. When introducing the turbine in the domain the domain height of 400 m seems to short. The turbine represents an 'obstacle' and generates more turbulence and a more complicated flow behavior than case the case with only waves. The power curve seems to reach a stable

development for case a and c after approximately 170 sec, but for the b case a slight increase in generated power can be detected after approximately 250 sec. This can be an indication that the simulation time are too short for the opposed case. Because of the limitation in number of grid cells, we could not 'afford' to put the turbine in the middle of the domain in a 1200 wide domain where no boundary effects were present. Instead, the turbine needed to be placed far downstream in the domain. By doing so, we cannot exclude boundary effects entirely and this has to be taken into considerations when interpreting the results.

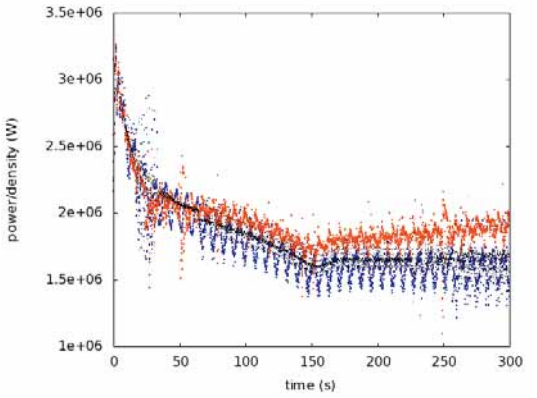

Fig. 5. Generated rotor power per density (Wm^3/kg) for the three different cases; wind and swell in the same direction (blue), wind and swell in the opposite direction (red) and wind over a surface with low roughness (black). The simulation time was 300 sec. Noise in the curves are due to start up effect every time the simulations had to be restarted due to technical problems.

In Figure 6-8 the forces in the rotor rotational tangential direction (hereafter named the tangential force) on each blade are shown for two different time steps. The left graph in every figure corresponds to 334 seconds and the right graphs are plotted half a wave period later, i.e. at 338 seconds. This will give a picture of the variation in the tangential force on each blade during two different wave positions. There are slightly more spread in the forces in case a – when the wave is aligned with the wind. Case b – with waves is opposing the wind, gives larger forces than case a and c.

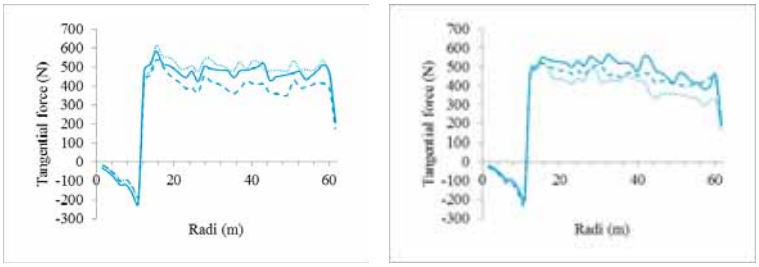

Fig. 6. Case a) Aligned situation. Tangential force (N) along the rotor blade for each blade 334 sec (left) and 338 sec (right). Blade 1 – solid line, blade 2 - broken line, blade 3 - dotted line.

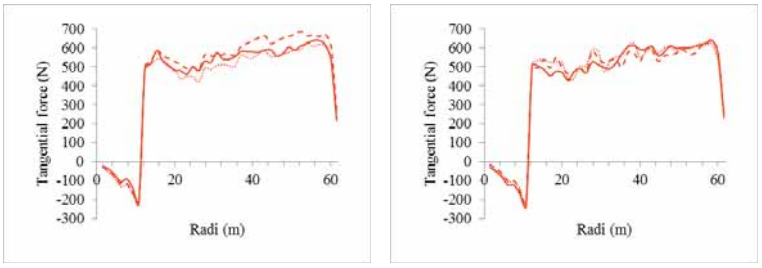

Fig. 7. Case b) Oppose situation. Forces in the rotor rotational tangential direction (N) along the rotor blade for each blade after 334 sec (left) and 338 sec (right). Blade 1 – solid line, blade 2 - broken line, blade 3 - dotted line.

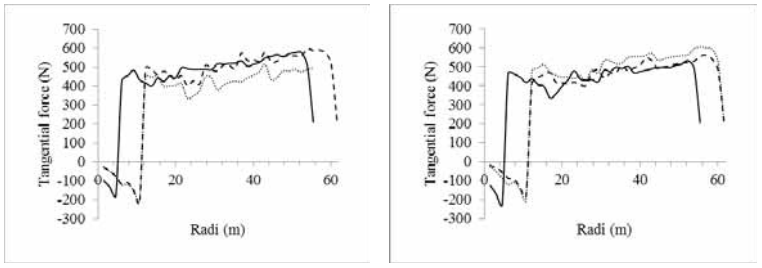

Fig. 8. Case c, flat surface. Forces in the rotor rotational tangential direction (N) along the rotor blade for each blade after 351 sec (left) and 355 sec (right). Blade 1 – solid line, blade 2 - broken line, blade 3 - dotted line.

6. Conclusions and suggestion for future studies

A combined CFD set up where an actuator line representation of a turbine operates in wave influenced wind is developed. These WIWiTS results show that wave influenced wind affects the wind turbine performance.

Before introducing the wind turbine in the simulation domain, wave simulations on a two-dimensional set up were conducted. These simulations showed that the influence of the wave extend tens of meters up in the atmosphere and will affect the wind in the swept area of wind turbines. Several simulations were performed and some general observations is that in a fast moving swell regime a wave that oppose the wind field will create larger turbulence levels (predicted directly from the k-epsilon model) than if the wave was aligned with the wind or with no wave present. More detailed turbulence analyses are however required to investigate this phenomenon further. When working with URANS predictions from the k-epsilon model, the results should be coupled with turbulence calculations related to the large-scale motion generated by the waves. This should be topic for future work and improvements.

The wave movements result in oscillations in the power output when the turbine operates in underrated wind with a torque controller. The wave movements periodically modify the wind profiles up to approximately 100 metre over the sea surface. The wind turbine with the nacelle at 88 metre height with rotor radius of 61 metre will experience these fluctuations and it will lead to slightly larger tangential forces than comparable situations over a flat surface. Also more spread in the forces was observed when the wind and the wave was aligned to each other.

There are indications that the domain is too small for the WIWiTS and complete grid independence was not reached. Therefore these results can only serve as an indication of the impact wave influenced wind may have on wind turbine performance. Nevertheless, it is interesting to note the relative differences between conditions with swell aligned with

the wind field, opposing the wind field and over a surface with low roughness (no waves). The swell shown has amplitude of 4 metre and it is unrealistic that such a large swell will persist for a longer time. More simulations with lower swell height and more realistic sea states are recommended.

The wave influenced wind will affect the turbine performance, as well as the loads, but it is not possible to conclude if this influence is significant in relation to the natural turbulent structure of the atmosphere and the varying atmospheric stability. We have here developed and demonstrated the use of a flexible open source CFD set up, and hopefully this will motivate further studies in this area.

Acknowledgements

This work was made possible by funding from the Norwegian Research Council Industrial PhD-program (198257) and from StormGeo. The work is also a part of the Norwegian Centre for Offshore Wind Energy (NORCOWE) under grant 193821/S60 from the Research Council of Norway (RCN). NORCOWE is a consortium with partners from industry and science, hosted by Christian Michelsen Research. The authors would like to acknowledge Theodor Ivesdal at the University of Stavanger for is outstanding technical help with the Linux cluster.

References

[1] Kalvig S, Gudmestad OT, Winther N. Exploring the gap between 'best knowledge' and 'best practice' in boundary layer meteorology for offshore wind energy. Wind Energy 2013;17(1). doi: 10.1002/we.1572

[2] Semedo A, Saetra Ø, Rutgersson A, Kahma KK, Pettersson H. Wave-induced wind in the marine boundary layer. Journal of the Atmospheric Sciences 2009;66:2256-2271.

[3] Ocampo-Torres F, García-Nava H, Durazo R, Osuna P, Díaz Méndez G, Graber H. The INTOA Experiment: A study of ocean-atmospher interactions under moderate to strong offshore winds and opposing swell conditions in the Gulf of Tehuantepec, Mexico. Boundary-Layer Meteorology 2011;138(3):433-451. doi: 10.1007/s10546-010-9561-5

[4] Lange B, Larsen S, Højstrup J, Barthelmie R. Importance of thermal effects and sea surface roughness for offshore wind resource assessment. Journal of Wind Engineering and Industrial Aerodynamics, Volume 92, Issue 11, September 2004, Pages 959-988, ISSN 0167-6105, http://dx.doi.org/10.1016/j.jweia.2004.05.005.

[5] Stull RB. An introduction to boundary layer meteorology. Vancouver: Atmospheric and Oceanographic Sciences Library, Springer; 1988.

[6]Barthelmie R J, Palutikof JP, Davies TD. Estimation of sector roughness lengths and the effect on prediction of the vertical wind speed profile. Boundary-Layer Meteorology 1993; 66(1-2):19-47. doi: 10.1007/BF00705458

[7] Motta M, Barthelmie RJ, Volund P. The influence of non-logarithmic wind speed profiles on potential power output at Danish offshore sites. Wind Energy 2005;8(2):219-236. doi: 10.1002/we.146

[8] Sathe A, Mann J, Barlas T, Bierbooms WAAM, van Bussel GJW. Influence of atmospheric stability on wind turbine loads. Wind Energy 2012;16(7). doi: 10.1002/we.1528

[9] Edson J, Crawford T, Crescenti J, Farrar T, Frew N, Gerbi G, Helmis C, Hristov T, Khelif D, Jessup A, Jonsson H, Li M, Mahrt L, McGillis W, Plueddemann A, Shen L, Skyllingstad E, Stanton T, Sullivan P, Sun J, Trowbridge J, Vickers D, Wang S, Wang Q, Weller R, Wilkin J, Williams AJ, Yue DKP, Zappa C. The coupled boundary layers and air-sea transfer experiment in low winds. Bulletin of the American Meteorological Society 2007;88(3):341-356.

[10] Sørensen JN, Shen WZ. Numerical modeling of wind turbine wakes. J. Fluid Eng. 2002;124:393-399. doi: 10.1115/1.1471361

[11] Jonkman J, Butterfield S, Musial W, Scott G. Definition of a 5-MW Reference Wind Turbine for Offshore System Development. National Renewable Energy Laboratory, Rept. NREL/TP-500-38060, Golden, CO, 2009.

[12] Kalvig S, Manger E, Kverneland R. A method for wave driven wind simulations with CFD. Energy Procedia 2013;35:148-156, ISSN 1876-6102, http://dx.doi.org/10.1016/j.egypro.2013.07.168

[13] Churchfield MJ, Lee S and Moriarty P. Overview of the simulator for offshore wind farm application (SOWFA) National Renewable Energy Laboratory, Golden, CO, USA 03 May 2012 http://wind.nrel.gov/designcodes/simulators/sowfa/ accessed January 2014.

[14] Launder BE, Spalding DB. The numerical computation of turbulent flows, Computer Methods in Applied Mechanics and Engineering, 3 (2), Pages 269–289, 1974, DOI: 10.1016/0045-7825(74)90029-2

[15] Sullivan PP, Edson JB, Hristov T, McWilliams JC. Large-eddy simulations and observations of atmospheric marine boundary layers above nonequilibrium surface waves. Journal of the Atmospheric Sciences 2008;65(4):1225-1245.

[16] OpenFOAM; http://www.openfoam.com/ (retrieved 09.01.2014)

[17] Kalvig S, Manger E, Hjartager B. Comparing different CFD wind turbine modelling approaches with wind tunnel measurements. IOP conference Series. In review.

[18] Churchfield MJ, Lee S, Michalakes J, Moriarty PJ. A numerical study of the effects of atmospheric and wake turbulence on wind turbine dynamics. Journal of Turbulence 2012. doi: 10.1080/14685248.2012.668191

[19] Martínez LA, Leonardi S, Churchfield MJ, Moriarty PJ. A comparison of actuator disc and actuator line wind turbine models and best practices for their use. 50th AIAA Aerospace Sciences Meeting and Exhibit, Nashville, TN, Jan. 9–12, AIAA, Washington D.C., 2012.
[20] Troldborg N. Actuator line modeling of wind turbine wakes. PhD Thesis 2008, Technical University of Denmark, Lyngby, Denmark.

Paper 6

Kalvig S, Eliassen L and Manger E. : “On offshore wind turbine fatigue caused by wave influenced wind”

2nd Symposium on OpenFOAM in Wind Energy, Conference May 2014, Boulder, Colorado, USA.

On Offshore wind turbine fatigue caused by wave influenced wind

Siri Kalvig[1,a], Lene Eliassen[2] and Eirik Manger[3]

[1]University of Stavanger/StormGeo, 4010 Stavanger
[2]NTNU/Statkraft, 7491 Trondheim, Norway
[3]Acona Flow Technology, 3732 Skien, Norway

Abstract. A wave influenced wind turbine simulator (WIWiTS) is developed and results from these simulations are used for fatigue analyses. WIWiTS is based on the Simulator for Offshore Wind Farm Application (SOWFA) developed at NREL. The simulations are transient with an unsteady Reynolds-Averaged Navier-Stokes (URANS) approach. An actuator line representation of the turbine is placed in a domain where the wave and wind are aligned with each other and opposed to each other. Simulations with four different wave states are compared to a reference case with no waves, but the inlet wind is the same for all cases. The wave will influence the wind field, which in turn affects the equivalent fatigue damage both at the blade root and at the tower base. In a relatively low wind regime (8 m/s in a height of 400 m) our simplified simulations show that the wave influenced wind increase the fatigue damage compared to a situation with no waves, especially for the cases where the wave opposes the wind field.

1 Introduction

All though it is known that fast moving waves in a low wind regime will influence the whole depth of the marine atmospheric boundary layer (MABL) [1], it is still uncertain to what extent the wave influenced wind field will affect an offshore wind turbine or a wind farm [2]. The aim of this study is to investigate if a wave influenced wind field will affect the wind turbine loads and fatigue. This will be done by the use of computational fluid dynamic (CFD) and by introducing a moving wave surface in the actuator line simulations of wind turbine performance and couple this with a structural response code. In the following, this combined setup with integrated wave simulations will be referred to as Wave Influenced Wind Turbine Simulations (WIWiTS).

In this study, we only look at the possible effect the waves will have on the wind. In the MABL there is of cause a close interaction between the wind field and the sea surface where heat and momentum is exchanged. A real representation of the varying wind and wave field is a huge task and very computational requiring. The problem thus had to be simplified. First of all, we only look at how the waves influence the wind field and not the other way around. Hence, the waves are seen as a solid moving wave surface. A neutral atmosphere is anticipated, so no buoyancy effects or heat exchange is

[a] Corresponding author: siri.kalvig@stormgeo.com

considered. In addition, the Coriolis force is neglected, and since we are studying processes on a relatively small scale in a short period, this is believed to be a valid assumption. The wave field can be divided into a wind-generated wave field (characterized by short periods and relatively low phase speed) and waves that have propagated away from the source origin or swell (characterized by longer periods and faster phase speed). While wind-waves are normally aligned with the local wind, the local wind direction is not always correlated with the swell direction. Sometimes winds can completely oppose the swell field and this is known to give rise to interesting situations with increased turbulence levels over the sea surface [3]. We choose to study cases where the wind is aligned to the wind field and opposing the wind field, and compare this to a control run over a flat surface. The waves chosen will then need to be swell-like waves. These waves can also be fairly well represented by a sinusoidal shape.

This wave influenced wind field will then interact with a wind turbine. For the wind turbine modelling part, the Simulator for Offshore Wind Farm Application (SOWFA) [4], developed at the National Renewable Energy Laboratory (NREL), was used.

In section 2, we give a brief description of the different models that are used and a description of the simulation characteristics. The results are presented and discussed in section 3 and we conclude and give suggestion for further usage in section 4.

2 Description of the work

2.1 Wave generation, actuator line model and FAST

All CFD simulations are done with the open source CFD toolbox OpenFOAM [5]. The waves were generated by the use of a moving mesh approach. Each grid cell moves up and down, reaching its maximum elevation at different time increments according to a sinusoidal function, and the movement looks like a wave propagating - much like the surface particles in a real ocean wave. In [6] a more detailed description of the model is available.

Churchfield [4] implemented Sørensen and Shen's actuator line method [7] in SOWFA. Here, the turbine rotor blades are represented as span-wise sections with airfoil characteristics. The model requires various input parameters. We have used the airfoil characteristics of NREL's 5 MW turbine. Other input parameters such as number of span-wise airfoil sections (segments), and the Gaussian width factor (related to the impact area for the force calculated in every blade segments) is determined after best practise, see e.g. [8, 9,10].

In SOWFA it is possible to activate a coupling to FAST which is an aeroelastic computer-aided engineering tool for horizontal axis wind turbines [11]. The actuator line CFD simulations will then replace the blade element momentum (BEM) part that is usually used with FAST. FAST will calculate the structural response and feed this back into the CFD simulations. Now various output parameters regarding blade loads can be analyzed and used for fatigue calculations.

The bases for these CFD simulations are the Navier-Stokes equations and the continuity equation for an incompressible Newtonian fluid [12]. Our wave generation method was built from the OpenFOAM specific solver pimpleDyMFoam, and SOWFA is built from the OpenFOAM specific solver pisoFoam. Originally, SOWFA was set up for Large Eddy Simulations (LES), but we use an Unsteady Reynold Average Navier-Stokes (URANS) approach. The original solver for SOWFA was modified to include our wave generating method and in order to run using the URANS approach. As turbulent closure, we have used the standard k-epsilon model [13]. These modifications of existing solvers and implementation of a new wave generation method has resulted in the combined WIWiTS setup.

2.3 Simulation characteristics

Several waves can be superimposed on each other to create different sea states, but we used only one wave, a swell like wave. We varied the period (T_p) and length (L). Following the dispersion relation in deep water, the wave speed c then depends only on the wavelength. We studied four different waves in combination with a wind field with reference wind speed of 8 m/s in 400 m height. The simulation cases are listed in Table 1.

Table 1. WIWiTS cases. The wave speed c will be aligned with the wind (+) or opposed with the wind (-).

Case (named after the period, T_p)	Wave parameters
6 sec, aligned and opposed	a = 2 m, L = 56.2 m, c = (+/-) 9.4 m/s
7 sec, aligned and opposed	a = 2 m, L = 76.4 m, c = (+/-) 10.9 m/s
8 sec, aligned and opposed	a = 2 m, L = 100.0 m, c = (+/-) 12.5 m/s
10 sec, aligned and opposed	a = 2 m, L = 155.9 m, c = (+/-) 15.6 m/s
No Wave, reference case	a = 0 m, L = 0 m, c = 0 m/s

The computational domain was 700 m x 260 m x 400 m with the turbine placed 550 m from the inlet (Figure 1a and 1b). Grid dependency studies performed on a two-dimensional setup (without turbine representation) showed that in order to have grid independent solutions, a very fine mesh is preferable. Also, the domain must be large to minimize boundary effects. This resulted in hundreds of millions of cells when used on an equivalent three-dimensional case. Simulations on such a mesh were not feasible. The mesh was instead constructed with a background-graded mesh having a refinement towards the wave surface and a refined area around the turbine rotor. This resulted in a cell size of approximately one meter near the wave surface inside the refined area. The domain length and possibly also the height is believed to be too short to avoid all boundary effects, but the simulations will nevertheless give indications on the relative differences in fatigue for different wave conditions compared to a no-wave situation.

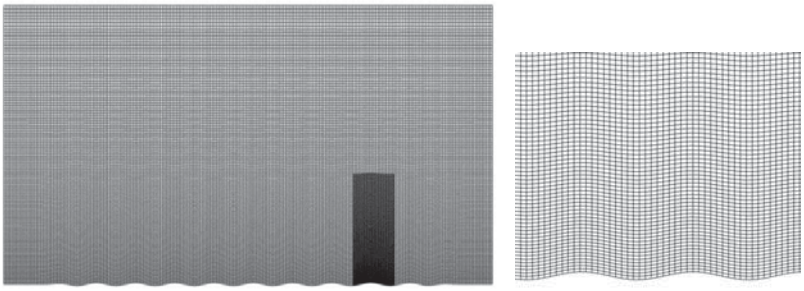

Figure 1a. Illustration of the WIWiTS domain. The WIWiTS mesh is graded near the surface and refined in a region around the turbine.

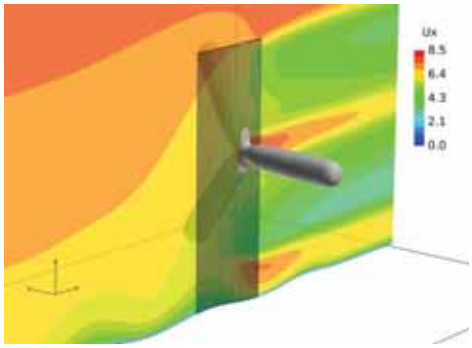

Figure 1b. An actuator line representation of the NREL 5 MW turbine is introduced in the moving wave domain. Shaded area shows the grid cells around the turbine. The horizontal velocities are shown as colour contours (m/s).

For pressure and velocities calculations, WIWiTS uses PIMPLE, which is a hybrid version of the PISO-SIMPLE algorithm [12]. For the calculation of the gradient term and the Laplacian term in the Navier-Stoks equations, Gauss linear discretization schemes were used and for the convective term, the Gauss upwind scheme was used. The boundary condition used for the different paches are listed in Table 2.

Table 2. Boundary conditions on the different patches for the WIWiTS, with OpenFoam specific naming. On the ground patch, the boundary conditions for U will be different in the case of a flat surface (fixedValue) compared to a moving wave surface (movingWallVelocity).
*Full openFOAM specific name: atmBoundaryLayerInletVelocity (logarithmic wind profile with $U_{400m} = 8$ m/s and roughness length, $z_0 = 0.0002$ m)

Field	Inlet	Outlet	top	sides	Ground
U, wind velocity	ABLvelocity*	zeroGradient	slip	slip	movingWallVelocity / fixedValue
P, pressure	zeroGradient	fixedValue	slip	slip	zeroGradient
k, turbulent kinetic energy	fixedValue	zeroGradient	slip	slip	kqRWallFunction
epsilon, turbulent dissipation of energy	fixedValue	zeroGradient	slip	slip	epsilonWallFunction;
nut, viscosity	fixedValue	zeroGradient	slip	slip	nutkRoughWallFunction

2.2 Fatigue calculations

Fatigue damage is based on a combination of material properties and load history. The material property gives information regarding the maximum number of cycles that the material can withstand with a given stress amplitude. This is normally given as an S-N curve [14];

(1)

$$log\, N = log\, \bar{a} - m\, log\, \Delta\sigma$$

where N is the predicted number of cycles to failure for the stress range $\Delta\sigma$, $\bar{a}$ is the intercept of the design S-N curve with the log N axis and m is the negative inverse slope of the S-N curve. A glass epoxy material for the blade is assumed, where the slope $m = 9$, and intercepts the curve, $\bar{a}$ at 70 MPa. The load history from the simulation will provide the bending moment, from which one can estimate the stress. From the stress history, the number of amplitudes at a given stress range can be estimated. For large simulations, the stress ranges are divided into blocks. The number of cycles with a stress range within the block will be n. The fatigue damage, D, is calculated using the Palmer-Miner rule:

(2)

$$D = \sum_{i=1}^{k} \frac{n_i}{N_i} = \frac{1}{\bar{a}} \sum_{i=1}^{k} n_i \cdot (\Delta\sigma_i)^m$$

where k is the number of stress blocks, n_i is the number of stress cycles in block i and N_i is the number of cycles to failure at a constant stress range $\Delta\sigma_i$. A combination of the probability of the wind conditions over a year combined with the fatigue damage from a simulation will give the expected fatigue damage over a year, and the inverse of the damage would be the expected lifetime.

In this study, the aim is not to investigate the lifetime of the structure, but rather the effect of the change in wind profile due to the wave influencing the wind profile. The equivalent damage load is a measurement of the damage load relative to another simulation. We will use the no wave simulation as a reference to the different simulations with different wave periods (see Table 1.). The definition of the equivalent fatigue load is:

(3)

$$\Delta\sigma_{EQ} = \left(\frac{\sum (\Delta\sigma_i)^m N_i}{N_{EQ}} \right)^{1/m}$$

where N_{EQ} is the equivalent number of cycles in the simulation. Here, N_{EQ} is the number of cycles needed for the equivalent fatigue damage in the reference simulation (no waves) to be one.

The stress at the blade root, σ, is estimated using the following relation:

(4)

$$\sigma = \frac{M \cdot y}{I}$$

where M is the bending moment of the, y is the radius of the outer diameter of the blade root, and I is the moment of inertia of the circular cylinder at the blade root. Only the bending moments in flapwise direction are evaluated, as the gravitational force is dominating the bending moment in edgewise direction. The first 200 seconds of the simulation is discarded due to start-up transients.

3 Results and discussion

Both the direction of the wave and the wave state will affect the wind profile over the rotor swept area. In Figure 2 only horizontal wind profiles for one of the four wave cases are shown (T_p=10 sec) as well as wind profiles for the no wave case. Profiles are sampled 300 meters from the inlet and at a position

close to the wind turbine at 495 meters (5 meters in front of the wind turbine). The wind profile figures illustrate that the waves have an effect on the wind field. Since the aim of this study is to examine the possible effect of this fluctuating wind field on the wind turbine, we will in the following investigate stress on the blades and the tower.

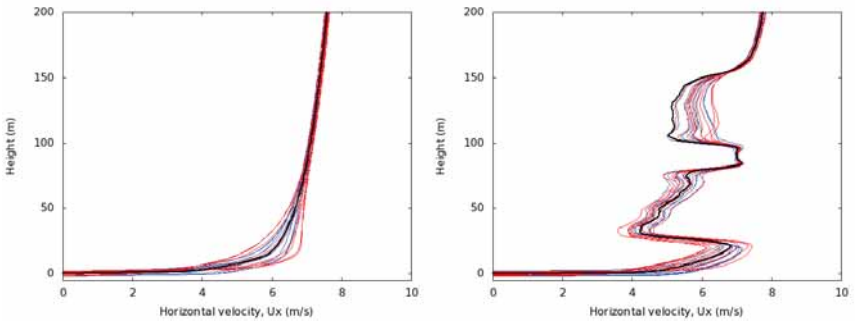

Figure 2. Profile of horizontal wind (m/s) 300 m from the inlet (left) and 495 m from the inlet (right) from case with wave period of 10 sec and from the no wave case (see Table 1). Wind and wave in the same direction (blue), wind and wave in the opposite direction (red) and no wave case (black). Profiles are sampled over approximately one wavelength.

Figure 3 shows the stress at the blade root due to the flapwise moment after removing the start-up transients. The top graph is for the opposed wave condition, while the bottom graph is the aligned wave condition. Both graphs only consider the last 100 seconds in the fatigue calculations.

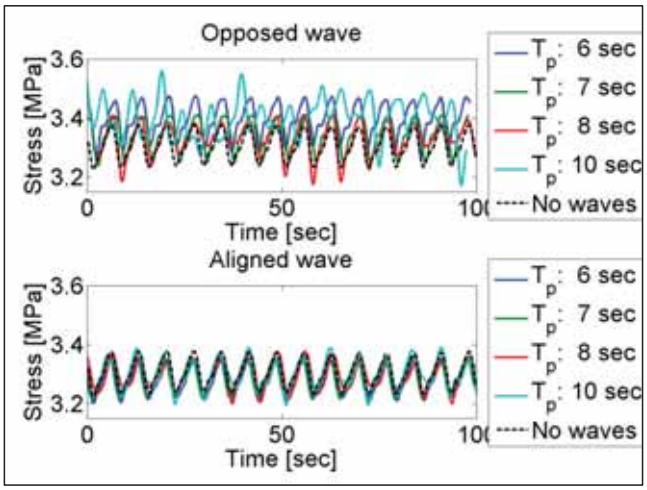

Figure 3. Stress at the blade root due to the flapwise bending moment at the blade root.

It is clear that the stress variations are larger in the opposed wave condition relative to the aligned wave condition. This is true for all wave conditions with opposed wind investigated. However, regarding the aligned wind cases the stress is not notably affected. The reference case with no waves is included in both graphs, and it coincides very well with the simulations considering aligned wind. Therefore, we expect that the difference in fatigue will not be large for the aligned case.

The opposed wave condition shows large variations in the stress range. Especially the waves with long periods show a large variation in stress. There seems to be a periodicity in the lower range of the stress for some of the wave conditions, as illustrated in Figure 5.

Figure 4 shows the stress at the base of the tower. Similar to the results for the blade root moment, the aligned case has smaller stress ranges compared to the opposed wave condition. The mean value seems to correspond relatively well with the stress in the reference case with no waves. The mean stress from opposed wave condition is higher than the aligned wave condition and the no wave condition for the stress at the tower base. The stress range has a large variance for some wave periods, e.g. T_p= 8 sec.

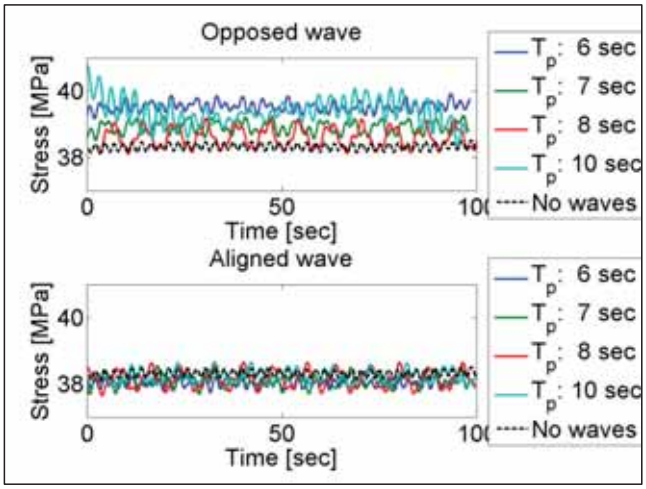

Figure 4: Stress at the blade root due to the tower bending moment at the tower base.

The stress at the blade root and at the tower root will have different periods. This is illustrated in Figure 5, where the stress at the root of all three blades are shown. Each blade has a period of 56 seconds at which they are oscillating. This period is the multiple of the period of the rotor rotation, 7 seconds, and the wave period, T_p. The stress transferred to the tower will however have a different period, which is similar to the waveperiod.

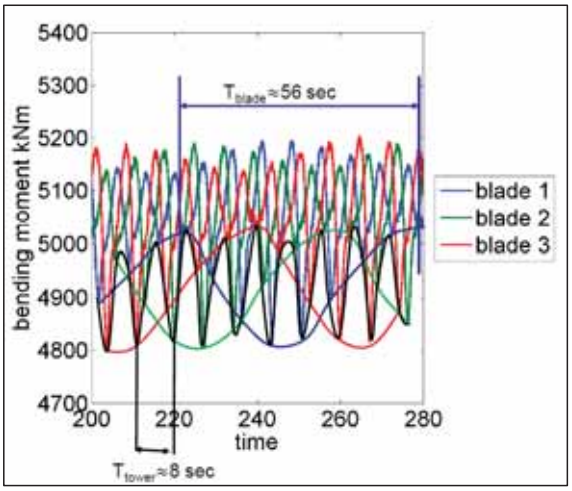

Figure 5. The stress for the three blades for opposed wave and period 8 seconds.

The frequency spectrum for the time simulation is shown in Figure 6 for all wave frequencies. The frequency of one rotation, 1P, is 0.14 Hz. 2P and 3P are integers of this frequency. It is evident that the rotational frequency, 1P, contains the most energy. This is where the mean vertical shear will be sampled. The turbulent winds are sampled at the higher multiples of the rotational frequency, i.e. 2P and 3P. The wave frequencies applied vary from 0.10 Hz to 0.17 Hz.

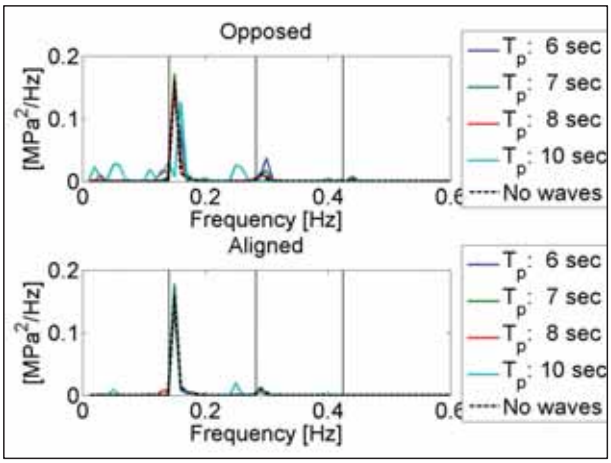

Figure 6. Frequency spectrum for the bending moment in the flapwise direction.

The frequency plot for the stress in the tower base is shown in Figure 7. The wave frequencies are visible in both the aligned and the opposed cases (wave period of 6-10 seconds corresponds to frequencies of 0.1-0.17 Hz). The intensity of the response spectrum varies with the period of the wave applied, and most energy is found for wave periods close to the rotational frequency 1P (here: 0.14 Hz). The only peak that is found in the reference case with no waves is at the 3P (0.42 Hz). This peak is due to the vertical shear of the mean wind profile, and is corresponding to the peak at 1P (0.14 Hz) for the bending moment in flapwise direction in Figure 6. The intensity of this peak is relatively similar for all simulations.

The small peak at around 0.3 Hz in Figure 7 may be the eigenfrequency of the tower. For a fully dynamic aero-hydro-elastic-servo response analysis, the response at this frequency is normally larger and will sometimes dominate the spectra. The analysis presented here is limited to an analysis with little ambient turbulence and no hydrodynamic load, and the excitation of this mode is therefore limited.

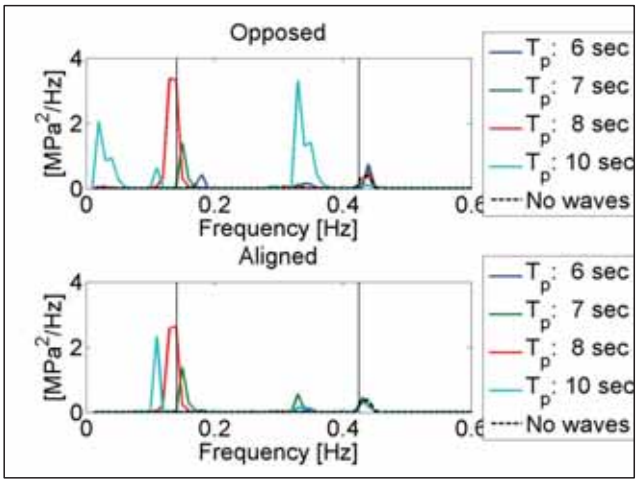

Figure 7. Frequency spectrum for the tower base bending moment.

The equivalent fatigue damages, shown in Table 3 and Table 4, are estimated using Equation 3. The length of the simulation is very limited, only 100 seconds. The equivalent damage is estimated using the no wave case as a reference load case.

Table 3. Equivalent fatigue damage at the blade root, considering flapwise bending moment, based on a 100 seconds simulation.

	$T_p = 6\,s$	$T_p = 7\,s$	$T_p = 8\,s$	$T_p = 10\,s$
No wave	1	1	1	1
Opposed	1.31	1.15	1.41	1.70
Aligned	1.01	0.98	1.06	1.19

Table 4. Equivalent fatigue damage at the tower base, based on a 100 seconds simulation.

	$T_p = 6\,s$	$T_p = 7\,s$	$T_p = 8\,s$	$T_p = 10\,s$
No wave	1	1	1	1
Opposed	1.42	1.52	2.36	2.37
Aligned	1.17	1.74	2.12	1.53

4 Conclusions and further suggestions

It has been challenging to validate the results. To our knowledge there does not exist similar work that we can compare our results with, nor observations. We have reason to believe that the domain size is too small and we cannot guarantee that boundary effects are not present. In addition, grid independency was not completely reached. Nevertheless, we think that these results demonstrate that the wave will influence the wind field, which in turn affect the equivalent fatigue damage at both the blade root and the tower base. In a relatively low wind regime (reference wind of 8 m/s in 400 m height) the wave influenced wind increases the fatigue damage compared to a situation with no waves, especially for the cases where the wave opposes the wind field. Of the four wave cases (eight simulations) studied, the larger wave periods (8 and 10 seconds) give rise to the highest equivalent loads, and these cases also result in the highest peaks in the frequency spectrum. It is currently not possible to state whether the effect of wave influenced wind gives a significant response on the wind turbine compared to other effects that causes fluctuations in the wind, i.e. varying stratification and natural turbulence fluctuations.

There is a need for longer stimulations time and more simulations in order to be able to conclude more specifically regarding the wave influenced wind impact on turbine performance and fatigue. Several sea states and wind regimes must be investigated, and it is also preferable to further develop the method here presented. Grid independency should be established and one should ensure that the computational domain is large enough. We have used an incompressible solver and one should consider implementing WIWiTS on a compressible solver. More realistic atmospheric conditions need to be implemented with buoyancy effect present. Different discretization schemes should be tested. The upwind schemes that we have used are known to be quite dissipative in URANS simulations, and a higher order scheme (e.g Quick) could generate more turbulence and hence change the results.

Acknowledgements

This work was made possible by funding from the Norwegian Research Council Industrial PhD-program (198257) and from StormGeo. The work is also a part of the Norwegian Centre for Offshore Wind Energy (NORCOWE) under grant 193821/S60 from the Research Council of Norway (RCN). NORCOWE is a consortium with partners from industry and science, hosted by Christian Michelsen Research. The authors would like to acknowledge Theodor Ivesdal at the University of Stavanger for his outstanding technical help with the Linux cluster.

References

1. P.P. Sullivan, J.B. Edson, T. Hristov, J.C. McWilliams. Large-eddy simulations and observations of atmospheric marine boundary layers above nonequilibrium surface waves. Journal of the Atmospheric Sciences, **65**(4), 1225-1245, (2008).
2. S. Kalvig, O.T. Gudmestad and N. Winther. Exploring the gap between "best knowledge" and "best practice" within the use of boundary layer meteorology for offshore wind energy, Wind Energ., **17**: 161–171. DOI: 10.1002/we.157 (2014)
3. F. Ocampo-Torres, H. García-Nava, R. Durazo, P. Osuna, G. Díaz Méndez, H. Graber. The INTOA Experiment: A study of ocean-atmospher interactions under moderate to strong offshore winds and opposing swell conditions in the Gulf of Tehuantepec, Mexico. Boundary-Layer Meteorology 2011;**138** (3):433-451. doi: 10.1007/s10546-010-9561-5 (2011)
4. M.J. Churchfield, S. Lee and P. Moriarty. Overview of the simulator for offshore wind farm application (SOWFA) National Renewable Energy Laboratory, Golden, CO, USA 03. May 2012 http://wind.nrel.gov/designcodes/simulators/sowfa/, retrieved January 2014
5. OpenFOAM; http://www.openfoam.com/ (retrieved 26. June 2014)
6. S. Kalvig, E. Manger and R. Kverneland. A method for wave driven wind simulations with CFD, Elsevier Energy Procedia, **35**, Pages 148-156, ISSN 1876-6102, http://dx.doi.org/10.1016/j.egypro.2013.07.168 (2013)
7. J.N. Sørensen and W.Z. Shen. Numerical modeling of wind turbine wakes. J. Fluid Eng. **124** 393-399 DOI: 10.1115/1.1471361 (2002)
8. L.A. Martínez, S. Leonardi, M.J. Churchfield and P.J. Moriarty. A comparison of actuator disc and actuator line wind turbine models and best practices for their use. 50th AIAA Aerospace Sciences Meeting and Exhibit, Nashville, TN, Jan. 9–12, AIAA, Washington D.C., (2012).
9. N. Troldborg. Actuator line modeling of wind turbine wakes. PhD Thesis, Technical University of Denmark, Lyngby, Denmark (2008)
10. A.M. Nodeland. Wake modelling using an actuator disk model in openFOAM. Master's thesis spring 2013, Norwegian University of Science and Technology, Department of Energy and Process Engineering, EPT-M-2013-85, Trondheim, Norway (2013)
11. J. Jonkman and M. Buhl. FAST User's Guide, NREL/EL-500-38230, NREL technical report, (2005). Accessible at: http://wind.nrel.gov/designcodes/simulators/fast/FAST.pdf
12. H.K. Veersteg, W. Malalasekera. *An Introduction to Computational Fluid Dynamics*, Essex, England: Pearson Education Limited, Second edition, (2007)
13. B.E. Launder, D.B. Spalding. The numerical computation of turbulent flows, Computer Methods in Applied Mechanics and Engineering, **3** (2), Pages 269–289 DOI: 10.1016/0045-7825(74)90029-2 (1974)
14. DNV, Design of offshore wind turbine structures, DNV-OS-J101, October (2010)